Acute Pulmonary Toxicity and Microglial Activation following Inhalation of Aerosolized
Engineered Nanomaterials in Rodents

By

PRIYA UPADHYAY
DISSERTATION

Submitted in partial satisfaction of the requirements for the degree of

DOCTOR OF PHILOSOPHY

in

Integrative Pathobiology

in the

OFFICE OF GRADUATE STUDIES

of the

UNIVERSITY OF CALIFORNIA

DAVIS

Approved:

Kent E. Pinkerton, Chair

Laura S. Van Winkle

Pamela J. Lein

Committee in Charge

2022

i

Abstract

Engineered nanomaterials (ENMs) are used in diverse consumer products including, but not limited to antibacterial agents, paints, food additives, cosmetics, rubber-curing agents, textile UV-absorbers, contrast elements for magnetic resonance imaging, heating agents for cancer thermotherapy, and carriers for drug and gene delivery. Nanomaterials possess a greater surface area to volume ratio yielding a greater reactive surface area and unique physiochemical properties, but potentially possessing greater biological activity and possible toxicity than their bulky counterparts. With more than 1800 ENM-based consumer products on the market, greater demands for nanomaterials may pose increased risk for consumer and occupational exposure, in particular for workers who manufacture, handle, and package ENMs and ENM-based products. Hence, there is a need to better understand and test the hazards of these nanomaterials and their effects on human health and the environment.

The aim of this study was to assess the potential implications of silver silicate ($Ag-SiO_2$), zinc oxide (ZnO) and reduced graphene oxide (rGO) to the respiratory tract, especially when inhaled. The focus of this study was on the upper respiratory tract composed of the nasal cavity and possible transport to the brain (via the olfactory bulb) and the lower respiratory tract formed by the bronchial tree and lung parenchyma. These two regions of the respiratory system were selected for study, based on unique patterns of particle deposition for each region and the potential implications for nanoparticles being retained in each of these regions following deposition.

To address the aim of our study, an acute, single day nose-only inhalation exposure regimen to aerosols of each nanomaterial was conducted in Sprague Dawley rats. Aerosols were well-characterized before and during the study. Animals were necropsied immediately (day 0) and on days 1, 7, 21 or day 56 post-exposure to ENMs. Bronchoalveolar lavage fluid, lung tissues and the nasal cavity with the contiguous olfactory bulbs were collected for assessment. Experiments were conducted to evaluate the pulmonary toxicity via BALF analysis, histological examination, gene expresssion and immunohistochemical staining. For the nasal cavity and olfactory bulb, histological examination and studies of microglial activation were conducted.

ACKNOWLEDGEMENTS

This thesis represents a milestone of more than 4 years of work in Toxic Pollutant Health Research Laboratory (TPHRL) located in Center for Health and the Environment, University of California, Davis. It was my home away from home. I was given many opportunities which sharpened my skills and helped me become a better scientist. These years in TPHRL represent my growth from a physician to a physician scientist.

First and foremost, I would like to thank Dr. Kent Pinkerton for providing guidance and support before and during my PhD journey. I have known him since I joined the lab as a volunteer and then continued working as a graduate student. Thank you, Dr. Pinkerton, for sharing your depth of knowledge, answering all my research questions and being patient with me. I could not imagine having a better mentor for my graduate study. I will forever be inspired by your humbleness, your passion for research and your expert knowledge in pulmonary pathology.

I would like to thank my committee members, Dr. Laura VanWinkle and Dr. Pamela Lein. Thank you for giving me constructive feedback and insightful comments which helped making my dissertation better. It was such an honor to have successful women scientists in my committee. Thank you, Dr. Van Winkle, for inspiring me to do better from day 1. I will always remember your words "write often and write early" and "negative data is still a data". To my wonderful GGIP family, thank you for being the base of my PhD and all the support throughout these years. Thank you, Dr. Sara Thomasy and Dr. Erin Kent. Thank you, Dr. Kevin Keel, for your advice when I was just starting graduate school.

Thank you to all the members of Pinkerton laboratory. This would not have been possible without you all. Thank you, Dale Uyeminami for your dedication during exposures and your patience to answer my questions as well as keeping in mind all the tiny details that we'd miss during the countless exposures. Ciara Fulgar and Savannah Mack's love for science, coffee talks and lunch meetings motivated me in many ways. Thank you, Emilia Laing, Radek Abarca, Yinyu Yuan and Krysta Zmich for helping me throughout my Phd years, for troubleshooting talks, embedding, sectioning and staining. Thank you, Morgan Poindexter and Ching Wen Wu for helping me with the experiments. It was fun working with Huong Huynh with her deep neurological knowledge. Thank you, Pinkerton lab for making early morning exposures and late-night necropsies fun. Thank you, Rona for all the editorial support.

To my friends and families, here and in Nepal, thank you for being my biggest cheerleaders and pillar of support. Mumma-Daddy for always being there and encouraging me from far. Swati for trying to understand whenever I explained my research. Mummy-Daddy, kakas-kakis for supporting me. Thank you Saurav for always checking up on me; Sampada, Aayush, Swikriti, Anisha, Pranabh and Prabhav for making me smile and laugh during those tiring thesis writing/pandemic days. To my

TABLE OF CONTENTS

Chapter Four: Pulmonary Response in Sprague Dawley Rats Following a Single Exposure to Aerosolized Graphene Oxide

Chapter Five: Inhalation of Silver Silicate Nanoparticles Leads to Transient and Differential Microglial Activation in the Rodent Olfactory Bulb

Chapter Six: Conclusions and Future Directions

List of Tables

List of Figures

CHAPTER 1

Introduction

The use of engineered nanomaterials (ENMs) has grown exponentially in the past two decades. Nanotechnology is defined as a discipline that "involves a wide range of technologies that measure, manipulate, or incorporate materials and/or features with at least one dimension between approximately 1 and 100 nanometers (nm). Nanomaterial applications exploit the properties of nanoscale components, distinct from bulk/macroscopic systems of identical composition. Nanoparticles are defined as particles with physical properties in two or three dimensions ranging from 1-100 nm (Standard 2012). Diverse in nature and utility, nanomaterials have created dramatic changes in our society through a myriad of commercial products, industrial applications, medical treatments, drug delivery and incorporation into thousands of everyday personal items. In the Nanotechnology Consumer Products Inventory (CPI), there are more than 1600 ENM-based consumer products (Bierkandt, Leibrock et al. 2018). Continual and greater demands for nanomaterials may pose increased risk for consumer and occupational exposure, in particular for workers who manufacture, handle, and package ENMs and ENM-based products. ENMs are used in diverse consumer products including but not limited to antibacterial agents, paints, food additives, cosmetics, rubber-curing agents, textile UV-absorbers, contrast elements for magnetic resonance imaging, heating agents for cancer thermotherapy, and carriers for drug and gene delivery. The physical size of these materials, with at least one dimension being 100 nm or less, provides them with unique properties not seen in identical materials of greater size (i.e. micron dimensions and larger). When compared to chemically identical bulk materials, nanomaterials possess a greater surface area to volume ratio yielding a greater reactive surface area and potentially greater toxicity than

their bulky counterparts (Fischer and Chan 2007). ENMs present a further challenge with possible health implications due to their size and ease of penetration into the body through a variety of pathways, such as dermal, ocular, inhalation, and digestion.

The goal of this dissertation is to explore the potential health implications of ENM exposure to the respiratory tract, especially when inhaled. The focus of this study will be in two primary regions of the respiratory tract: 1) the upper respiratory tract composed of the nasal cavity and 2) the lower respiratory tract formed by the bronchial tree and lung parenchyma. These two regions of the respiratory system have been selected for study, based on unique patterns of particle deposition for each region and the potential health implications for nanoparticles depositing in each of these regions.

It is well-established particles less than 10 microns can enter the respiratory tract. As the size of particles become smaller, the ease of their penetration into the respiratory system is enhanced with particles 2.5 microns or less entering and depositing into the deepest portions of the lungs formed by the alveoli. Nanoparticles have the greatest potential for deposition throughout the entire respiratory system. Although the nasal cavity serves as a primary filter for large airborne particles through deposition and clearance. The turbulent airflow created in the nose by the nasal turbinates allows for a high deposition of nanoparticles as well. This chapter will introduce the concepts of particle deposition, pathways of clearance and potential adverse outcomes associated with nanoparticles through an extensive review of the current literature. We will begin with a discussion of ENM effects on upper respiratory tract and nose to brain translocation, followed by EMN effects on the lower respiratory tract.

Route of Exposure

ENMs can enter the body via dermal, ocular, inhalation, and digestion routes. In addition to environmental and occupational exposure to ENMs, worldwide use of ENMs in biomedicine, therapeutics and diagnosis also represent a major source of exposure (Wu and Tang 2018). The route of exposure to ENMs influences the type and degree of effects observed. However, inhalation is the most common, and potentially the most harmful, route of exposure (Kreyling, Semmler-Behnke et al. 2006, Bierkandt, Leibrock et al. 2018).

The workplace, environment, and consumer products can act as the three major sources of inhalation exposure to humans (Bierkandt, Leibrock et al. 2018). In the workplace, employers may be exposed to ENMs at any stage of the synthesis process which can include manufacturing, packaging and transport (Kuhlbusch, Asbach et al. 2011, Oberbek, Kozikowski et al. 2019). Sprays and powders containing ENMs create the risk of inhalation exposure to consumers as they can produce aerosols within the vicinity of the breathing zone for users of these products (Lorenz, Hagendorfer et al. 2011). Similarly, ENMs can be released in the environment during production, handling, transport and use of ENM-based products (Bierkandt, Leibrock et al. 2018).

Nose as a port of entry
Function of Nose

The nose as a pyramidal-shaped structure that acts as a portal for the exchange of air between the external environment and the body. The nose helps to filter and

condition inhaled air before entering the lower respiratory tract. These functions to filter and condition the air are essential for the defense and protection of the lower respiratory tract (Harkema, Carey et al. 2006). Specialized vascular mucosa of the nasal cavity helps to regulate the temperature of the air, while humidity in the nose is maintained by the transudation of fluids through the mucosal epithelium and secretion from the mucosal glands and goblet cells lining extensive regions of the nasal cavity (Geurkink 1983). Vibrissae and the mucociliary flow contribute to the protective function of the nose. Vibrissae are the stiff hairs present at the nares to trap particles >3µm in the inhaled air. In contrast, particles in the range of 0.5 to 3 µm are trapped following deposition by the mucus lining layer in the nasal cavity (Geurkink 1983, Sahin-Yilmaz and Naclerio 2011). Mucus in the nasal cavity is secreted by mucous (goblet) cells and subepithelial glands.

Mucus covers a large portion of the nasal vestibule. Trapped particles in the mucus are removed from the nasal cavity by the beating of cilia to the nasopharynx, oropharynx, and esophagus and subsequent clearance from the body through the digestive tract. Present in mucus are antibodies, interferons, lysozymes and enzymes to contribute to the defense during the clearance of particles and micro-organisms. The nose also possesses reflex functions in the form of the sense of smell and the trigeminal nerve with endings found throughout the nasal wall. Olfaction is critical function of the nose.

The sense of smell or olfaction is one of the oldest evolutionary senses which develops in the embryo and aids in the search for food, mating and kin recognition, as well as in the identification of danger and enemies (Sarafoleanu, Mella et al. 2009,

Treloar, Miller et al. 2010). Rodents are obligate nose breathers with olfaction serving as a major function. The sense of smell also helps humans and rodents in locomotor activities and spatial orientation (Miller and Spear 2009, Hugill 2015). The olfactory pathway and the visual pathway are the only direct neural connections to the central nervous system (CNS) to the outside environment without involvement of the blood brain barrier (BBB) (Brai and Alberi 2018). Therefore, both the eye and the nasal cavity can serve as potential pathways for exogenous materials to gain access to the brain via the optic and olfactory nerve respectively. In addition, the trigeminal nerve of the nasal cavity could also serve to connect the olfactory neuroepithelium and nasal respiratory epithelium respectively to the brain (Mistry, Stolnik et al. 2009).

Comparative Anatomy and Physiology of the nose

The external nose is a pyramid-shaped muscular structure composed of frontal, maxillae and nasal bones along with soft tissues. The nasal septum divides the nasal cavity into two symmetrical structures, separated in the mid-sagittal plane by the nasal septum. The nasal cavity is composed of dorsal, ventral, medial and lateral walls. The total volume and surface area of the bilateral nasal cavity is 15 mL and 160 cm^2, respectively (Gizurarson 2012) in humans. In the adult rat the nasal volume is 257 mm^3 and surface area 1344 mm^2 (Gross, Swenberg et al. 1982).The nasal cavity is further divided into three regions: vestibular, respiratory and olfactory.

I.   Vestibular region: This area constitutes the anterior region of the nasal cavity and has a total surface area of 0.6 cm^2 in the human (Crowe, Greenlee et al. 2018). Nasolacrimal ducts and lateral nasal glands open in the vestibule of rodents. The

vestibular region is lined with stratified squamous epithelium and the presence of nasal hairs or vibrissae, which act as the first line of defense to filter the inhaled air.

II. Respiratory region: This area of the nose covers the major portion of the nasal cavity with a total surface area of 130 cm^2 (Watelet and Cauwenberge 1999). Within this region are three bony plates which compose the nasal turbinates or conchae consisting of the superior, middle and inferior turbinates to form air spaces known as the superior, middle and inferior meatus, respectively. This structural nature of the nose creates the turbulent airflow to help in temperature control, humidification and filtration of the inspired air. In rodents, turbinates have complex branching patterns and foldings. As rodents are obligate nasal breather, these complex turbinates provide a greater surface lining of olfactory epithelium (to be discussed further in the next section) and better protection to the lower respiratory tract. Due to differences in turbinates, the air flow pattern in human and rodents vary significantly (Harkema 2015). The respiratory region is lined with pseudostratified ciliated columnar epithelium composed of ciliated cells in addition to goblet and basal cells. The mucin secreted by goblet cells makes the mucus lining layer of the nose which traps and removes deposited particles from the inspired air. The cilia and microvilli associated with this cell type increase the surface area of the respiratory region. The maxillary branch of the trigeminal nerve innervates respiratory region of the nasal cavity. It should be noted the trigeminal nerve is also considered as a potential route for nose-to-brain transport of viruses, metals and therapeutics (Crowe, Greenlee et al. 2018). The

vascularity and large surface area of the respiratory portion of the nasal cavity may also contribute to the systemic absorption of metals and therapeutics from the nasal cavity (Ghadiri, Young et al. 2019).

III. Olfactory region: This region is in the upper portion or most dorsal aspect of the nasal cavity. The region is lined with pseudostratified columnar epithelium consisting of olfactory, sustentacular (supporting) and basal cells. The partition between the brain and the nasal cavity is formed by the cribriform plate of the ethmoid bone possessing numerous foramina. These foramina provide the connection between the brain and the nasal cavity via the olfactory nerve fascicles (Gray 2009, Gizurarson 2012). As already mentioned, the olfactory region contains basal cells, supporting or sustentacular cells, and the olfactory epithelial cells. This neural layer forms the trigeminal and olfactory neural composition of the olfactory epithelium. Axons of the olfactory neural cells synapse with mitral cells of the olfactory bulb. As these axons exit from the olfactory epithelium, they are enclosed in bundles by olfactory ensheathing cells which are present along the pathway from the olfactory epithelium to the olfactory bulb (Crowe, Greenlee et al. 2018, Yao, Murtaza et al. 2018). The perineural space between the ensheathing layer and the neural fibroblast layer is continuous with the subarachnoid space (Field, Li et al. 2003). It is due to the presence of these cell layers and axons, particles can be transported to the brain from the nasal cavity.

Deposition of ENM in the respiratory tract

Deposition of ENM in the respiratory tract is influenced by 1) the complex anatomical structure of the respiratory tract, 2) characteristics of the particles and 3) airflow patterns in the lungs (Bakand, Hayes et al. 2012, Darquenne 2020). Three major mechanisms that influence particle deposition are inertial impaction, gravitational sedimentation and Brownian diffusion (Figure 1). Particle deposition is also influenced by turbulent airflow, electrostatic precipitation and interception (Darquenne 2020).

When there is a sudden change in air flow due to the bifurcation of the airways, larger particles (>5µm) with are unable to be maintained in the laminar air flow. These larger particles are deposited in the nasopharyngeal region by inertial impaction. In the tracheobronchial region, smaller particles (1-8µm) deposit by interception and gravitational sedimentation. The mass of the particle influences gravitational deposition. Submicron (<1µm) and nanoparticles (<100nm) are deposited in the alveolar region by Brownian diffusion. Deposition by Brownian diffusion is inversely proportional to the particle size. Brownian motion is produced by small particles colliding with air molecules in the alveoli. Brownian motion allows particles to come into contact with the alveolar surfaces leading to deposition. Brownian diffusion can also lead to the deposition of particles less than 0.01µm in the nose, mouth and pharyngeal airways as well (Cohen, Zelikoff et al. 2000, Oberdörster, Oberdörster et al. 2005, Bakand, Hayes et al. 2012, Darquenne 2020). Nanoparticles carrying a charge surface can also be deposited in the lungs by electrostatic precipitation (Oberdörster, Oberdörster et al. 2005).

Clearance of ENM

Physical and chemical mechanisms can lead to the clearance of ENMs from the respiratory tract. Physical clearing processes include macrophage phagocytosis and transport along the mucociliary escalator. Chemical clearing processes include dissolution and physical breakdown of the particles (Oberdörster, Oberdörster et al. 2005, Madl and Pinkerton 2009). In addition to these classic clearance pathways, ENMs deposited in the respiratory tract are also removed by uptake and translocation of ENMs along sensory neurons into the ganglionic and CNS structures. Epithelial cell translocation of ENMs to the lung interstitium movement into lymphatic and circulatory systems represent additonal pathways or particle clearance from the respiratory tract (Oberdörster, Oberdörster et al. 2005, Elder, Gelein et al. 2006, Kreyling, Semmler-Behnke et al. 2006, Madl and Pinkerton 2009).

Epithelial Translocation

ENMs, due to their small size, are easily and deeply deposited into the alveolar region which can prove difficult to clear due to size (Witschi, Pinkerton et al. 2008). Compared to particles of larger size, ENMs are less efficiently phagocytosed by alveolar macrophages. This inefficiency in macrophage uptake can increase the translocation of ENMs through the alveolar epithelium (FERIN, OBERDÖRSTER et al. 1991, Kreyling, Semmler et al. 2004, Semmler-Behnke, Takenaka et al. 2007). Rats exposed to 20nm TiO_2 showed increased pulmonary retention, alveolar epithelial translocation, pulmonary inflammation and impaired clearance, compared to rats exposed to 250nm TiO_2 (Ferin and Oberdörster 1992, Ferin, Oberdorster et al. 1992, Oberdörster, Ferin et al. 1994). ENMs which are taken up by epithelial cells decrease their chances of being phagocytosed by macrophages, thus decreasing the rate of clearance of these particles

(Kreyling, Semmler et al. 2004, Semmler-Behnke, Takenaka et al. 2007). Thus, epithelial translocation is the major pathway for clearance of particles when they are not phagocytosed either due to their small size or due to particle overload of alveolar macrophages (Oberdörster, Oberdörster et al. 2005).

Nose to Brain Translocation

Nose to Brain Pathways

Three primary pathways have been identified in which particles and therapeutics can be transported from the nose to the brain. These are 1) the olfactory pathway, 2) the trigeminal pathway and 3) the systemic pathway.

I. Olfactory pathway: Following deposition of inhaled particles on the surface of the olfactory mucosa, translocation can take place through olfactory receptor neurons by way of a transcellular or paracellular pathway. The nasal epithelium with associated tight junctions, desmosomes and adherent junctions can allow particles to pass through the space between cells by means of a transcellular transport. As described previously, these particles can reach the olfactory bulb and cerebrospinal fluid (CSF) by way of the axons of the olfactory receptor neuron, since these axons cross the cribriform plate to reach the olfactory bulb as well as to other regions of the CNS (Athira, Prajitha et al. 2018, Bourganis, Kammona et al. 2018, Selvaraj, Gowthamarajan et al. 2018). The olfactory pathway can be further divided into an intra-neuronal pathway which includes olfactory neuron axons, as well as the extra-neuronal pathway that is associated with perineural channels (Chen,

Fawcett et al. 1998). The olfactory pathway has been extensively studied for the transport of therapeutics in the treatment of CNS diseases, due to the ability for rapid onset of action, fewer systemic side effects and the ability to bypass the BBB (Thorne and Frey 2001, Mistry, Stolnik et al. 2015, Bourganis, Kammona et al. 2018). The potential for the translocation of ENM from the nose to the brain via this pathway will be an area of discussion in this and other chapters.

II. Trigeminal pathway: The trigeminal nerve is the largest cranial nerve which supplies innervation and sensation to the face, while also assisting in biting and chewing. The trigeminal nerve innervates the respiratory and olfactory mucosa. The trigeminal pathway can also act as an alternative route for particle and therapeutic transport from the nose to the brain (Mistry, Stolnik et al. 2009). Trigeminal nerves enter the forebrain and hindbrain from the nasal cavity via the cribriform plate near the olfactory bulb, as well as through the anterior lacerated foramen found near the pons (Pardeshi and Belgamwar 2013). The trigeminal nerve has three branches: 1) ophthalmic, 2) maxillary and 3) mandibular. The ophthalmic branch innervates the dorsal nasal mucosa and anterior part of the nasal cavity, whereas the maxillary branch innervates the lateral walls of the nasal cavity. The mandibular branch has motor fibers and supply the muscles of mastication. These neural branches have the capacity to carry particles from the nasal mucosa, although there is no direct connection between the trigeminal nerve and the nasal mucosa. The three branches of the nerve synapse at the trigeminal ganglion, whereupon

the nerve enters the brainstem at the level of the pons and subsequently to the forebrain and hindbrain (Illum 2000, Pardeshi and Belgamwar 2013, Bourganis, Kammona et al. 2018).

III.   Systemic pathway: the highly vascular respiratory epithelium of the nasal cavity can be a primary contribution in the systemic transport of particles from the nose to the brain (Kozlovskaya, Abou-Kaoud et al. 2014). Lipophilic particles of small size and low molecular weight (mention size and weight) can easily enter the bloodstream and cross BBB in comparison to larger hydrophilic particles. However, these particles must overcome enxymatic and mucociliary clearance functions to be able to cross the BBB and enter the brain (Dhuria, Hanson et al. 2010, Kozlovskaya, Abou-Kaoud et al. 2014). These particles must also undergo hepatic and renal metabolism, thus increasing the potential for particle exposure and toxicity of other organs in the systemic uptake of particles (Dhuria, Hanson et al. 2010). An additional systemic pathway that has been less well studied is the venous blood-carotid artery blood supply pathway which eventually reaches the brain by a counter-current mechanism (Dhuria, Hanson et al. 2010). Particles in the blood can also enter the brain through the choroid plexus through passage to the CSF and diffusion into the brain parenchyma (Pardridge 2011, Bourganis, Kammona et al. 2018).

ENM movement to the brain via the olfactory pathway following- inhalation

Following deposition in the nasal cavity, ENMs can translocate to the brain with their presence signaled by activation and visualization within the parenchyma of the

CNS. Studies have shown the presence of AgNP in the OBs following inhalation (Ji et al. 2007; Sung et al. 2009). These studies demonstrated a dose-dependent increase in Ag content in the brain following inhalation of Ag nanoparticles. Genter et al. (2012) visualized Ag in the OBs and in the lateral ventricles using autometallography (Genter, Newman et al. 2012). Patchin et al. (2016) found Ag in the OBs along with the observation that the size of inhaled AgNP influenced the speed at which Ag translocates to the OB. 20nm AgNP rapidly translocated (following 1 day post-inhalation) to the OB, but the concentration of these particles rapidly decreased over time (7 to 21 days post-inhalation). In contrast, inhalation of 110nm AgNP resulted in slow, but progressive translocation of Ag to the OB over a post-inhalation period covering 56 days (Patchin, Anderson et al. 2016). Inhalation of MnNP has also been shown to lead to a significant increase in Mn concentration in the OB (Elder, Gelein et al. 2006). This novel study found when one naris was occluded, Mn concentration primarily increased in the OB of the ipsilateral side, suggesting nanoparticles entered the OB via inhalation and deposition on olfactory epithelium rather than by way of systemic routes such as the hematogenous transfer through the blood-brain barrier. Iron has also been demonstrated in the brain following intranasal instillation of Fe_2O_3 (. Wang et al. (2007). Fe was found in the OBs and brainstem, with noticeable preference of transfer through the olfactory and trigeminal nerves (Wang, Feng et al. 2007). These researchers also found Fe in the hippocampus, midbrain and cortex, suggesting widespread distribution of Fe in the brain following inhalation and uptake. Inhalation of PbNP was associated with accumulation of Pb in the hippocampus as well as localization in the brain endothelial cells, pericytes, and axons (Dumková, Smutná et al. 2017, Lebedová,

Nováková et al. 2018, Bláhová, Nováková et al. 2020). Following inhalation of PbNP, FeNP, and TiNP the hippocampus and striatum neurons demonstrated significant and sustained morphologic changes characterized by cellular swelling, vacuolization, and chromatin condensation and fragmentation (Wang, Chen et al. 2008, Wang, Wang et al. 2011, Dumková, Smutná et al. 2017, Lebedová, Nováková et al. 2018). In the hippocampus, pyramidal cells lost their pattern of regular and close arrangement as well as enlargement and elongation with neuronal tracts becoming more sparse (Wang, Chen et al. 2008, Dumková, Smutná et al. 2017). The presence of nanoparticles has been observed throughout the central nervous system following nasal inhalation as well as intranasal instillation, demonstrating a clear connection between the nasal cavity and the brain.

ENM-mediated neuroresponse and neurotoxicity

Following translocation to the CNS, ENMs are thought to mediate their effects via interaction with microglia and neurons. ENMs are recognized by microglia by binding to microglial surface receptors or through ENM engulfment by microglia. ENMs can act as a potent stimulus and are recognized by toll-like receptors 2 (TLR-2) and TLR-4 to induce activation of NF-kB, a transcriptional factor that directs transcription of various proinflammatory cytokines (Hutter, Boridy et al. 2010, Ze, Sheng et al. 2014). ENMs can also be taken up into microglia via phagocytosis, pinocytosis, and clathrin-mediated endocytosis (Luther, Petters et al. 2013, Ye, Raghnaill et al. 2013). ENMs can be translocated to intracellular lysosomes through the endo-lysosome pathway to activate the NLRP3 inflammasome to modulate the release of proinflammatory cytokines such

as IL-1β (Sun, Wang et al. 2013). An in vitro study by Wang et al. (2011) demonstrated following exposure to Fe_2O_3, microglia engulfment of NPs show an increase in cellular vesicles and lysosomes with subsequent swelling of endoplasmic reticulum (Wang, Wang et al. 2011). These findings suggest microglia increase their protein production following the uptake of NPs.

Microglia also proliferate and change phenotype to an activated state in response to the presence of ENM in the CNS. Microglial activation was noted following nose-only inhalation of quantum dots and AgNP (Hopkins, Patchin et al. 2014, Patchin, Anderson et al. 2016) . Intranasal instillation of FeNP induced microglial proliferation as well as microglial activation in the OBs (Wang, Wang et al. 2011). Ze et al (2014) found TiNP intranasal administration also caused proliferation of microglial cells (Ze, Sheng et al. 2014).

Microglia release proinflammatory cytokines to exert neurotoxic effects on the CNS. IL-1β and TNF-α were found to be elevated following intranasal instillation of ultrafine carbon black and intranasal instillation of TiNP (Yamamoto, Ahmed et al. 2006). An increase in cell surface proteins such as TLR, allows ENM to bind to microglia to further propagate the proinflammatory response. A similar proinflammatory response, was also noted following intranasal administration of AuNP and TiNP (Hutter, Boridy et al. 2010, Ze, Sheng et al. 2014). Elevation in the chemokines CCL2, CCL3, and CXCL9 was also noted following exposure to ultrafine carbon black, which act as a signal to attract additional microglia to the site of inflammation (Yamamoto, Ahmed et al. 2006).

Mechanism of microglial-mediated neuroresponse – Oxidative stress

Reactive oxygen species (ROS) is a byproduct of normal cellular metabolism. Its formation in health is slow and steady, which allow cellular antioxidant defense mechanisms to scavenge the ROS and prevent it from causing cell damage and death. However, oxidative stress can result in excess ROS that surpasses the cell's endogenous antioxidant capacity. The brain, in particular, is sensitive to oxidative stress since it requires abundant amounts of oxygen and contains many polysaturated fatty acids upon which free radicals can interact. The brain also exhibits lower levels of antioxidants compared to other organ systems (Clausen, Doctrow et al. 2010).

One of the products of oxidative stress is 8-hydroxy-2'-deoxyguanosine (8-OHdG). This is an oxidized nucleoside and acts as a marker for oxidative damage to DNA and RNA. Ze et al. (2013) found increased levels of 8-OHdG following 90 consecutive days of intranasal instillation of TiNP (Ze, Zheng et al. 2013).

One potential mechanism oxidative stress can mediate neurotoxicity is through lipid peroxidation. As mentioned earlier, the brain contains a large amount of lipids that readily interact with free radicals. Free radicals can selectively interact with lipids in the cell membrane, directly attack membrane proteins, and also induce crosslinking of lipid to protein or protein to protein (Sultana, Perluigi et al. 2013). Lipid peroxidation leads to altered membrane integrity and permeability and has been implicated in neurodegeneration disorders such as Alzheimer's disease and Parkinson's disease (Shichiri 2014). Malondialdehyde (MDA) and ThioBarbituric Acid Reactive Species

(TBARS) are end-products of lipid peroxidation and can act as markers of lipid peroxidation. Elevation in MDA and TBARS in the brain has been found following inhalation of Ag and Pb (Lebedová, Nováková et al. 2018, Bláhová, Nováková et al. 2020). Intranasal instillation of TiO_2 leads to lipid peroxidation and increases in MDA in a dose-dependent manner. Wang et al. (2008) and Ze et al. (2013) found intranasal instillation of Ti led to lipid peroxidation and an increase in MDA in a dose-dependent manner (Wang, Chen et al. 2008, Ze, Zheng et al. 2013). Wu et al. (2011) found following intranasal instillation of SiO_2 an elevation in H_2O_2 and MDA along with a significant decrease in GSH activity (Wu, Wang et al. 2011) . H_2O_2 can activate the transcriptional factor NF-κB, which in turn can enhance an proinflammatory response. The elevation in MDA as well as a decrease in GSH is suggestive of a significant oxidative stress that has overwhelmed the cell's ability to respond.

Another surrogate marker of oxidative stress in the brain is the glial fibrillary acidic protein (GFAP). GFAP is an intermediate filament protein in the cytoskeleton of astroglia and has been identified as a specific biomarker for the activation of astrocytes (Lumpkins, Bochicchio et al. 2008). Reactive astrocytosis provides many support functions in the CNS, including glutathione production to protect against ROS damage, resistance in the spread of inflammation as well as stabilization of extracellular fluid and ion balance. However, activation of astrocytes can also lead to neurodegenerative processes such as scar formation and loss of normal neural function (Kim, Park et al. 2019). GFAP upregulation has been found in the CA4 region of the hippocampus following inhalation of TiNP in a dose-dependent manner (Wang, Chen et al. 2008). An additional study found an increase in GFAP just 1 week after intranasal instillation of

CuNP (Liu, Gao et al. 2014). Inhaled MnNP is also associated with increased GFAP expression along with the upregulation of inflammatory cytokines such as TNF-α and macrophage inflammatory protein-2 (Elder, Gelein et al. 2006).

Heme oxygenase-1 (HO-1) is produced in response to oxidative stress. HO-1 activation in neurons confer protective effects against oxidative damage and cell death, but its upregulation has also been implicated in neurodegenerative disorders such as Alzheimer's Disease (Schipper 2007, Hung, Liou et al. 2008). Expression of HO-1 gene as well as HO-1 protein has been found to be elevated in the hippocampus of AgNP-treated mice (Davenport, Hsieh et al. 2015).

ENM mediated Pulmonary toxicity

When inhaled ENMs is deposited in the distal airways, aggregated ENMs are taken up by alveolar macrophages. These cells which phagocytose ENMs are cleared from airway through a variety of routes including the mucociliary escalator or lymphatic drainage (Thompson, Sayers et al. 2014). However, ENMs can cause frustrated phagocytosis releasing ROS and OS causing cell death (Murphy, Schinwald et al. 2012). When the lung is exposed to excessive ENMs, the clearance capacity of macrophages can be impaired, to increase inflammation and damage to lung cells (Morrow 1988, Donaldson and Tran 2002). Therefore, retention of ENMs in the lungs might cause toxic effects due to particle tissue overload and particle-cell interaction (Rothen-Rutishauser, Blank et al. 2008).

ENMs have been found to cause inflammatory responses in the lung tissue. Carbon nanotubes (CNT) activate the inflammasome in alveolar macrophages leading to the secretion of IL-1β and IL-18. These proinflammatory cytokines cause lysosomal disruption and ROS production (Palomaki, Valimaki et al. 2011, Meunier, Coste et al. 2012, Sun, Wang et al. 2013). In a study by Lam et al (2004), instillation of carbon black or quartz particles in comparion to single-walled CNT in the lungs of mice demonstrated a greater development of interstitial inflammation and epithelioid granuloma after 7 and 90 days of exposure (Lam, James et al. 2004). Similarly, exposure to titanium dioxide (TiO$_2$) ENM caused pulmonary neutrophilia, increased lymphocytes and eosinophilia (Goncalves, Chiasson et al. 2010, Larsen, Roursgaard et al. 2010, Rossi, Pylkkänen et al. 2010). There was increased production of CXCL-1, TNF-α and IL-8 (Goncalves, Chiasson et al. 2010, Rossi, Pylkkänen et al. 2010). Inhalation of 10mg/m^3 zinc oxide (ZnO) ENMs for 4 weeks in rats caused transient increase in total cells and neutrophils without persistent inflammation (Morimoto, Izumi et al. 2016). In another study, intratracheal instillation of ZnO (200,400, 800 µg/kg) caused an increase in total cells and protein levels after 7 days post-exposure (Wang, Li et al. 2017). Eosinophilia, proliferation of airway epithelial cells and goblet cell hyperplasia was observed after 24 hours, while pulmonary interstitial fibrosis was observed 4 weeks after intratracheal instillation of ZnO in rats (Cho, Duffin et al. 2011). Inflammatory markers, IL-12, MIP-1a, CINC-1,-2, and HO-1 were in increased in BALF after exposure to ZnO ENMs (Adamcakova-Dodd, Stebounova et al. 2014, Morimoto, Izumi et al. 2016). Decreased lung function and enhanced inflammation were observed in mice and rats exposed to Ag ENMs by inhalation (Sung, Ji et al. 2008, Stebounova, Adamcakova-Dodd et al.

2011, Braakhuis, Gosens et al. 2014, Seiffert, Buckley et al. 2016, Silva, Anderson et al. 2016). Short-term inhalation exposure to Ag ENMs was associated with size-dependent pulmonary toxicity. Exposure to 15nm Ag ENM in rats resulted in significantly increased neutrophilia, lactate dehydrogenase, MCP-1, IL-1β and total glutathione level in comparison to animals exposed to 410 nm Ag ENM (Braakhuis, Gosens et al. 2014). In a study by Sung et al. (2008), tidal volume and minute volume decreased in rats exposed to Ag ENM for 90 days. In this same study, total cells, macrophages, lymphocytes, polymorphonuclear cells, albumin and LDH were significantly increased (Sung, Ji et al. 2008). Pulmonary toxicity depends upon size, dose and surface modifications of ENMs (Anderson, Silva et al. 2015, Silva, Anderson et al. 2015, Alessandrini, Vennemann et al. 2017). Exposure to Ag ENM can cause size-dependent delayed peak and short-term pulmonary inflammation and cytotoxicity (Silva, Anderson et al. 2016).

Mechanism of pulmonary toxicity – Oxidative Stress

The primary mechanisms of ENM-induced pulmonary toxicity are ROS generation and oxidative stress (Nel, Xia et al. 2006, Li, Xia et al. 2008, Ferreira, Cemlyn-Jones et al. 2013). With ENM exposure, excess ROS production occurs in the lungs to overburden the natural antioxidant defenses by depletion of glutathione (GSH) and accumulation of oxidized glutathione (GSSG). Oxidative stress due to decreased GSH/GSSG ratio causes cell injury (Nel, Xia et al. 2006).

ENMs produce ROS by various mechanisms (Nel, Xia et al. 2006, Li, Xia et al. 2008, Madl, Plummer et al. 2014). First is the generation of superoxide ions and hydroxyl ions by electron hole pairs during electron donor or capture interactions. Electron hole pairs in ENMs surface are formed by UV activation (Li, Xia et al. 2008). Second, excited energy property of semiconductor ENMs lead to jumping of electrons from conduction band to oxygen releasing superoxide ions. Third, metal ions generated from the dissolution of ENMs catalyze ROS generation. Fourth mechanism is the generation of superoxide ions by transition metals on the surface of ENMs via the Fenton reaction (Li, Xia et al. 2008). These intrinsic properties of ENMs contribute to the production of ROS as well as ENM-tissue or ENM-cell interaction cause further ROS generation (Nel, Xia et al. 2006).

Excessive production of ROS leads to activation of the cytokine cascade and intracellular signaling targets including receptor tyrosine kinases, mitogen activated protein kinases and transcription factors to trigger the transcription and expression of genes responsible for inflammation and fibrosis (Bonner 2007). IL-1β also promotes the formation of immature collagenous tissue in the lung by expressing platelet-derived growth factor (PDGF)-AA and PDGF receptor-α to increase the production of myofibroblasts. TNF-α also increases the production of transforming growth factor (TGF)-β enhancing collagen deposition by myofibroblasts (Li, Xia et al. 2008).

Conclusion

ENMs continue to have broad applications in society today. Large scale industrial production and commercialization of ENMs based products continues to grow rapidly grow with increased demand for consumer products containing ENMs such as cosmetics, electronics, personal care and medicine. Such diverse applications lead to an inevitable increase for human exposure. There are sufficient experimental and occupational studies to elevate safety concerns for exposure to ENMs. As the concentration of airborne ENMs is higher in the industrial setting, workers who manufacture and package ENMs based products are at increased risk of exposure. Therefore, it is paramount to understand the route of exposure, the fate of ENMs entering the body and potential acute and chronic effects caused such exposure.

In this literature review chapter, we have provided an in-depth foundation for the route of exposure, deposition patterns and clearance mechanisms for ENMs in upper and lower respiratory tract. Although there are in vivo and in vitro toxicity studies, there continues to be a knowledge gap for those mechanisms involved in the acute effects of ENM exposure. Only a limited number of studies have focused on upper respiratory tract and nose to brain translocation of ENMs. As ENMs can bypass blood brain barrier via olfactory pathway, this may represent a major route for therapeutics to reach the brain. However, additional studies are needed to understand the nose to brain pathway and toxic effects of ENMs in the brain. Small differences in the characteristics of ENMs can cause major changes in the biological effects. So, more studies need to focus on proper characterization of ENMs. Despite the extensive and advanced use of ENMs, further understanding the factors and mechanisms influencing ENMs toxicity will bridge

the knowledge gap of ENMs and help in creating safe nanoparticle exposure and application in humans.

The goal of the research presented in this dissertation is to narrow the knowledge gap regarding toxic effects exerted by ENMs, to create a safe environment for workers and consumers. Metal oxides (zinc oxide and silver silicate) and carbon based ENM (graphene oxide) are chosen based on their excessive use in consumer products. This study will help us to better understand the health implications of inhaling ENMs by assessing pulmonary toxicities, translocation from the nasal cavity to the OB, and subsequent activation of microglial cells, resident macrophages of the Central Nervous System (CNS), following acute nose-only inhalation exposures.
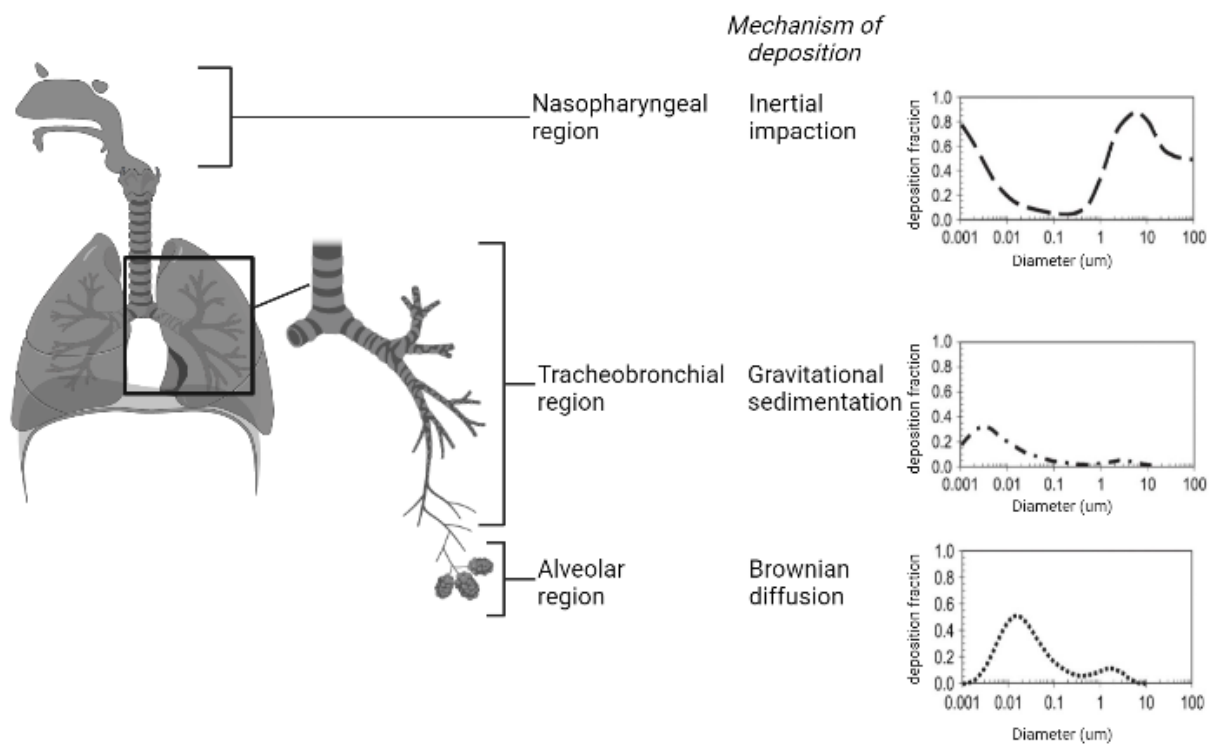
Figure 1. Mechanism of deposition in different region of respiratory tract. Particle deposition probability is adapted from *Madl et al. 2009.*

References

1. Adamcakova-Dodd, A., L. V. Stebounova, J. S. Kim, S. U. Vorrink, A. P. Ault, P. T O'Shaughnessy, V. H. Grassian and P. S. Thorne (2014). "Toxicity assessment of zinc oxide nanoparticles using sub-acute and sub-chronic murine inhalation models." Particle and fibre toxicology **11**(1): 1-15.

2. Alessandrini, F., A. Vennemann, S. Gschwendtner, A. U. Neumann, M. Rothballer, T. Seher, M. Wimmer, S. Kublik, C. Traidl-Hoffmann and M. Schloter (2017). "Pro-inflammatory versus immunomodulatory effects of silver nanoparticles in the lung: the critical role of dose, size and surface modification." Nanomaterials **7**(10): 300.

3. Anderson, D. S., R. M. Silva, D. Lee, P. C. Edwards, A. Sharmah, T. Guo, K. E. Pinkerton and L. S. Van Winkle (2015). "Persistence of silver nanoparticles in the rat lung: Influence of dose, size, and chemical composition." Nanotoxicology **9**(5): 591-602.

4. Athira, S. S., N. Prajitha and P. V. Mohanan (2018). "Interaction of nanoparticles with central nervous system and its consequences." American Journal of Research in Medical Sciences **4**(1): 12-32.

5. Bakand, S., A. Hayes and F. Dechsakulthorn (2012). "Nanoparticles: a review of particle toxicology following inhalation exposure." Inhalation toxicology **24**(2): 125-135.

6. Bierkandt, F. S., L. Leibrock, S. Wagener, P. Laux and A. Luch (2018). "The impact of nanomaterial characteristics on inhalation toxicity." Toxicology research **7**(3): 321-346.

7. Bláhová, L., Z. Nováková, Z. Večeřa, L. Vrlíková, B. Dočekal, J. Dumková, K. Křůmal, P. Mikuška, M. Buchtová and A. Hampl (2020). "The effects of nano-sized PbO on

biomarkers of membrane disruption and DNA damage in a sub-chronic inhalation study on mice." Nanotoxicology **14**(2): 214-231.

8. Bonner, J. C. (2007). "Lung fibrotic responses to particle exposure." Toxicologic pathology **35**(1): 148-153.

9. Bourganis, V., O. Kammona, A. Alexopoulos and C. Kiparissides (2018). "Recent advances in carrier mediated nose-to-brain delivery of pharmaceutics." European Journal of Pharmaceutics and Biopharmaceutics **128**: 337-362.

10. Braakhuis, H. M., I. Gosens, P. Krystek, J. A. Boere, F. R. Cassee, P. H. Fokkens, J. A. Post, H. Van Loveren and M. V. Park (2014). "Particle size dependent deposition and pulmonary inflammation after short-term inhalation of silver nanoparticles." Particle and fibre toxicology **11**(1): 1-16.

11. Brai, E. and L. Alberi (2018). "Olfaction, among the first senses to develop and decline." Sensory Nervous System: 65.

12. Chen, X.-Q., J. R. Fawcett, Y.-E. Rahman, T. A. Ala and W. H. Frey II (1998). "Delivery of nerve growth factor to the brain via the olfactory pathway." Journal of Alzheimer's Disease **1**(1): 35-44.

13. Cho, W.-S., R. Duffin, S. E. Howie, C. J. Scotton, W. A. Wallace, W. MacNee, M. Bradley, I. L. Megson and K. Donaldson (2011). "Progressive severe lung injury by zinc oxide nanoparticles; the role of Zn2+ dissolution inside lysosomes." Particle and fibre toxicology **8**(1): 1-16.

14. Clausen, A., S. Doctrow and M. Baudry (2010). "Prevention of cognitive deficits and brain oxidative stress with superoxide dismutase/catalase mimetics in aged mice." Neurobiology of aging **31**(3): 425-433.

15. Cohen, M. D., J. T. Zelikoff and R. B. Schlesinger (2000). Pulmonary immunotoxicology, Springer Science & Business Media.

16. Crowe, T. P., M. H. W. Greenlee, A. G. Kanthasamy and W. H. Hsu (2018). "Mechanism of intranasal drug delivery directly to the brain." Life sciences **195**: 44-52.

17. Darquenne, C. (2020). "Deposition mechanisms." Journal of aerosol medicine and pulmonary drug delivery **33**(4): 181-185.

18. Davenport, L. L., H. Hsieh, B. L. Eppert, V. S. Carreira, M. Krishan, T. Ingle, P. C. Howard, M. T. Williams, C. V. Vorhees and M. B. Genter (2015). "Systemic and behavioral effects of intranasal administration of silver nanoparticles." Neurotoxicology and teratology **51**: 68-76.

19. Dhuria, S. V., L. R. Hanson and W. H. Frey II (2010). "Intranasal delivery to the central nervous system: mechanisms and experimental considerations." Journal of pharmaceutical sciences **99**(4): 1654-1673.

20. Donaldson, K. and C. L. Tran (2002). "Inflammation caused by particles and fibers." Inhalation toxicology **14**(1): 5-27.

21. Dumková, J., T. Smutná, L. Vrlíková, P. Le Coustumer, Z. Večeřa, B. Dočekal, P. Mikuška, L. Čapka, P. Fictum and A. Hampl (2017). "Sub-chronic inhalation of lead oxide nanoparticles revealed their broad distribution and tissue-specific subcellular localization in target organs." Particle and fibre toxicology **14**(1): 1-19.

22. Elder, A., R. Gelein, V. Silva, T. Feikert, L. Opanashuk, J. Carter, R. Potter, A. Maynard, Y. Ito and J. Finkelstein (2006). "Translocation of inhaled ultrafine manganese oxide particles to the central nervous system." Environmental health perspectives **114**(8): 1172-1178.

23. Ferin, J. and G. Oberdörster (1992). "Translocation of particles from pulmonary alveoli into the interstitium." Journal of Aerosol Medicine **5**(3): 179-187.

24. Ferin, J., G. Oberdorster and D. Penney (1992). "Pulmonary retention of ultrafine and fine particles in rats." Am J Respir Cell Mol Biol **6**(5): 535-542.

25. FERIN, J., G. OBERDÖRSTER, S. C. SODERHOLM and R. GELEIN (1991). "Pulmonary tissue access of ultrafine particles." Journal of aerosol medicine **4**(1): 57-68.

26. Ferreira, A., J. Cemlyn-Jones and C. R. Cordeiro (2013). "Nanoparticles, nanotechnology and pulmonary nanotoxicology." Revista Portuguesa de Pneumologia (English Edition) **19**(1): 28-37.

27. Field, P., Y. Li and G. Raisman (2003). "Ensheathment of the olfactory nerves in the adult rat." Journal of neurocytology **32**(3): 317-324.

28. Fischer, H. C. and W. C. Chan (2007). "Nanotoxicity: the growing need for in vivo study." Current opinion in biotechnology **18**(6): 565-571.

29. Genter, M. B., N. C. Newman, H. G. Shertzer, S. F. Ali and B. Bolon (2012). "Distribution and systemic effects of intranasally administered 25 nm silver nanoparticles in adult mice." Toxicologic pathology **40**(7): 1004-1013.

30. Geurkink, N. (1983). "Nasal anatomy, physiology, and function." Journal of allergy and clinical immunology **72**(2): 123-128.

31. Ghadiri, M., P. M. Young and D. Traini (2019). "Strategies to enhance drug absorption via nasal and pulmonary routes." Pharmaceutics **11**(3): 113.

32. Gizurarson, S. (2012). "Anatomical and histological factors affecting intranasal drug and vaccine delivery." Current drug delivery **9**(6): 566-582.

33. Goncalves, D., S. Chiasson and D. Girard (2010). "Activation of human neutrophils by titanium dioxide (TiO2) nanoparticles." Toxicology in Vitro **24**(3): 1002-1008.

34. Gray, H. (2009). Gray's anatomy, Arcturus Publishing.

35. Gross, E. A., J. A. Swenberg, S. Fields and J. Popp (1982). "Comparative morphometry of the nasal cavity in rats and mice." Journal of anatomy **135**(Pt 1): 83.

36. Harkema, J. R. (2015). Comparative anatomy and epithelial cell biology of the nose. Comparative biology of the normal lung, Elsevier**:** 7-19.

37. Harkema, J. R., S. A. Carey and J. G. Wagner (2006). "The nose revisited: a brief review of the comparative structure, function, and toxicologic pathology of the nasal epithelium." Toxicologic pathology **34**(3): 252-269.

38. Hopkins, L. E., E. S. Patchin, P.-L. Chiu, C. Brandenberger, S. Smiley-Jewell and K. E. Pinkerton (2014). "Nose-to-brain transport of aerosolised quantum dots following acute exposure." Nanotoxicology **8**(8): 885-893.

39. Hugill, K. (2015). "The senses of touch and olfaction in early mother–infant interaction." Journal of Health Visiting **3**(12): 654-658.

40. Hung, S.-Y., H.-C. Liou, K.-H. Kang, R.-M. Wu, C.-C. Wen and W.-M. Fu (2008). "Overexpression of heme oxygenase-1 protects dopaminergic neurons against 1-methyl-4-phenylpyridinium-induced neurotoxicity." Molecular pharmacology **74**(6): 1564-1575.

41. Hutter, E., S. Boridy, S. Labrecque, M. Lalancette-Hébert, J. Kriz, F. M. Winnik and D. Maysinger (2010). "Microglial response to gold nanoparticles." ACS nano **4**(5): 2595-2606.

42. Illum, L. (2000). "Transport of drugs from the nasal cavity to the central nervous system." European journal of pharmaceutical sciences **11**(1): 1-18.

43. Kim, Y., J. Park and Y. K. Choi (2019). "The role of astrocytes in the central nervous system focused on BK channel and heme oxygenase metabolites: A review." Antioxidants **8**(5): 121.

44. Kozlovskaya, L., M. Abou-Kaoud and D. Stepensky (2014). "Quantitative analysis of drug delivery to the brain via nasal route." Journal of controlled release **189**: 133-140.

45. Kreyling, W. G., M. Semmler-Behnke and W. Möller (2006). "Health implications of nanoparticles." Journal of Nanoparticle Research **8**(5): 543-562.

46. Kreyling, W. G., M. Semmler and W. Möller (2004). "Dosimetry and toxicology of ultrafine particles." Journal of Aerosol Medicine **17**(2): 140-152.

47. Kuhlbusch, T. A., C. Asbach, H. Fissan, D. Göhler and M. Stintz (2011). "Nanoparticle exposure at nanotechnology workplaces: a review." Particle and fibre toxicology **8**(1): 1-18.

48. Lam, C.-W., J. T. James, R. McCluskey and R. L. Hunter (2004). "Pulmonary toxicity of single-wall carbon nanotubes in mice 7 and 90 days after intratracheal instillation." Toxicological sciences **77**(1): 126-134.

49. Larsen, S. T., M. Roursgaard, K. A. Jensen and G. D. Nielsen (2010). "Nano titanium dioxide particles promote allergic sensitization and lung inflammation in mice." Basic & clinical pharmacology & toxicology **106**(2): 114-117.

50. Lebedová, J., Z. Nováková, Z. Večeřa, M. Buchtová, J. Dumková, B. Dočekal, L. Bláhová, P. Mikuška, I. Míšek and A. Hampl (2018). "Impact of acute and subchronic inhalation exposure to PbO nanoparticles on mice." Nanotoxicology **12**(4): 290-304.

51. Li, N., T. Xia and A. E. Nel (2008). "The role of oxidative stress in ambient particulate matter-induced lung diseases and its implications in the toxicity of engineered nanoparticles." Free radical biology and medicine **44**(9): 1689-1699.

52. Liu, Y., Y. Gao, Y. Liu, B. Li, C. Chen and G. Wu (2014). "Oxidative stress and acute changes in murine brain tissues after nasal instillation of copper particles with different sizes." Journal of nanoscience and nanotechnology **14**(6): 4534-4540.

53. Lorenz, C., H. Hagendorfer, N. von Goetz, R. Kaegi, R. Gehrig, A. Ulrich, M. Scheringer and K. Hungerbühler (2011). "Nanosized aerosols from consumer sprays: experimental analysis and exposure modeling for four commercial products." Journal of nanoparticle Research **13**(8): 3377-3391.

54. Lumpkins, K. M., G. V. Bochicchio, K. Keledjian, J. M. Simard, M. McCunn and T. Scalea (2008). "Glial fibrillary acidic protein is highly correlated with brain injury." Journal of Trauma and Acute Care Surgery **65**(4): 778-784.

55. Luther, E. M., C. Petters, F. Bulcke, A. Kaltz, K. Thiel, U. Bickmeyer and R. Dringen (2013). "Endocytotic uptake of iron oxide nanoparticles by cultured brain microglial cells." Acta biomaterialia **9**(9): 8454-8465.

56. Madl, A. K. and K. E. Pinkerton (2009). "Health effects of inhaled engineered and incidental nanoparticles." Critical reviews in toxicology **39**(8): 629-658.

57. Madl, A. K., L. E. Plummer, C. Carosino and K. E. Pinkerton (2014). "Nanoparticles, lung injury, and the role of oxidant stress." Annual review of physiology **76**: 447-465.

58. Meunier, E., A. Coste, D. Olagnier, H. Authier, L. Lefèvre, C. Dardenne, J. Bernad, M. Béraud, E. Flahaut and B. Pipy (2012). "Double-walled carbon nanotubes trigger IL-1β release in human monocytes through Nlrp3 inflammasome activation." Nanomedicine: Nanotechnology, Biology and Medicine **8**(6): 987-995.

59. Miller, S. S. and N. E. Spear (2009). "Olfactory learning in the rat immediately after birth: unique salience of first odors." Developmental psychobiology **51**(6): 488-504.

60. Mistry, A., S. Stolnik and L. Illum (2009). "Nanoparticles for direct nose-to-brain delivery of drugs." International journal of pharmaceutics **379**(1): 146-157.

61. Mistry, A., S. Stolnik and L. Illum (2015). "Nose-to-brain delivery: investigation of the transport of nanoparticles with different surface characteristics and sizes in excised porcine olfactory epithelium." Molecular pharmaceutics **12**(8): 2755-2766.

62. Morimoto, Y., H. Izumi, Y. Yoshiura, T. Tomonaga, T. Oyabu, T. Myojo, K. Kawai, K. Yatera, M. Shimada and M. Kubo (2016). "Evaluation of pulmonary toxicity of zinc oxide nanoparticles following inhalation and intratracheal instillation." International journal of molecular sciences **17**(8): 1241.

63. Morrow, P. (1988). "Possible mechanisms to explain dust overloading of the lungs." Toxicological Sciences **10**(3): 369-384.

64. Murphy, F. A., A. Schinwald, C. A. Poland and K. Donaldson (2012). "The mechanism of pleural inflammation by long carbon nanotubes: interaction of long fibres with macrophages stimulates them to amplify pro-inflammatory responses in mesothelial cells." Particle and fibre toxicology **9**(1): 1-15.

65. Nel, A., T. Xia, L. Madler and N. Li (2006). "Toxic potential of materials at the nanolevel." science **311**(5761): 622-627.

66. Oberbek, P., P. Kozikowski, K. Czarnecka, P. Sobiech, S. Jakubiak and T. Jankowski (2019). "Inhalation exposure to various nanoparticles in work environment—contextual information and results of measurements." Journal of Nanoparticle Research **21**(11): 1-24.

67. Oberdörster, G., J. Ferin and B. E. Lehnert (1994). "Correlation between particle size, in vivo particle persistence, and lung injury." Environmental health perspectives **102**(suppl 5): 173-179.

68. Oberdörster, G., E. Oberdörster and J. Oberdörster (2005). "Nanotoxicology: an emerging discipline evolving from studies of ultrafine particles." Environmental health perspectives **113**(7): 823-839.

69. Palomaki, J., E. Valimaki, J. Sund, M. Vippola, P. A. Clausen, K. A. Jensen, K. Savolainen, S. Matikainen and H. Alenius (2011). "Long, needle-like carbon nanotubes and asbestos activate the NLRP3 inflammasome through a similar mechanism." ACS nano **5**(9): 6861-6870.

70. Pardeshi, C. V. and V. S. Belgamwar (2013). "Direct nose to brain drug delivery via integrated nerve pathways bypassing the blood–brain barrier: an excellent platform for brain targeting." Expert opinion on drug delivery **10**(7): 957-972.

71. Pardridge, W. M. (2011). "Drug transport in brain via the cerebrospinal fluid." Fluids and Barriers of the CNS **8**(1): 7.

72. Patchin, E. S., D. S. Anderson, R. M. Silva, D. L. Uyeminami, G. M. Scott, T. Guo, L. S. Van Winkle and K. E. Pinkerton (2016). "Size-dependent deposition, translocation, and microglial activation of inhaled silver nanoparticles in the rodent nose and brain." Environmental health perspectives **124**(12): 1870-1875.

73. Rossi, E. M., L. Pylkkänen, A. J. Koivisto, M. Vippola, K. A. Jensen, M. Miettinen, K. Sirola, H. Nykäsenoja, P. Karisola and T. Stjernvall (2010). "Airway exposure to silica-coated TiO2 nanoparticles induces pulmonary neutrophilia in mice." Toxicological Sciences **113**(2): 422-433.

74. Rothen-Rutishauser, B., F. Blank, C. Mühlfeld and P. Gehr (2008). "In vitro models of the human epithelial airway barrier to study the toxic potential of particulate matter." Expert opinion on drug metabolism & toxicology **4**(8): 1075-1089.

75. Sahin-Yilmaz, A. and R. M. Naclerio (2011). "Anatomy and physiology of the upper airway." Proceedings of the American Thoracic Society **8**(1): 31-39.

76. Sarafoleanu, C., C. Mella, M. Georgescu and C. Perederco (2009). "The importance of the olfactory sense in the human behavior and evolution." Journal of medicine and life **2**(2): 196.

77. Schipper, H. M. (2007). "Biomarker potential of heme oxygenase-1 in Alzheimer's disease and mild cognitive impairment."

78. Seiffert, J., A. Buckley, B. Leo, N. G. Martin, J. Zhu, R. Dai, F. Hussain, C. Guo, J. Warren and A. Hodgson (2016). "Pulmonary effects of inhalation of spark-generated silver nanoparticles in Brown-Norway and Sprague–Dawley rats." Respiratory research **17**(1): 1-15.

79. Selvaraj, K., K. Gowthamarajan and V. V. S. R. Karri (2018). "Nose to brain transport pathways an overview: Potential of nanostructured lipid carriers in nose to brain targeting." Artificial Cells, Nanomedicine, and Biotechnology **46**(8): 2088-2095.

80. Semmler-Behnke, M., S. Takenaka, S. Fertsch, A. Wenk, J. Seitz, P. Mayer, G. Oberdörster and W. G. Kreyling (2007). "Efficient elimination of inhaled nanoparticles from the alveolar region: evidence for interstitial uptake and subsequent reentrainment onto airways epithelium." Environmental health perspectives **115**(5): 728-733.

81. Shichiri, M. (2014). "The role of lipid peroxidation in neurological disorders." Journal of clinical biochemistry and nutrition: 14-10.

82. Silva, R. M., D. S. Anderson, L. M. Franzi, J. L. Peake, P. C. Edwards, L. S. Van Winkle and K. E. Pinkerton (2015). "Pulmonary effects of silver nanoparticle size, coating, and dose over time upon intratracheal instillation." Toxicological Sciences **144**(1): 151-162.

83. Silva, R. M., D. S. Anderson, J. Peake, P. C. Edwards, E. S. Patchin, T. Guo, T. Gordon, L. C. Chen, X. Sun, L. S. Van Winkle and K. E. Pinkerton (2016). "Aerosolized Silver Nanoparticles in the Rat Lung and Pulmonary Responses over Time." Toxicol Pathol **44**(5): 673-686.

84. Standard, A. (2012). "Standard Terminology Relating to Nanotechnology."

85. Stebounova, L. V., A. Adamcakova-Dodd, J. S. Kim, H. Park, P. T. O'Shaughnessy, V. H. Grassian and P. S. Thorne (2011). "Nanosilver induces minimal lung toxicity or inflammation in a subacute murine inhalation model." Particle and fibre toxicology **8**(1): 1-12.

86. Sultana, R., M. Perluigi and D. A. Butterfield (2013). "Lipid peroxidation triggers neurodegeneration: a redox proteomics view into the Alzheimer disease brain." Free Radical Biology and Medicine **62**: 157-169.

87. Sun, B., X. Wang, Z. Ji, R. Li and T. Xia (2013). "NLRP3 inflammasome activation induced by engineered nanomaterials." Small **9**(9-10): 1595-1607.

88. Sung, J. H., J. H. Ji, J. U. Yoon, D. S. Kim, M. Y. Song, J. Jeong, B. S. Han, J. H. Han, Y. H. Chung and J. Kim (2008). "Lung function changes in Sprague-Dawley rats after prolonged inhalation exposure to silver nanoparticles." Inhalation toxicology **20**(6): 567-574.

89. Thompson, E. A., B. C. Sayers, E. E. Glista-Baker, K. A. Shipkowski, A. J. Taylor and J. C. Bonner (2014). "Innate immune responses to nanoparticle exposure in the lung." Journal of environmental immunology and toxicology **1**(3): 150.

90. Thorne, R. G. and W. H. Frey (2001). "Delivery of neurotrophic factors to the central nervous system." Clinical pharmacokinetics **40**(12): 907-946.

91. Treloar, H. B., A. M. Miller, A. Ray and C. A. Greer (2010). "Development of the olfactory system." The neurobiology of olfaction **20092457**: 131-155.

92. Wang, B., W. Y. Feng, M. Wang, J. W. Shi, F. Zhang, H. Ouyang, Y. L. Zhao, Z. F. Chai, Y. Y. Huang and Y. N. Xie (2007). "Transport of intranasally instilled fine Fe 2 O 3 particles into

the brain: micro-distribution, chemical states, and histopathological observation." Biological trace element research **118**(3): 233-243.

93. Wang, D., H. Li, Z. Liu, J. Zhou and T. Zhang (2017). "Acute toxicological effects of zinc oxide nanoparticles in mice after intratracheal instillation." International journal of occupational and environmental health **23**(1): 11-19.

94. Wang, J., C. Chen, Y. Liu, F. Jiao, W. Li, F. Lao, Y. Li, B. Li, C. Ge and G. Zhou (2008). "Potential neurological lesion after nasal instillation of TiO2 nanoparticles in the anatase and rutile crystal phases." Toxicology Letters **183**(1-3): 72-80.

95. Wang, Y., B. Wang, M.-T. Zhu, M. Li, H.-J. Wang, M. Wang, H. Ouyang, Z.-F. Chai, W.-Y. Feng and Y.-L. Zhao (2011). "Microglial activation, recruitment and phagocytosis as linked phenomena in ferric oxide nanoparticle exposure." Toxicology letters **205**(1): 26-37.

96. Watelet, J.-B. and P. V. Cauwenberge (1999). "Applied anatomy and physiology of the nose and paranasal sinuses." Allergy **54**: 14-25.

97. Witschi, H. R., K. E. Pinkerton, L. S. Van Winkle and J. A. Last (2008). "Toxic responses of the respiratory system." Casarett & Doull's Toxicology. The Basic Science of Poisons. 5th ed. New York, NY: McGraw-Hill Health Professions Division: 609-630.

98. Wu, J., C. Wang, J. Sun and Y. Xue (2011). "Neurotoxicity of silica nanoparticles: brain localization and dopaminergic neurons damage pathways." ACS nano **5**(6): 4476-4489.

99. Wu, T. and M. Tang (2018). "Review of the effects of manufactured nanoparticles on mammalian target organs." Journal of Applied Toxicology **38**(1): 25-40.

100.   Yamamoto, S., S. Ahmed, M. Kakeyama, T. Kobayashi and H. Fujimaki (2006). "Brain cytokine and chemokine mRNA expression in mice induced by intranasal instillation with ultrafine carbon black." Toxicology letters **163**(2): 153-160.

101.   Yao, R., M. Murtaza, J. T. Velasquez, M. Todorovic, A. Rayfield, J. Ekberg, M. Barton and J. St John (2018). "Olfactory ensheathing cells for spinal cord injury: sniffing out the issues." Cell transplantation **27**(6): 879-889.

102.   Ye, D., M. N. Raghnaill, M. Bramini, E. Mahon, C. Åberg, A. Salvati and K. A. Dawson (2013). "Nanoparticle accumulation and transcytosis in brain endothelial cell layers." Nanoscale **5**(22): 11153-11165.

103.   Ze, Y., L. Sheng, X. Zhao, J. Hong, X. Ze, X. Yu, X. Pan, A. Lin, Y. Zhao and C. Zhang (2014). "TiO 2 nanoparticles induced hippocampal neuroinflammation in mice." PloS one **9**(3): e92230.

104.   Ze, Y., L. Zheng, X. Zhao, S. Gui, X. Sang, J. Su, N. Guan, L. Zhu, L. Sheng and R. Hu (2013). "Molecular mechanism of titanium dioxide nanoparticles-induced oxidative injury in the brain of mice." Chemosphere **92**(9): 1183-1189.

CHAPTER 2

Acute Pulmonary Toxicity in Rats following Inhalation of 1% Silver Silicate Nanomaterial

ABSTRACT

Silver nanoparticles (Ag NP) are used primarily as an anti-bacterial in numerous commercial applications in biomedical devices, antibacterial solutions, wound dressing, baby bottles, disinfectants, textiles, pesticides, and dietary supplements. Silver-silica composites prolong the antibacterial action of Ag NP. Increased use of silver silicate ($AgSiO_2$) NP has also increased the risk of inhalation and toxicity during manufacture and commercial use of $AgSiO_2$ NP products. The primary objective of this study is to determine if acute exposure by inhalation of $AgSiO_2$ NP induces inflammation in the lungs. 8-week-old male and female Sprague Dawley rats were randomly assigned to either $AgSiO_2$ NP inhalation (n=42) or sham control (n=30) groups. Rats were exposed to aerosolized 1% AgSiO2 NP (20 nm) for 6 hours. Animals were then examined on days 0, 1, 7, 21 and 56 post exposure (PE). Bronchoalveolar lavage (BAL) was collected from the right lung to assess protein concentration, cell number, viability, and cell differentials. The left lung was inflation-fixed, embedded and sectioned for histopathological analysis. Particle aerosol was characterized by gravimetric measurement, x-ray fluorescence, cascade impactor and transmission electron microscopy during the 6-hour inhalation exposure period. Animals exposed to 1% $AgSiO_2$ demonstrated a significant increase in total cells in BAL on days 0, 1 and 7 PE ($p<0.05$). Macrophages and neutrophils were significantly increased on days 0, 1 and 7 PE in animals exposed to 1% $AgSiO_2$. In a similar pattern, eosinophils demonstrated significant increases on days 0, 7 and 21 following 1% $AgSiO_2$ inhalation. Histopathological scoring showed significantly increased bronchiolar inflammation on day 0, 1 and 7, while perivascular inflammation was noted on days 0, 1, 7 and 21. Alveolar inflammation was noted only on days 0 and 1. Average $AgSiO_2$ aerosol mass

was 5.66+/- 2.87 mg/m^3. Ag concentration in the aerosol using XRF analysis was 5.6

+/- 2.0 mg/m^3. The mass median aerodynamic diameter of the aerosol was 1.87 +/-

0.26 µm. TEM demonstrated some agglomeration of AgSiO$_2$ nanoparticles following

aerosolization ranging from 21 to 370 nm in size. Following acute inhalation of 1%

AgSiO$_2$, rats developed an acute inflammation that possibly persists as long as 21 day

PE as indicated by significant increases in total cells, macrophages, neutrophils, and

eosinophils influx to the lungs. These findings strongly suggest 1% AgSiO$_2$ can induce

acute to subacute inflammation and are not completely harmless when inhaled.

INTRODUCTION

Silver nanoparticles (AgNPs), including silver silicate nanoparticles (Ag-SiO$_2$ NPs), are engineered metal nanomaterials with diverse commercial applications. AgNPs are the most common NP used in diverse products, representing 50% of all nanomaterial based consumer products (McINTYRE 2012, Inshakova and Inshakov 2017). Antibacterial and antimicrobial properties of Ag have further enhanced the use of AgNPs in industries including healthcare, electronics, beauty and textiles (Burdușel, Gherasim et al. 2018). AgNPs is commonly used in wound dressings and antiseptic sprays. Silver silicate (Ag-SiO$_2$) is a type of AgNP supported on silica, which helps to reduce particle agglomeration (Jiang, Liu et al. 2005). Ag-SiO$_2$ NPs are also used as antimicrobial additives for wound dressings and in catalytic reduction of toxic dyes in industry (Egger, Lehmann et al. 2009, Chu, Peng et al. 2012).

Increased demand for AgNP-based materials has led to increased production to increase the risk of exposure of workers during the manufacturing and packaging of these materials. Exposure to AgNPs can be by way of dermal absorption, ocular contact, oral ingestion, or inhalation. However, inhalation is the most common route of exposure. Inhalation of AgNPs may occur during manufacturing or commercial application or by aerosolized commercial products or drug therapies and wound sprays containing silver. As nanoparticles are small, they can readily enter the body and potentially exert toxic effects.

Permissible Exposure Limits (PELs) have been developed by the Occupational Safety and Health Administration (OSHA) to protect workers against the health effects of exposure to hazardous substances. Recommended Exposure Limit (REL) for AgNPs

43

(<100 nm primary particle size) is 0.9 µg/m^3 (Kuempel, Roberts et al. 2021). However, there are still uncertainties regarding the exposure limit of AgNPs.

AgNPs cause inflammatory reactions in lung tissue. Rats and mice exposed to AgNPs by inhalation demonstrated decreased lung function and increased lung inflammation (Sung, Ji et al. 2008, Stebounova, Adamcakova-Dodd et al. 2011, Braakhuis, Gosens et al. 2014, Seiffert, Buckley et al. 2016, Silva, Anderson et al. 2016). Although numerous studies have evaluated the toxicity of AgNPs, there is no in-vivo assessment of Ag-SiO$_2$. In a study done by Pittol et.al., exposure of Ag-SiO$_2$ to L-919 murine fibroblast cells did not cause any toxicity which was explained by no significant increase in micronucleus frequency or decrease in cell viability (Pittol, Tomacheski et al. 2018).

Pulmonary toxicity depends upon size, dose and surface modifications of NPs (Anderson, Patchin et al. 2015, Anderson, Silva et al. 2015, Silva, Anderson et al. 2015, Alessandrini, Vennemann et al. 2017). Therefore, the need remains to assess the toxic effects of Ag-SiO$_2$. We have chosen exposure by inhalation as the most comparable to human exposure for the safety assessment for both environmental and occupational exposure (Landsiedel, Ma-Hock et al. 2012).

To better understand the acute toxic responses of Ag-SiO$_2$ NPs following a single aerosol exposure, we exposed Sprague Dawley rats to Ag-SiO$_2$ NPs in a nose-only inhalation system for a single 6 hour period. Bronchoalveolar lavage, lung histology, immunohistochemistry, and gene expression were done to assess potential toxic responses.

MATERIALS AND METHODS

Silver Silicate nanoparticles

The Ag-SiO$_2$ NPs used in the present study were synthesized, characterized and supplied in powder form by the National Institute of Environmental Health Sciences Centers for Nanotechnology Health Implications Research Consortium. Ag-SiO$_2$ NPs were synthesized by flame spray pyrolysis as silver (~8nm) supported on silica (~7nm) (3.79% w/w) (Beltran-Huarac, Zhang et al. 2018). The powdered Ag-SiO$_2$ NPs were 10.64 ± 7.10 nm in diameter prior to suspension in endotoxin-free water at a concentration of 1 mg/ml for aerosolization. The primary particle size, primary particle size distribution, and size factor were characterized by imaging analysis with a transmission electron microscope (TEM). Crystallinity, density and chemical composition were characterized by X-ray diffraction, pycnometer, and inductively coupled plasma mass spectrometry (ICP-MS) respectively (Beltran-Huarac, Zhang et al. 2018).

Nose-only Inhalation Exposure System

The Ag-SiO$_2$ ENM aerosol was generated to create a more realistic inhalation exposure. The aerosol nebulization system (Figure 2.1) was designed at the Center for Health and the Environment at the University of California, Davis, (Anderson, Patchin et al. 2015, Silva, Anderson et al. 2016). Briefly, a BGI 6-jet Collison nebulizer (Waltham, Massachusetts) was used to aerosolize ENM suspensions as fine droplets. The suspension in the nebulizer was constantly stirred and maintained on ice to reduce ENM aggregation. An oil-free compressor (California Air Tools, San Diego, California)

was used to generate compressed air for the nebulizer. The compressed air was dehumidified using compressed air dryers (Wilkerson, Richland, MI) and filtered with a Motor Gard M-610 filter (Motor Gard, Manteca, California) to generate the aerosolized suspension. The suspension droplets were passed through a custom-fabricated heater and two diffusion dryers (TSI, Shoreview, Minnesota) to remove water and create dry particle aggregates. The aggregates were passed through a Krypton-85 charge neutralizer to reduce static charge and to minimize agglomeration of the dried particles entering the 48-port nose-only exposure system. Steel piping connected all the components of the system. The pressure in the nebulizer was 20 psi, while the exposure chamber was at 0.5 to 1 inch of negative water pressure compared to the room air pressure.

During the time of exposure, each rat was housed in a cylindrical nose-only exposure tube (Teague Enterprises, Woodland, California). The tubes were connected to the exposure system for delivery of the Ag-SiO$_2$ aerosol. Sham filtered air control rats were also placed in nose-only inhalation tubes in the same room as the nose-only inhalation exposure system.

Exposure Characterization

Temperature and relative humidity of the exposure system were monitored during the 6-hour exposure period. Four mass concentration, three TEM, three x-ray fluorescence (XRF), and two cascade impactor samples were collected. Total mass concentration was determined by gravimetric measurement using 25-mm Pallflex membrane filters (TX40HI20-WW, Pall Life Sciences, Port Washington, New York). These filters were housed in a portable sampler connected to a nose-only port for

sampling of the aerosol within the inhalation system at 1 L/min for 15 minutes. XRF samples were collected on 3.0µm 25-mm Pall Teflo filters (P/N R2I025, Pall Life Sciences, Port Washington, New York) at 3 L/min for 5 minutes to determine the Zn mass concentration of the ZnO aerosol (Chester Labnet, Tigard, Oregon). An eight-stage Mercer style cascade impactor was used to determine the particle agglomerate size range. A 25-mm Pallflex membrane filter was used on each stage to collect particles at a flow rate of 1 L/min for 30 minutes. For visualization of Ag-SiO$_2$ NPs by transmission electron microscopy (TEM), aerosolized samples were collected on a formvar carbon film supported on a 400-mesh copper grid (3 mm in diameter; Ted Pella, Reading, California). Images were acquired using a Phillips CM-12 TEM operating at 120 kV (Anderson, Patchin et al. 2015).

Animal Protocol

The inhalation study was conducted in agreement with regulations set by University of California, Davis Institutional Animal Care and Use Committee (IACUC) institutional animal care and use committeeunder NIH guidelines. Male Sprague Dawley rats 12 weeks of age were purchased from Envigo Laboratory (Fremont, California). Prior to exposure, the animals were housed two per cage, with Purina 5001 regular laboratory rodent diet (Newco Distributors, Rancho Cucamonga, California) and water provided ad libitum. Rats were acclimated in nose-only exposure tubes daily for one week prior to the experiment. The residence time in the tubes was gradually increased to acclimate rats to a single 6-hour exposure to filtered air (FA) or aerosolized Ag-SiO$_2$.

The animals were randomly assigned to five treatment groups and five control groups with 6 rats/treatment group and 6 rats/control group. Due to space limitations in the exposure chamber, animals scheduled for necropsy at 0, 1, or 7 days post-exposure (PE) were exposed on a different day than those necropsied on day 21 and day 56 PE. However, all procedures were performed in an identical manner to maintain consistency.

Necropsy, Bronchoalveolar Lavage, and Tissue collection

At the start of each necropsy performed on days 0,1, 7, 21 and 56 PE, an overdose of Beuthanasia-D (7.5 ml/kg) (MWI Veterinary Supply Company, Los Angeles, CA, 90074) was used to provide a quick and humane death. Cardiac puncture was performed, and blood was collected in a 12-ml round bottom tube for centrifugation at 2000 revolutions per min (rpm) for 15 min. The resulting blood plasma was collected and stored at -80°C for later use.

Following blood collection, the trachea was cannulated, and the left main bronchus was clamped. The right middle, caudal and accessory lobes were lavaged, flash-frozen, and stored at -80°C for later use. Briefly, the lobes were lavaged three times with a single 7-ml aliquot of sterile phosphate-buffered saline (PBST, Sigma Aldrich, St.Louis, MO) in a 12-ml syringe for collection of bronchoalveolar lavage fluid (BALF). The BALF was collected in a 15-ml round bottom tube and centrifuged for 15 min at 2000 rpm and 4°C. The resulting BALF supernatant was decanted and stored for further analysis, while the cell pellet was resuspended in 2 ml of sterile PBST. Trypan blue was used to count the total viable and non-viable cells. A 100-µl aliquot of resuspended cells was used to prepare cytospin slides for cell differentials.

The left lung was unclamped and inflation-fixed at a hydrostatic pressure of 30 cm with 4% paraformaldehyde for 1 hour. The fixed lung was subsequently stored in 4% paraformaldehyde for 24 hours before transfer to 70% ethanol.

Histological Analysis

The left lung was cut into four transverse slices (cranial to caudal), dehydrated in a graded series of ethanol (70%, 95% and 100%), placed through three series of toluene and paraffin, and embedded in paraffin in cassettes. The paraffin sections were cut to 5-µm thickness using a microtome (HM 355, Microm, Walldorf, Germany) and placed on Superfrost slides (Fisher Scientific, Pittsburgh, PA) for histopathological or immunohistochemical staining.

For the H&E-staining procedure, tissue sections were deparaffinized, stained with Harris hematoxylin (American MasterTech), differentiating solution (American MasterTech), Bluing solution (American MasterTech), and eosin Y (American MasterTech) before coverslipping. For AB-PAS staining, tissue sections were deparaffinized, hydrated, treated with 3% acetic acid (American MasterTech), stained with Alcian blue (American MasterTech), treated with 0.5% periodic acid (American MasterTech) and Schiff reagents (American MasterTech), and coverslipped.

Histopathologic Assessment

Semi-quantitative histologic analysis of 5 lung tissue sections/ animal stained with hematoxylin and eosin (H&E) was performed to determine the presence of cellular infiltrates, epithelial abnormalities, and mucous hyperplasia. The degree of inflammation and cellularity were evaluated in the alveolar, perivascular, bronchiolar, and pleural

regions of the lungs for each rat using a previously described method (Silva, Anderson et al. 2015). Scoring was done by two individuals who were blinded to the treatment received by animals. Briefly, the severity and extent of pathology were determined using a severity score ranging from 0–3; 0 being normal and 3 being markedly inflamed in a particular region of the tissue (Table 2.1). The extent score was defined as the relative area of tissue observed with pathological changes. Extent scores included 0 (no lung involvement), 1 (≤1/3rd lung involvement), 2 (>1/3rd to ½ involvement) and 3 (>1/2 involvement). The overall score of lung inflammation was determined by multiplying severity and extent scores (Overall score = severity × extent).

Immunohistochemistry

Paraffin-embedded tissue sections were deparaffinized in three changes of toluene before hydration in graded ethanol. For antigen retrieval, the slides were then immersed in ethylene diamine tetra acetic acid (EDTA; Thermo Fisher Scientific, pH=8) in a decloaker at 123°C for 2 minutes, then 85°C for 10 seconds, and cooled for 45 minutes. After cooling, the sections were rinsed with PBST + 1000µl tween (PBST; Sigma Aldrich, St.Louis, MO) and treated with 3% hydrogen peroxide for 10 minutes to block endogenous peroxidase activity and prevent false-positive staining results. The sections were subsequently washed in PBST three times and treated with Protein Block (Dako, Carpinteria, CA) for 10 minutes to preclude non-specific binding of the primary antibody. Afterward, the sections were incubated for 1 hour at room temperature with the anti-heme oxygenase -1 (anti HO-1, 1:1000 dilution, ab13243, AbCam) primary antibodies or PBS (for negative control slides). After washing with PBST, the sections were incubated with secondary antibodies, biotinylated affinity-purified goat anti-rabbit

immunoglobulin G (Catalog no. K4403, Dako), for 30 minutes at room temperature. The sections were then rinsed with PBST three times and incubated in 3,3'-diaminobenzidine (DAB) and substrate (Catalog no. K3568, Dako) for 5 minutes. Harris's Hematoxylin (MasterTech, Inc., Lodi, CA) was used to counterstain the tissue sections before coverslipping with ClearMount™ permanent mounting medium (Thermo Fisher Scientific). The sections were observed using brightfield microscopy for qualitative analysis of HO-1 staining.

Gene Expression

TRI-Reagent® (Sigma Aldrich) was used to homogenize and preserve ribonucleic acid (RNA) from the right caudal lobe. RNA was extracted according to the manufacturer's instructions of an RNA isolation kit (Zymo Research, Irvine, CA) and converted to complementary deoxyribonucleic acid (cDNA) using Applied Biosystems' High-Capacity cDNA Reverse Transcription Kit (Foster City, CA). Gene-specific forward and reverse primer (0.2 µm), cDNA (2 µl/reaction), and SYBR Green nucleic acid stain (10 µl/reaction; Applied Biosystems) were used for quantitative polymerase chain reaction (qPCR). Using the ΔΔ-Ct method, gene expression of inflammatory markers interleukin-1β (*IL-1β*), chemokine ligand-1 *(CXCL-1),* tumor necrosis factor-α *(TNF-α),* and monocyte chemoattractant protein-1 *(MCP-1)* and oxidative stress marker hemeoxygenase-1 *(HO-1)* were analyzed and standardized to the expression of the Ribosomal Protein S13 (RPS13) housekeeping gene (Livak and Schmittgen 2001). Gene primers were designed using Primer3 primer design software (Untergasser, Cutcutache et al. 2012).

Statistical Analysis

JMP 13 statistical software (Cary, NC) was used for the sample size calculation and data analysis. Outliers for BALF and histopathology data were determined by box plots. The cleaned data were then assessed for deviations from the assumptions of the Analysis of Variance (ANOVA) and transformed to meet the requirements of normality and equal variance as needed. ANOVAs and post-hoc Tukey's tests for each BALF endpoint were performed at a significance level of $p \leq 0.05$ to determine the main effects between the independent variables (post-exposure necropsy day and treatment). Semi-quantitative histopathological scores were assessed using a non-parametric Kruskal-Wallis test.

RESULTS

Ag-SiO$_2$ Aerosol Characterization

Aerosol characterization found Ag-SiO$_2$ NPs in nanopure water suspension were optimally aerosolized with only moderate agglomeration. The gravimetric Ag-SiO$_2$ aerosol mass concentration measured was 4.9 ± 2.3 mg/m^3, while the Ag concentration alone as measured by XRF was 0.17 ± 0.01 mg/m^3. These results suggest the suspension of Ag-SiO$_2$ NPs in nanopure water did not alter the mass concentration of the aerosol. The median aerosol diameter measured by cascade impactor was 1.9 ± 0.3 µm, and the size (diameter) distribution of the Ag-SiO$_2$ NPs based on TEM ranged from 21 to 370 nm (Figures 2.2 and 2.3 respectively). The aerosol diameter measured by the cascade impactor suggested that there was particle agglomeration, but size distribution based on TEM suggested that approximately 50% of Ag-SiO$_2$ NPs were less than 100 nm in diameter to permit inhalation and deposition in the lungs.

BALF Analysis

BALF analysis demonstrated a significant increase ($p<0.05$) in total number of cells on days 0, 1 and 7 post-exposure to Ag-SiO$_2$ (Figure 2.4 A). By day 21 the total BAL cell numbers were comparable to control animals. Macrophage and neutrophil numbers in Ag-SiO$_2$ exposed rats on days 0, 1 and 7 post-exposure were significantly higher ($p < 0.05$) than in control animals (Figure 2.4 B,C). Significantly increased numbers of eosinophils were observed on day 0 and 7 post-exposure to Ag-SiO$_2$ ($p < 0.05$) (Figure 2.4 D). However, by day 21 all inflammatory cells had returned to control levels.

Histopathologic Analysis

Semiquantitative histopathological scores of lung tissue sections showed no significant inflammatory changes in the lung parenchyma, alveoli, bronchioles, perivascular or pleural region for any time point between control animals and animals exposed to Ag-SiO$_2$.

Qualitative differences were noted in lung parenchyma. On day 0 and day 1 post-exposure, a mild influx of macrophages was noted (Figure 2.5). No changes were observed on days 7, 21 or 56 post-exposure.

Lung tissue sections stained with AB-PAS were analyzed for airway goblet cells between control and ZnO exposed animals. No significant differences were observed between the two groups.

Immunohistochemistry

Positively-stained macrophages for HO-1 antibody were observed in sub-pleural region of the lungs of Ag-SiO$_2$ exposed animals (Figure 2.6). Qualitative analysis showed the presence of HO-1 staining only on day 1 PE with little staining noted on days 0, 7, 21 and 56 PE to Ag-SiO$_2$.

Gene Expression

Expression of *IL-1β, TNF-α, CXCL-1, MCP-1* and *HO-1* were analyzed in right caudal lobe of lungs on days 0, 1, 7, 21 and 56 PE to Ag-SiO$_2$. No statistically significant differences were noted between animals exposed to Ag-SiO$_2$ and FA.

DISCUSSION

Acute exposure to AgNPs by inhalation can lead to a short, but significant inflammatory reaction in the lungs. There have been numerous studies done to demonstrate the toxicity of AgNPs in lung tissues, but no in-vivo inhalation study has been done to evaluate Ag-SiO$_2$ NPs. Ag-SiO$_2$ NPs are used as antimicrobial additives for wound dressings and in catalytic reduction of toxic dyes in industries (Egger, Lehmann et al. 2009, Chu, Peng et al. 2012). The objective of this study was to evaluate the acute toxicity of Ag-SiO$_2$ in rats following inhalation. We exposed rats in a nose-only inhalation chamber for 6 hours and allowed for a recovery period of up to 56 days post-exposure. We chose the inhalation route to mimic potential occupational and environmental exposures. The use of a nose-only inhalation system helped to minimize nanoparticle deposition on the fur and subsequent ingestion of these particles. 1% Ag-SiO$_2$ provided by NIEHS was fully characterized before and during the experiment.

In this study, the aerosolized silver nanoparticle concentration was 4.9 ± 2.3 mg/m^3. The Occupational Safety and Health Administration (OSHA) has set the exposure limit for silver nanoparticles at 0.01 mg/m^3 per 8-hour time weighted average. The maximal time-weighted average of aerosolized silver has been found to be up to 0.289 mg/m^3 manufacturing plants for silver (Lee, Ahn et al. 2012). Our study's aerosolized silver concentration can be the equivalent of an environment with high occupational exposure to aerosolized silver without personal safety measures.

Pulmonary injury, inflammation and vascular permeability were determined by BAL cell counts and cell differentials (Yoshiura, Fujisawa et al. 2019). In our study, the number of total cells in the BAL were significantly increased on days 0, 1 and 7 following exposure to Ag-SiO$_2$. Macrophages and neutrophils were significantly increased on day 0 and remained elevated untill day 7 post-exposure to Ag-SiO$_2$. Eosinophils were also noted to be significantly higher on day 0 and day 7 post-exposure to Ag-SiO$_2$ compared to FA control animals. By day 21, inflammatory cells had returned to levels similar to those observed in control animals. In a study by Silva et.al. (2016), a delayed, but short-lived inflammatory response was observed when rats were exposed to 20 nm and 110 nm AgNPs in a nose-only inhalation chamber. The duration of exposure was similar to our study, i.e., 6 hours for 1 day with necropsies performed on days 1, 7, 21 and 56 following exposure. In contrast to our study, inflammatory cells in BAL and histopathological changes peaked at day 7 and persisted until day 21 post exposure (Silva, Anderson et al. 2016).

In another study of longer duration, rats were exposed to 18nm AgNPs for 90 days. Following exposure, the tidal volume and minute volume were found to be

decreased, along with inflammatory changes noted in the BAL, as well as histological changes in the lungs following a much longer duration of exposure for 90 days (Sung, Ji et al. 2008).

In another study conducted in mice with AgNPs for 10 days, total cells, macrophages and neutrophils in BALF were increased significantly on days 0 and day 21 post-exposure. As noted in our study, no lung injury was observed in the histopathological assessment of lung tissue sections (Stebounova, Adamcakova-Dodd et al. 2011). However, all these studies used AgNPs, not Ag-SiO$_2$.

In an in-vitro study, L-929 murine fibroblast cell was treated with Ag-SiO$_2$. MTT (3-(4,5-dimethylthiazol-2-yl)-2,5 diphenyltetrazolium bromide), CBPI (cytokinesis-block proliferation index) and micronucleus assay was done to assess the toxicity. No significant micronucleus frequency increase or cell viability reduction were observed (Pittol, Tomacheski et al. 2018). Characterization of provided Ag-SiO$_2$ done by NIEHS has shown that silica in Ag-SiO$_2$, used in our study, is amorphous with 0% crystallinity. It has been studied that amorphous silica is non-toxic (Brunner, Wick et al. 2006, Pittol, Tomacheski et al. 2018). So, one of the reasons of non-toxic nature of Ag-SiO$_2$ in comparison to AgNPs can be explained by the presence of an amorphous silicate. The hydrophilic characteristic of silica can also influence the toxicity. It can reduce the nonspecific binding of proteins and release of AgNPs, thus reducing the toxicity (Hu, Liu et al. 2008, Hu, Fawcett et al. 2012, Agnihotri, Mukherji et al. 2013). In addition, duration of exposure (6 hour, single day) in current study might not be sufficient to elicit long lasting pulmonary inflammation with distinct histopathological changes.

In summary, future studies with sub-acute and chronic durations would be helpful to further evaluate the toxicity of Ag-SiO$_2$ NPs in the lungs.

CONCLUSION

The results of present study suggest that single 6-hour exposure to Ag-SiO$_2$ results in acute and short-term pulmonary inflammation in the form of increased total cells, macrophages and neutrophils in BALF on days 0, 1 and 7 post-exposure. Inflammatory cells returned to control levels by day 21. Hence, these findings suggest Ag-SiO$_2$ when inhaled into lungs are not completely harmless and can be associated with short-term inflammation.

TABLES

Table 2.1: Semi-quantitative histopathology severity scoring rubric

Score	Description
0	Normal. Thin alveolar walls, with very few free macrophages and no inflammatory cells in the lumen. Respiratory epithelium 1 cell-layer thick. Normal smooth muscle and submucosal layers. Vascular endothelium may contain some influxing monocytes and a few inflammatory cells. No visible particle agglomerates. Little/no cells at the pleura.
1	PMNs present in perivascular cuffs, airway submucosa, and alveolar airspaces. Influx of monocytes and macrophages into alveolar airspaces and monocytes in perivascular cuffs.
2	Presence of PMNs, macrophages, and monocytes in alveolar airspaces, along with cellular debris (exudate). Influxing cells in the perivascular cuffs and/or airway submucosa. Thickened alveolar walls.
3	Presence of PMNs and/or foamy and/or irregular macrophages (e.g., multi-nucleated, or exhibiting loss of membrane integrity) and cellular exudate in the airspaces.

Table 2.2. Aerosol characterization

Method	Endpoint (units)	Measurement
Gravimetry	Mass Concentration (mg Ag-SiO$_2$/m^3)	4.9 ± 2.3
X-ray Fluorescence	Ag Mass Concentration (mg Ag/m^3)	0.17 ± 0.01
Cascade Impactor	Mass median aerodynamic diameter (μm)	1.9 ± 0.3

FIGURES

Figure 2.1. Aerosol Nebulization System.

A 6-jet Collison nebulizer was used to aerosolize particles in suspension as aqueous droplets. Water was removed by a heater and diffusion dryers. Krypton-85 beta emission source neutralized particle charge. Dry particles were delivered to the nose-only exposure chamber.
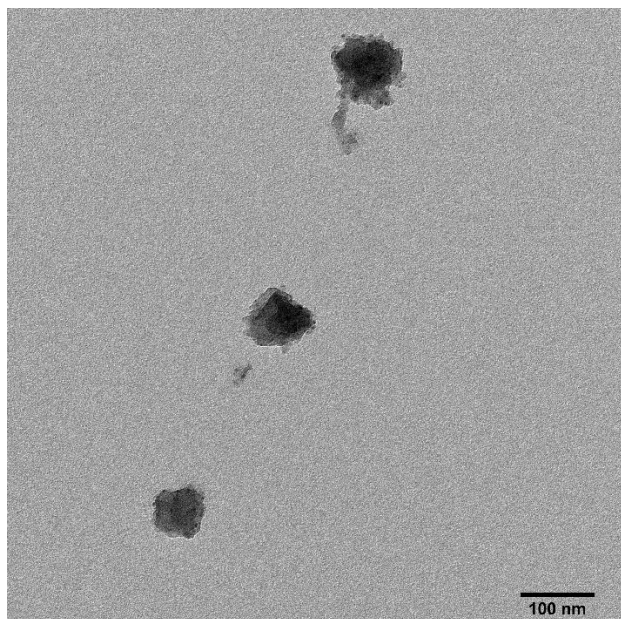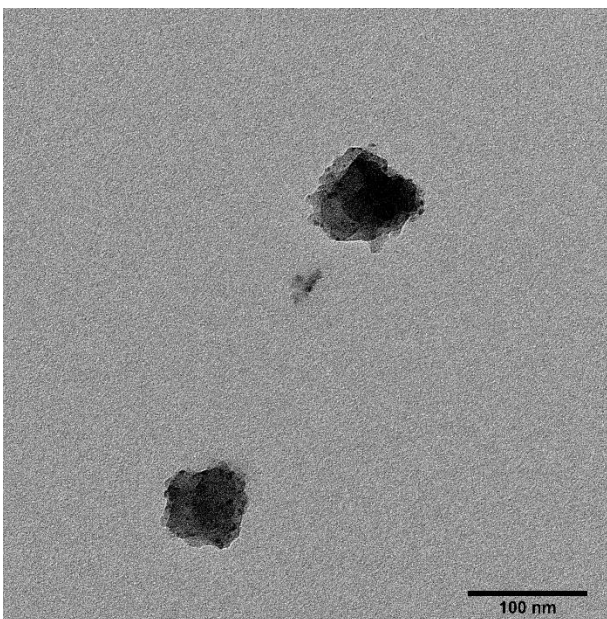
Figure 2.2. Morphology of Aerosolized Ag-SiO$_2$

Transmission electron micrographs (TEM) of aerosolized Ag-SiO$_2$. Figure A is at a lower

magnification (scale bar, 100 nm). Figure B is at a higher magnification (scale bar, 100

nm) showing agglomerated Ag-SiO$_2$ NPs.
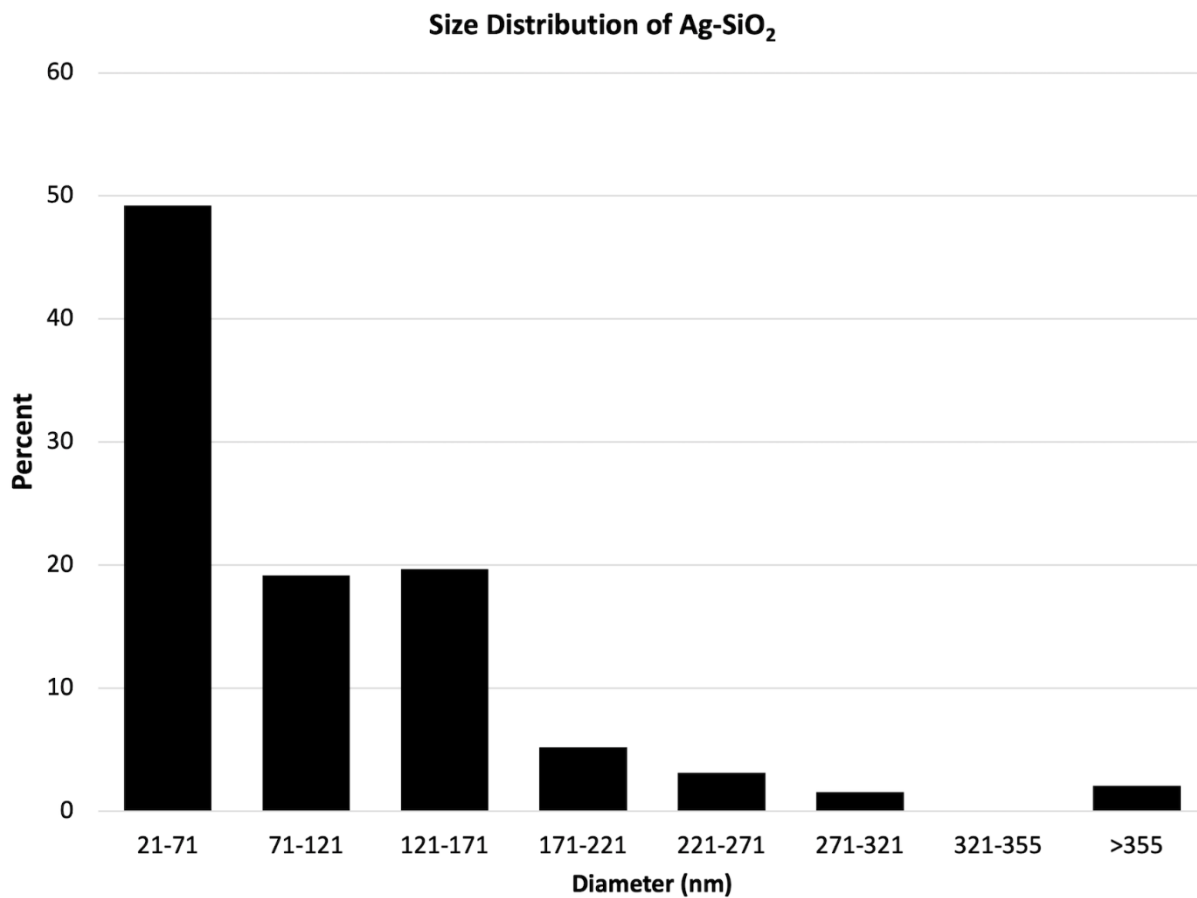
Figure 2.3. Graph of the size (diameter) distribution of aerosolized silver silicate (Ag-SiO$_2$) nanoparticles measured by transmission electron microscopy.
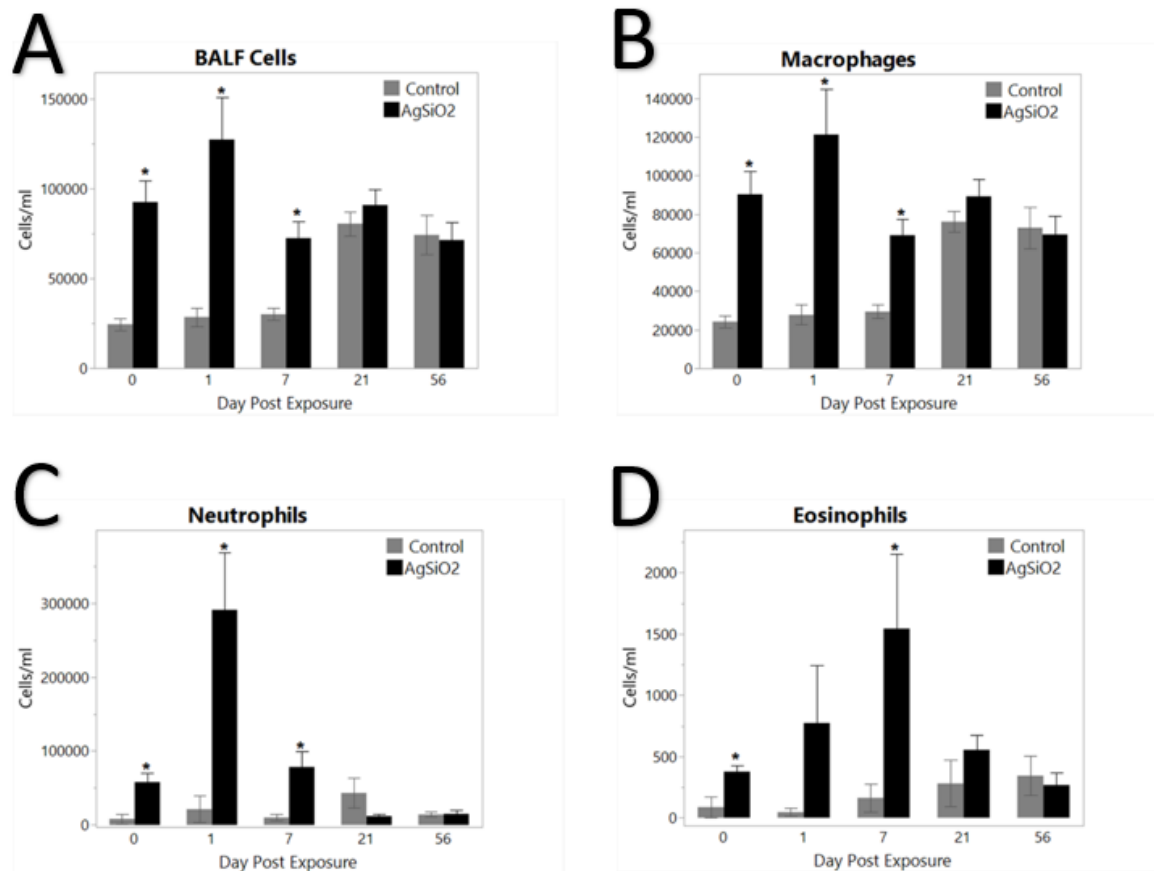
Figure 2.4. Total cells (A), Macrophages (B), Neutrophils (C) and Eosinophils (D) from bronchoalveolar lavage of rats exposed to filtered air (control) or Ag-SiO₂. Rats were necropsied on days 0, 1, 7, 21 or 56 post exposure. Statistical analysis was performed by ANOVA to compare between treatment groups. * = significant difference ($p < 0.05$) between control and Ag-SiO₂ exposed group for the same day. (n=6 rats/ group/ time point).
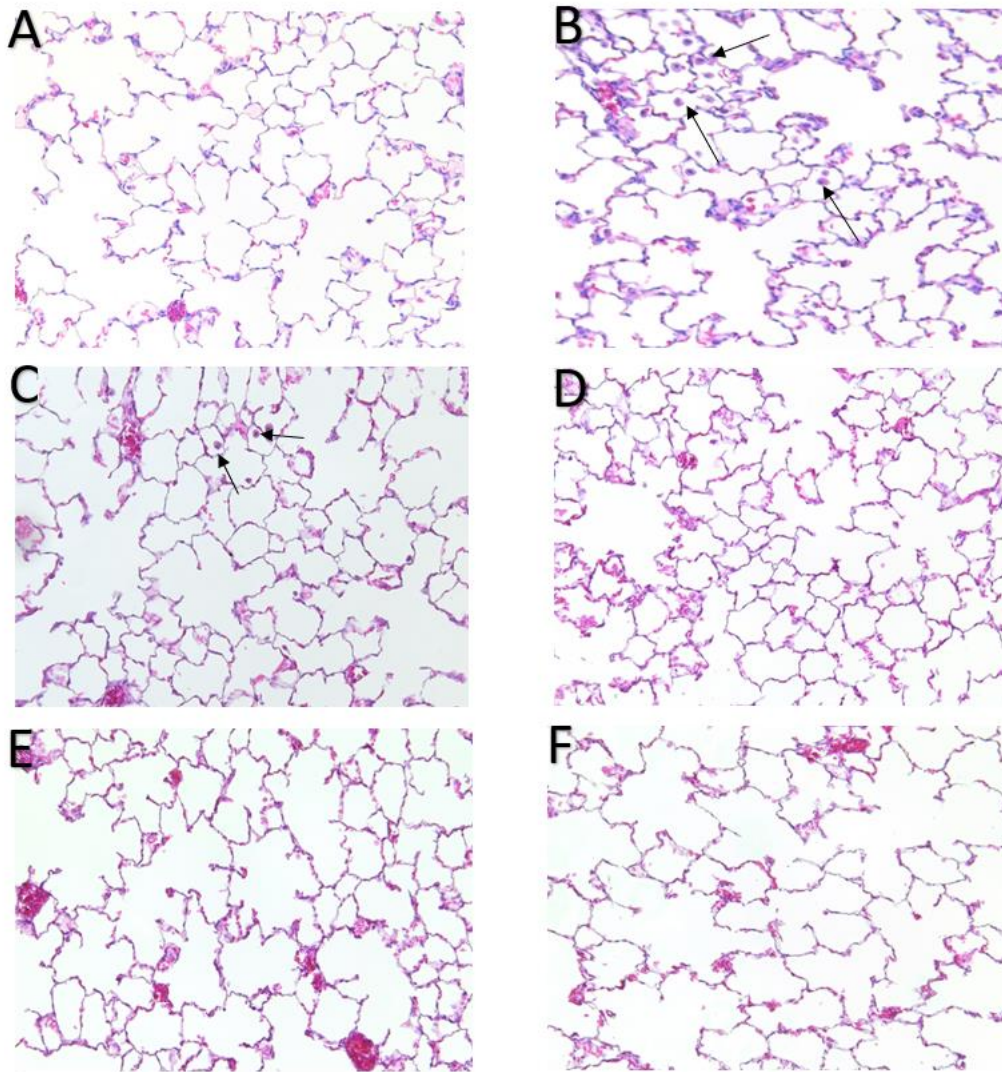
Figure 2.5. Representative brightfield microscopy images of H & E stained lung tissue sections at 20X magnification showing control animals (**A**) and animals exposed to Ag-SiO$_2$ on day 0 PE (**B**), day 1 PE (**C**), day 7 PE (**D**), day 21 PE (**E**) and day 56 PE (**F**). Arrows indicate the presence of increased number of macrophages in the subpleural alveoli of the lungs. (Scale bar= 50µm)
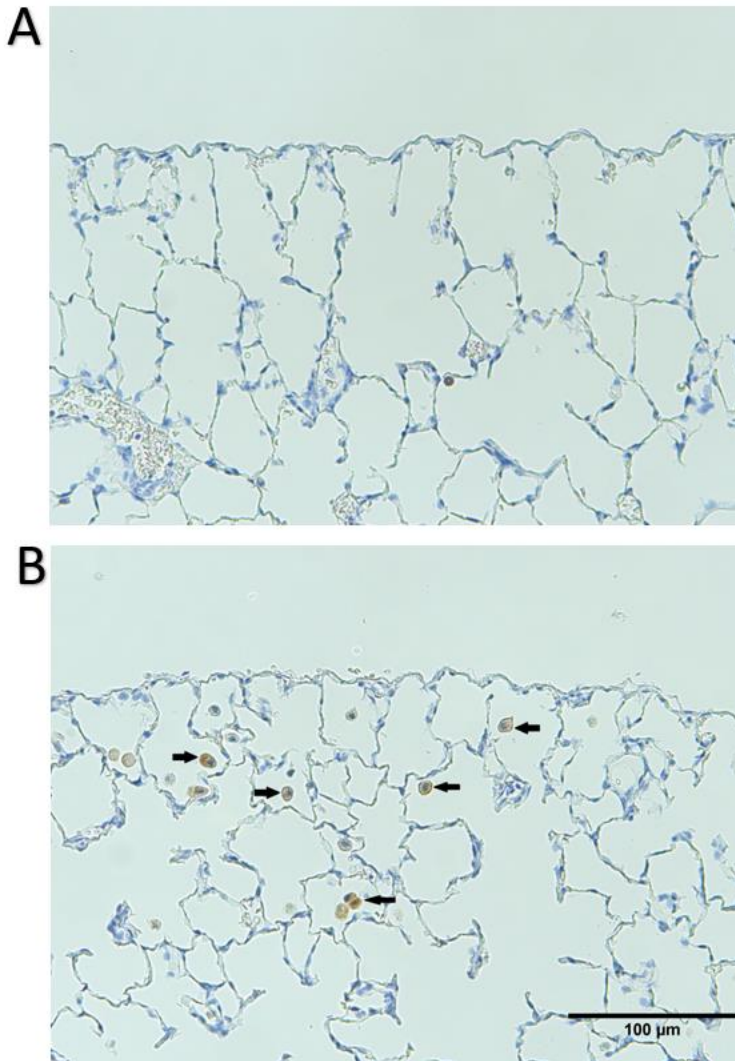
Figure 2.6. Lung tissue sections, at 20X magnification, immunochemically stained with anti-heme oxygenase-1 for control (**A**) and post-exposure day 1 (**B**). Arrows point to cells with heme oxygenase-1, a marker for oxidative stress. Positive cells appear to be macrophages. (Scale bar= 100μm)

References

1. Agnihotri, Shekhar, Soumyo Mukherji, and Suparna Mukherji. 2013. 'Immobilized silver nanoparticles enhance contact killing and show highest efficacy: elucidation of the mechanism of bactericidal action of silver', *Nanoscale*, 5: 7328-40.

2. Alessandrini, Francesca, Antje Vennemann, Silvia Gschwendtner, Avidan U Neumann, Michael Rothballer, Tanja Seher, Maria Wimmer, Susanne Kublik, Claudia Traidl-Hoffmann, and Michael Schloter. 2017. 'Pro-inflammatory versus immunomodulatory effects of silver nanoparticles in the lung: the critical role of dose, size and surface modification', *Nanomaterials*, 7: 300.

3. Anderson, D. S., E. S. Patchin, R. M. Silva, D. L. Uyeminami, A. Sharmah, T. Guo, G. K. Das, J. M. Brown, J. Shannahan, T. Gordon, L. C. Chen, K. E. Pinkerton, and L. S. Van Winkle. 2015. 'Influence of particle size on persistence and clearance of aerosolized silver nanoparticles in the rat lung', *Toxicol Sci*, 144: 366-81.

4. Anderson, Donald S, Rona M Silva, Danielle Lee, Patricia C Edwards, Arjun Sharmah, Ting Guo, Kent E Pinkerton, and Laura S Van Winkle. 2015. 'Persistence of silver nanoparticles in the rat lung: Influence of dose, size, and chemical composition', *Nanotoxicology*, 9: 591-602.

5. Beltran-Huarac, Juan, Zhenyuan Zhang, Georgios Pyrgiotakis, Glen DeLoid, Nachiket Vaze, and Philip Demokritou. 2018. 'Development of reference metal and metal oxide engineered nanomaterials for nanotoxicology research using

high throughput and precision flame spray synthesis approaches', *NanoImpact*, 10: 26-37.

6. Braakhuis, Hedwig M, Ilse Gosens, Petra Krystek, John AF Boere, Flemming R Cassee, Paul HB Fokkens, Jan Andries Post, Henk Van Loveren, and Margriet VDZ Park. 2014. 'Particle size dependent deposition and pulmonary inflammation after short-term inhalation of silver nanoparticles', *Particle and fibre toxicology*, 11: 1-16.

7. Brunner, Tobias J, Peter Wick, Pius Manser, Philipp Spohn, Robert N Grass, Ludwig K Limbach, Arie Bruinink, and Wendelin J Stark. 2006. 'In vitro cytotoxicity of oxide nanoparticles: comparison to asbestos, silica, and the effect of particle solubility', *Environmental science & technology*, 40: 4374-81.

8. Burdușel, Alexandra-Cristina, Oana Gherasim, Alexandru Mihai Grumezescu, Laurențiu Mogoantă, Anton Ficai, and Ecaterina Andronescu. 2018. 'Biomedical applications of silver nanoparticles: an up-to-date overview', *Nanomaterials*, 8: 681.

9. Chu, Chia-Yu, Fu-Chuo Peng, Ying-Fang Chiu, Hsing-Chuan Lee, Chien-Wen Chen, Jiun-Chiou Wei, and Jiang-Jen Lin. 2012. 'Nanohybrids of silver particles immobilized on silicate platelet for infected wound healing', *PloS one*, 7: e38360.

10. Egger, Salome, Rainer P Lehmann, Murray J Height, Martin J Loessner, and Markus Schuppler. 2009. 'Antimicrobial properties of a novel silver-silica nanocomposite material', *Applied and environmental microbiology*, 75: 2973-76.

11. Hu, Lianghai, John Paul Fawcett, and Jingkai Gu. 2012. 'Protein target discovery of drug and its reactive intermediate metabolite by using proteomic strategy', *Acta Pharmaceutica Sinica B*, 2: 126-36.

12. Hu, Shang-Hsiu, Ting-Yu Liu, Hsin-Yang Huang, Dean-Mo Liu, and San-Yuan Chen. 2008. 'Magnetic-sensitive silica nanospheres for controlled drug release', *Langmuir*, 24: 239-44.

13. Inshakova, Elena, and Oleg Inshakov. 2017. "World market for nanomaterials: structure and trends." In *MATEC web of conferences*, 02013. EDP Sciences.

14. Jiang, Zhong-Jie, Chun-Yan Liu, and Lu-Wei Sun. 2005. 'Catalytic properties of silver nanoparticles supported on silica spheres', *The Journal of Physical Chemistry B*, 109: 1730-35.

15. Kuempel, Eileen D, Jenny R Roberts, Gary Roth, Ralph D Zumwalde, Drew Nathan, Ann F Hubbs, Douglas Trout, and George Holdsworth. 2021. 'Health effects of occupational exposure to silver nanomaterials'.

16. Landsiedel, Robert, Lan Ma-Hock, Hans-Juergen Haussmann, Ben van Ravenzwaay, Martin Kayser, and Karin Wiench. 2012. 'Inhalation studies for the safety assessment of nanomaterials: status quo and the way forward', *Wiley Interdisciplinary Reviews: Nanomedicine and Nanobiotechnology*, 4: 399-413.

17. Lee, Ji Hyun, Kangho Ahn, Sun Man Kim, Ki Soo Jeon, Jong Seong Lee, and Il Je Yu. 2012. 'Continuous 3-day exposure assessment of workplace manufacturing silver nanoparticles', *Journal of Nanoparticle Research*, 14: 1-10.

18. Livak, Kennth J, and Thomas D Schmittgen. 2001. 'Analysis of relative gene expression data using real-time quantitative PCR and the 2− ΔΔCT method', *methods*, 25: 402-08.

19. McINTYRE, ROBIN A. 2012. 'Common nano-materials and their use in real world applications', *Science progress*, 95: 1-22.

20. Pittol, Michele, Daiane Tomacheski, Douglas Naue Simões, Vanda Ferreira Ribeiro, and Ruth Marlene Campomanes Santana. 2018. 'Evaluation of the toxicity of silver/silica and titanium dioxide particles in mammalian cells', *Brazilian Archives of Biology and Technology*, 61.

21. Seiffert, Joanna, Alison Buckley, Bey Leo, Nicholas G Martin, Jie Zhu, Ranran Dai, Farhana Hussain, Chang Guo, James Warren, and Alan Hodgson. 2016. 'Pulmonary effects of inhalation of spark-generated silver nanoparticles in Brown-Norway and Sprague–Dawley rats', *Respiratory research*, 17: 1-15.

22. Silva, R. M., D. S. Anderson, J. Peake, P. C. Edwards, E. S. Patchin, T. Guo, T. Gordon, L. C. Chen, X. Sun, L. S. Van Winkle, and K. E. Pinkerton. 2016. 'Aerosolized Silver Nanoparticles in the Rat Lung and Pulmonary Responses over Time', *Toxicol Pathol*, 44: 673-86.

23. Silva, Rona M, Donald S Anderson, Lisa M Franzi, Janice L Peake, Patricia C Edwards, Laura S Van Winkle, and Kent E Pinkerton. 2015. 'Pulmonary effects of silver nanoparticle size, coating, and dose over time upon intratracheal instillation', *Toxicological sciences*, 144: 151-62.

24. Stebounova, Larissa V, Andrea Adamcakova-Dodd, Jong Sung Kim, Heaweon Park, Patrick T O'Shaughnessy, Vicki H Grassian, and Peter S Thorne. 2011.

'Nanosilver induces minimal lung toxicity or inflammation in a subacute murine inhalation model', *Particle and fibre toxicology*, 8: 1-12.

25. Sung, Jae Hyuck, Jun Ho Ji, Jin Uk Yoon, Dae Seong Kim, Moon Yong Song, Jayoung Jeong, Beom Seok Han, Jeong Hee Han, Yong Hyun Chung, and Jeongyong Kim. 2008. 'Lung function changes in Sprague-Dawley rats after prolonged inhalation exposure to silver nanoparticles', *Inhalation toxicology*, 20: 567-74.

26. Untergasser, Andreas, Ioana Cutcutache, Triinu Koressaar, Jian Ye, Brant C. Faircloth, Maido Remm, and Steven G. Rozen. 2012. 'Primer3--new capabilities and interfaces', *Nucleic acids research*, 40: e115-e15.

27. Yoshiura, Yukiko, Yuri Fujisawa, Taisuke Tomonaga, Hiroto Izumi, Takako Oyabu, Toshihiko Myojo, Masaru Kubo, Manabu Shimada, and Yasuo Morimoto. 2019. 'Comparison of Responses in Rat Lung Following Inhalation and Intratracheal Administration of Nanoparticles.' in, *In Vivo Inhalation Toxicity Screening Methods for Manufactured Nanomaterials* (Springer).

CHAPTER 3

Inhaled Engineered Zinc Oxide Nanoparticles Induce Acute

Toxicity in the Lungs of Rats

ABSTRACT

Zinc Oxide nanoparticles (ZnO NPs) are commercially used as antibacterial, antifungal, anti-corrosive, and UV filtering agents. Increased consumer product use has created concerns for the potential increased risk by inhalation of these nanoparticles during synthesis and commercial application. The primary objective of this study is to determine if acute, one day inhalation of ZnO NPs induces inflammation in the lungs. Male Sprague Dawley rats were randomly assigned to sham control (filtered air, n=12) or ZnO inhalation (n=24). Exposure was to aerosolized 50-nm diameter ZnO for a single 6-hour period with necropsy at 0, 1, 7, or 21 days post exposure (PE). Bronchoalveolar lavage (BAL) was collected from the right lung to determine cell number, viability, and differentials, along with supernatant protein concentration. The left lung was inflation-fixed, embedded, and sectioned for histopathologic analysis. The particle aerosol was characterized by gravimetric, x-ray fluorescence, cascade impactor, and transmission electron microscopic analyses. BAL comparisons between the control and ZnO exposed rats revealed statistically significant ($p < 0.05$) decreases in viable cells and increases in macrophages, neutrophils, and protein on PE days 0, 1, and 7. These findings were supported by lung histopathology, with the greatest inflammation observed on PE days 1 and 7, along with greater numbers of HO-1-stained macrophages in the airways and subpleural regions, of ZnO exposed versus sham control rats. Thus, the cumulative findings suggest ZnO inhalation causes short-term inflammation and oxidative stress.

INTRODUCTION

The concept of nanotechnology began in the 1980s (Pietroiusti, Stockmann-Juvala et al. 2018). Today there are more than 1,600 engineered nanomaterial (ENM)-based consumer products on the global market, with annual sales in the US alone of $70 million (Pietroiusti, Stockmann-Juvala et al. 2018). Zinc oxide (ZnO) is one of the largest globally produced metal oxides with a total production of 0.1-1.2 million tons/year (Swain, Rao et al. 2016). ZnO nanomaterials have a high surface-area-to-volume ratio compared to that of typical ZnO particles with larger diameters. Thus, ZnO NMs have a significant potential of greater toxicity due to a larger reactive surface area compared to that of ZnO particles with larger diameters.

ZnO ENMs are widely used in textiles, pharmaceuticals, cosmetics, and biomedical and electronic applications (Kołodziejczak-Radzimska and Jesionowski 2014). Since ZnO ENMs have antimicrobial properties, they are used in drugs and cosmetics (Dobrucka, Dlugaszewska et al. 2018, Siddiqi, ur Rahman et al. 2018, Jiang, Lin et al. 2020, Wiesmann, Tremel et al. 2020). Due to their high photostability, dispersive properties, and ability to absorb UV radiation without skin irritation (Cho, Duffin et al. 2011), ZnO ENMs are major constituents found in sunscreen lotions and creams (Subramaniam, Prasad et al. 2019).

The high demand for nanomaterials poses increased risks for occupational exposure, with the greatest risk in workers who manufacture, handle, and package ENMs and ENM-based products. Studies have shown inhalation of ZnO particles in workers who develop metal fume fever (Kao, Chen et al. 2012, Vandebriel and De Jong 2012, Monsé, Hagemeyer et al. 2018). Permissible Exposure Limits (PELs) have been

developed by the Occupational Safety and Health Administration (OSHA) to protect

workers against the health effects of exposure to hazardous substances. OSHA's

regulatory PEL for ZnO is 5–10 mg/m^3 as an 8-hour time-weighted average (Vogel and

Cassee 2018). However, there remain uncertainties as to the exposure levels and

associated toxicities of ENMs in occupational settings lacking proper emissions

controls. Under such conditions, the surrounding community and environment may also

be exposed to industrially-produced ENMs (Seaton, Tran et al. 2010).

ZnO ENMs have been reported to cause toxic effects by dermal, ingestion, and

inhalation routes of exposure (Buzea, Pacheco et al. 2007, De Matteis 2017). In an

occupational setting, exposure to ZnO-based products occurs most commonly by

inhalation during synthesis, manufacturing, handling, packaging, and disposal (Singh

2019). A number of studies have examined the toxicity of ZnO ENMs using exposure

methods such as intranasal or intratracheal instillation, as well as oropharyngeal

aspiration, rather than by inhalation which is physiologically more comparable to human

exposure (Gao, Yang et al. 2013, Jacobsen, Stoeger et al. 2015, Saptarshi, Feltis et al.

2015, Morimoto, Izumi et al. 2016, Wang, Li et al. 2017, Wang, Zhang et al. 2020).

Inhalation studies are critical for safety assessments of environmental and

occupational exposures (Landsiedel, Ma-Hock et al. 2012). Chronic exposure to ZnO

aerosols in a whole-body chamber has resulted in acute, but transient inflammation

(Adamcakova-Dodd, Stebounova et al. 2014, Chuang, Juan et al. 2014, Morimoto,

Izumi et al. 2016). Very few studies (Klein, Wiench et al. 2012, Areecheewakul,

Adamcakova-Dodd et al. 2020) have done a single-day, nose-only inhalation exposure

to assess the toxicity of ZnO nanomaterials. Therefore, single-day acute studies are

necessary as a means to detect early pathogenesis and its progression and/or regression after the exposure to ZnO ENM.

To better understand the acute toxic responses of ZnO ENMs following a single exposure, we exposed Sprague Dawley rats to a ZnO aerosol in a nose-only inhalation system for 6 hours. Toxic responses were quantitatively and qualitatively assessed using bronchoalveolar lavage, lung histology, immunohistochemistry, and gene expression.

MATERIALS AND METHODS

Zinc Oxide nanomaterials

ZnO ENMs 50 nm in diameter were supplied by the National Institutes of Health (NIH) Health Effects of Nanomaterials Consortium as a powder. Physicochemical characterization of the ENMs was completed by the T.H. Chan School of Public Health-National Institute of Environmental Health Sciences (HSPH-NIEHS) Nanosafety Center at Harvard University. ZnO ENMs were synthesized by flame spray with mean diameter of 45.7 ± 17.4 nm. Primary particle size was determined by X-ray diffraction and transmission electronic microscope (TEM) image analysis. Primary particle size distribution and size factor were characterized by TEM image analysis by Image J. Crystallinity and density was characterized by X-ray diffraction and pycnometer respectively (Beltran-Huarac, Zhang et al. 2018).

Nose-only Inhalation Exposure System

A ZnO ENM aerosol was generated to facilitate a more realistic inhalation exposure. Provided powdered form of ZnO ENMs was made into a suspension in a

nanopure water at 1mg/ml concentration. The aerosol nebulization system (Figure 3.1) was designed at the University of California, Davis, Center for Health and the Environment (Anderson, Patchin et al. 2015, Silva, Anderson et al. 2016). Briefly, a BGI 6-jet Collison nebulizer (Waltham, Massachusetts) was used to aerosolize ENM suspensions as fine droplets. The suspension in the nebulizer was constantly stirred and kept on ice to reduce ENM aggregation. An oil-free compressor (California Air Tools, San Diego, California) was used to generate compressed air for the nebulizer. The compressed air was dehumidified using compressed air dryers (Wilkerson, Richland, MI) and filtered with a Motor Gard M-610 filter (Motor Gard, Manteca, California) to aerosolize the suspension. The suspension droplets were passed through a custom-fabricated heater and two diffusion dryers (TSI, Shoreview, Minnesota) to remove water and create dry particle aggregates. The aggregates were passed through a Krypton-85 charge neutralizer to reduce static charge and minimize agglomeration of the dried particles entering the 48-port nose-only exposure system. Steel piping connected all the components of the system. The pressure in the nebulizer was 20 psi, while the exposure chamber was at 0.5 to 1 inch of negative water pressure compared to the room air pressure.

During the time of exposure, each rat was housed in a cylindrical nose-only exposure tube (Teague Enterprises, Woodland, California). The tubes were connected to the exposure system for the ZnO aerosol exposures or placed on a table in the same room as the exposure system for the filtered air (control) exposures.

Exposure Characterization

Temperature and relative humidity of the exposure system were monitored during the 6-hour exposure period. Four mass concentration, three TEM, three x-ray fluorescence (XRF), and two cascade impactor samples were collected. Total mass concentration was determined by gravimetric measurement of 25-mm Pallflex membrane filters (TX40HI20-WW, Pall Life Sciences, Port Washington, New York). These filters were housed in a portable sampler connected to a nose-only port for sampling of the aerosol within the inhalation system at 1 L/min for 15 minutes.

XRF samples were collected on 3.0µm 25-mm Pall Teflo filters (P/N R2I025, Pall Life Sciences, Port Washington, New York) at 3 L/min for 5 minutes to determine the Zn mass concentration of the ZnO aerosol (Chester Labnet, Tigard, Oregon). An eight-stage Mercer style cascade impactor was used to determine the particle agglomerate size range. A 25-mm Pallflex membrane filter was used on each stage to collect particles at a flow rate of 1 L/min for 30 minutes. For visualization of ZnO ENM by transmission electron microscopy (TEM), aerosolized samples were collected on a formvar carbon film supported on a 400-mesh copper grid (3 mm in diameter; Ted Pella, Reading, California). Images were acquired using a Phillips CM-12 TEM operating at 120 kV (Anderson, Patchin et al. 2015).

Animal Protocol

The inhalation study was conducted in agreement with regulations set by University of California, Davis Institutional Animal Care and Use Committee (IACUC) institutional animal care and use committee under NIH guidelines. Male Sprague Dawley rats 12 weeks of age were purchased from Envigo Laboratory (Fremont, California). Prior to exposure, the animals were housed two per cage, with

Purina 5001 regular laboratory rodent diet (Newco Distributors, Rancho Cucamonga, California) and water provided ad libitum. Rats were acclimated in nose-only exposure tubes daily for one week prior to the experiment. The residence time in the tubes was gradually increased to acclimate rats to a single 6-hour exposure to filtered air or aerosolized ZnO.

The animals were randomly assigned to four treatment groups and four control groups with 6 rats/treatment group and 3 rats/control group. Due to space limitations in the exposure chamber, animals scheduled for necropsy at 0, 1, or 7 days post exposure (PE) were exposed on a different day than those necropsied on day 21 PE. However, all procedures were performed in an identical manner to maintain consistency.

Necropsy, Bronchoalveolar Lavage, and Tissue collection

At the start of each necropsy performed on days 0,1, 7, and 21 PE, an overdose of Beuthanasia-D (7.5 ml/kg) (MWI Veterinary Supply Company, Los Angeles, CA, 90074) was used to provide a quick and humane death. Cardiac puncture was performed, and blood was collected in a 12-ml round bottom tube for centrifugation at 2000 revolutions per min (rpm) for 15 min. The resulting blood plasma was collected and stored at -80°C for later use.

Following blood collection, the trachea was cannulated, and the left main bronchus was clamped. The right middle, caudal and accessory lobes were lavaged, flash-frozen, and stored at -80°C for later use. Briefly, the lobes were lavaged three times with a single 7-ml aliquot of sterile phosphate-buffered saline (PBST, Sigma Aldrich, St.Louis, MO) in a 12-ml syringe for collection of bronchoalveolar lavage fluid

(BALF). The BALF was collected in a 15-ml round bottom tube and centrifuged for 15 min at 2000 rpm and 4°C. The resulting BALF supernatant was decanted and stored for further analysis, while the cell pellet was resuspended in 2 ml of sterile PBST. Trypan blue was used to count the total viable and non-viable cells. A 100-µl aliquot of resuspended cells was used to prepare cytospin slides for cell differentials.

The left lung was unclamped and inflation-fixed at a hydrostatic pressure of 30 cm with 4% paraformaldehyde for 1 hour. The fixed lung was subsequently stored in 4% paraformaldehyde for 24 hours before transfer to 70% ethanol.

Histological Analysis

The left lung was cut into four transverse slices (cranial to caudal), dehydrated in a graded series of ethanol (70%, 95% and 100%), placed through three series of toluene and paraffin, and embedded in paraffin in cassettes. The paraffin sections were cut to 5-µm thickness using a microtome (HM 355, Microm, Walldorf, Germany) and placed on Superfrost slides (Fisher Scientific, Pittsburgh, PA) for histopathological or immunohistochemical staining.

For H&E-staining procedure, the tissue sections were deparaffinized, stained with Harris hematoxylin (American MasterTech), differentiating solution (American MasterTech), Bluing solution (American MasterTech), and eosin Y (American MasterTech) before coverslipping. For AB-PAS staining, the tissue sections were deparaffinized, hydrated, treated with 3% acetic acid (American MasterTech), stained with Alcian blue (American MasterTech), treated with 0.5% periodic acid (American MasterTech) and Schiff reagents (American MasterTech), and coverslipped.

Histopathologic Assessment

Semi-quantitative histologic analysis of lung tissue sections stained with hematoxylin and eosin (H&E) was performed to determine the presence of cellular infiltrates, epithelial abnormalities, and mucous hyperplasia. The levels of inflammation and cellularity were evaluated in the alveolar, perivascular, bronchiolar, and pleural regions of the lungs for each rat using a previously described method (Silva, Anderson et al. 2015). Briefly, the severity and extent of pathology were determined using a severity score ranging from 0–3; 0 being normal and 3 being markedly inflamed in a particular region of the tissue (Table 1). The extent score was defined as the relative area of tissue observed with pathological changes. Extent scores included 0 (no lung involvement), 1 ($\leq$1/3rd lung involvement), 2 (>1/3rd to ½ involvement) and 3 (>1/2 involvement). The overall score of lung inflammation was determined by multiplying severity and extent scores (Overall score = severity × extent).

Immunohistochemistry

Paraffin-embedded sections were deparaffinized in three changes of toluene before hydration in graded ethanol. For antigen retrieval, the slides were then immersed in ethylene diamine tetra acetic acid (EDTA; Thermo Fisher Scientific, pH=8) in a decloaker at 123°C for 2 minutes, then 85°C for 10 seconds, and cooled for 45 minutes. After cooling, the sections were rinsed with PBST + 1000µl tween (PBST; Sigma Aldrich, St.Louis, MO) and treated with 3% hydrogen peroxide for 10 minutes to block endogenous peroxidase activity and prevent false-positive staining results. The sections were subsequently washed in PBST three times and treated with Protein Block (Dako, Carpinteria, CA) for 10 minutes to preclude non-specific binding of the primary antibody.

Afterward, the sections were incubated for 1 hour at room temperature with the anti-heme oxygenase -1 (anti HO-1, 1:1000 dilution, ab13243, AbCam) primary antibodies or PBS (for negative control slides). After washing with PBST, the sections were incubated with secondary antibodies, biotinylated affinity-purified goat anti-rabbit immunoglobulin G (Catalog no. K4403, Dako), for 30 minutes at room temperature. The sections were then rinsed with PBST three times and incubated in 3,3'-diaminobenzidine (DAB) and substrate (Catalog no. K3568, Dako) for 5 minutes. Harris's Hematoxylin (MasterTech, Inc., Lodi, CA) was used to counterstain the tissue sections before coverslipping with ClearMount^{TM} permanent mounting medium (Thermo Fisher Scientific). 3 sections/rat were observed using brightfield microscopy for qualitative analysis of HO-1 staining. Qualitative observation was done with no scoring scales used.

Gene Expression

TRI-Reagent® (Sigma Aldrich) was used to homogenize the right caudal lobe and preserve ribonucleic acid (RNA). RNA was extracted according to the manufacturer's instructions of an RNA isolation kit (Zymo Research, Irvine, CA) and converted to complementary deoxyribonucleic acid (cDNA) using Applied Biosystems' High-Capacity cDNA Reverse Transcription Kit (Foster City, CA). Gene-specific forward and reverse primer (0.2 μm), cDNA (2 μl/reaction), and SYBR Green nucleic acid stain (10 μl/reaction; Applied Biosystems) were used for quantitative polymerase chain reaction (qPCR). Using the ΔΔ-Ct method, gene expression of inflammatory markers interleukin-1β (*IL-1β), chemokine ligand-1 (CXCL-1),* tumor necrosis factor-α *(TNF-α),* and monocyte chemoattractant protein-1 *(MCP-1)* and oxidative stress marker

hemeoxygenase-1 *(HO-1)* were analyzed and standardized to the expression of the Ribosomal Protein S13 (RPS13) housekeeping gene (Livak and Schmittgen 2001). Gene primers were designed using Primer3 primer design software (Untergasser, Cutcutache et al. 2012).

Statistical Analysis

JMP 13 statistical software (Cary,NC) was used for the sample size calculation and data analysis. Outliers for BALF and histopathology data were determined by box plots. The cleaned data were then assessed for deviations from the assumptions of the Analysis of Variance (ANOVA) and transformed to meet the requirements of normality and equal variance as needed. ANOVAs and post-hoc Tukey's tests for each BALF endpoint were performed at a significance level of $p \leq 0.05$ to determine the main effects between the independent variables (post-exposure necropsy day and treatment). Semi-quantitative histopathological scores were assessed using a non-parametric Kruskal-Wallis test.

RESULTS

Aerosol Characterization

The powdered ZnO ENMs provided by the NIEHS were found to be endotoxin-free (Beltran-Huarac, Zhang et al. 2018). They were resuspended in nanopure water at a concentration of 1mg/ml.

Characterization results of the ZnO aerosol sampled during the 6-hour exposure period are shown in Table 3.2. Samples were taken during 6 hours inhalation exposure to ZnO on both exposure days. The results are shown as an average of samples taken

during the 6-hour inhalation exposure to ZnO. The mean mass concentration of ZnO was 4.23 ± 1.27 mg/m^3 standard deviation. XRF analysis of aerosolized ZnO determined mean zinc concentration of the aerosol to be 2.25 mg/m^3 ± 0.23 as standard deviation. Mass median aerodynamic diameter calculated from the cascade impactor samples was 3.57 µm. TEM images of the ZnO (Figure 3.2) aerosol in the exposure chamber demonstrated varying degrees of particle agglomeration.

BALF Analysis

BALF analysis demonstrated a significant ($p < 0.05$) difference between ZnO- and control-exposed animals at day 0 PE, with the former exhibiting almost two times the number of cells/mL relative to the latter (Figure. 3.3A). Notably, ZnO-exposed rats also had more nonviable BALF cells than their control-exposed counterparts on PE days 0, 1, and 7 (Figure. 3.3B; $p<0.05$). By day 21 PE, the number of nonviable cells was comparable between the exposure two groups. While the supernatant protein concentration was significantly increased at day 7 PE in animals exposed to ZnO compared to filtered air (Figure. 3.3C; $p <0.05$), it returned to the control level by day 21 PE. Significant increases were also observed in macrophages on day 0 PE (Figure. 3.3D; $p <0.05$), neutrophils on days 0 and 1 PE (Figure. 3.3E; $p <0.05$), and eosinophils on day 1 PE (Figure 3.3F; $p <0.05$). The number of inflammatory cells resolved by day 21 PE.

Histopathological Analysis

A normal pulmonary architecture of the airways and bronchiolar epithelium and the more distal alveoli was observed in sham control animals exposed only to filtered air.

Semi-quantitative histopathologic scores (table 4.1) of lung tissue sections demonstrated significant alveolar inflammation on days 1 and 7 following exposure to ZnO compared to filtered air control animals (Figure 4.4A; $p<0.05$). Inflammation was due to a large influx of macrophages (Figure 4.5), which peaked on day 7 and resolved by day 21 PE. The influx of macrophages also contributed to airway (bronchiolar) inflammation, which was significantly higher in ZnO-exposed rats compared to their control counterparts on day 7 PE (Figure. 4.4B; *p<0.05*).

Lung tissue sections stained with AB-PAS were analyzed for airway goblet cells between control and ZnO exposed animals. No significant differences were observed between the two groups.

Immunohistochemistry

Abundant positively-stained macrophages were observed in lung tissue sections of ZnO exposed animals stained with HO-1 antibody (Figure 6). Lung sections of ZnO-exposed rats necropsied on day 7 PE stained the greatest number of cells than observed in rats necropsied on days 0, 1, and 21 PE. Qualitative analysis showed minimal staining on day 0 and an absence of staining on day 21 PE in animals exposed to ZnO.

Gene Expression

qPCR analysis was used to examine gene expression for IL-1β, CXCL-1, TNF-α, HO-1 and MCP-1 cytokines on PE days 0,1,7 and 21. No statistically significant differences were observed between the ZnO- and control-exposed groups at any of the PE timepoints examined (Figure S1).

DISCUSSION

The objective of the present study was to optimize the ZnO inhalation exposure to evaluate the acute toxicity of ZnO nanoparticles in rats. We used a single, 6-hour exposure period and allowed the rats to recover for up to 21 days post exposure. A number of studies have used intratracheal instillation or oropharyngeal aspiration administration of ZnO nanoparticles to the lungs, while inhalation of ZnO nanomaterials provides a more realistic route for occupational and environmental exposure and use of a nose only system minimizes the deposition on fur and ingestion. Deposition and clearance patterns for particles following inhalation exposure in animals can be compared to the real world setting (Madl and Pinkerton 2009). Inhalation of ZnO from welding fumes, as well as exposure to ZnO in the manufacturing environment are primary concerns for ZnO toxicity (Adamcakova-Dodd, Stebounova et al. 2014). ZnO was fully characterized before and during the 6 hours exposure time period.

The United States OSHA recommends 8-hour time-weighted average (TWA) exposure limits of 5 mg/m^3 for ZnO fumes and respirable ZnO dust. In the present study, the mean mass concentration of ZnO ENM aerosol was 4.23 ± 1.27 mg/m^3 standard deviation. This concentration is similar to the maximum recommended TWA limit for ZnO fume and respirable ZnO dust. The average diameter of the ZnO ENMs provided by NIH was 50 nm. However, the cascade impactor showed a mass median

aerodynamic diameter of ZnO as 3.57 µm, suggesting extensive agglomeration of the ZnO particles in the experimental aerosol.

BAL findings collected from the respiratory tract can be helpful in detecting pulmonary inflammation (du Bois, Drent et al.). Measuring cell counts, cell differentials, and protein concentrations in BALF are means to determine pulmonary injury, inflammation, and vascular permeability (Yoshiura, Fujisawa et al. 2019). In our study, the total number of cells recovered in BALF increased significantly immediately following the end of exposure, with non-viable cells significantly greater in animals exposed to ZnO when compared to control animals on days 0, 1, and 7 days post-exposure. Macrophage and neutrophil in ZnO exposed animals were significantly increased immediately post-exposure (day 0), while neutrophils remained elevated along with an increase in eosinophil number 1 day -postexposure in ZnO exposed animals. A significant increase in protein concentration in BALF from day 0 to post-exposure day 7 suggested a mild, but statistically significant level of sustained injury and inflammation in animals exposed to ZnO. However, by 21 days post-exposure to ZnO, all biomarkers examined in this study had returned to levels similar to control. Morimoto et al exposed F344 rats to ZnO particles (2 and 10 mg/m^3) by inhalation for 4 weeks (6h/day, 5d/week), with necropsies at 3 days, 1 week, 1 month, 3 months, or 6 months following the last day of exposure (Morimoto, Izumi et al. 2016). Transient increases in total cell and neutrophil numbers were most notable in animals exposed to 10 mg/m^3. The exposure concentration and duration used was much higher than the current study. Wang et al used intratracheal instillation of ZnO (200, 400 and 800 µg/kg) to observe an increase in total cell number and total protein in BALF supernatant at 7

days following instillation (Wang, Li et al. 2017). However, intratracheal instillation

delivers a much higher dose at a faster rate than inhalation and is not an optimal

physiological administration route for approximating inhalation exposure over time (Madl

and Pinkerton 2009). In another study, Yoshiura et al. found that the total protein

concentration in BALF after intra tracheal instillation of ZnO in rats was significantly

higher than in rats exposed by inhalation (Yoshiura, Fujisawa et al. 2019).

Histopathologic analysis of lung tissue sections showed acute but transient

inflammation. An influx of macrophages in the alveolar regions was noted on days 1 and

7 PE. Similarly, bronchiolar inflammation was highest on day 7 PE. However, by 21

days PE, inflammation had resolved. A further study demonstrated no significant

changes in lung histology of mice 3 weeks following aerosol exposure to ZnO for 13

weeks (3.5 mg/m3, 4hrs/day) which indicates transient toxicity of ZnO in given dose

(Adamcakova-Dodd, Stebounova et al. 2014). In the present study,

immunohistochemical staining revealed HO-1-stained macrophages. HO-1 maintains

oxidant-antioxidant homeostasis. It is the marker of oxidative stress that is activated

during inflammation (Araujo, Zhang et al. 2012).

Inflammatory markers *IL-1β, CXCL-1, TNF-α, HO-1 and MCP-1* were measured

in lung homogenates. *IL-1β* and *TNF-α* are pro-inflammatory cytokines that activate

inflammatory cells (Elsabahy and Wooley 2013). The cytokines *MCP-1* and *CXCL-1*

attract monocytes and neutrophils, respectively, to sites of inflammation and injury

(Yadav, Saini et al. 2010, Sawant, Poluri et al. 2016). No significant changes were

observed in any of these biomarkers, but they have been identified in other studies of

ZnO exposure. In a study by Morimoto et al., *HO-1* in the BALF was increased

transiently in rats exposed to 10 mg/m^3 of ZnO for four weeks (6 hours/day, 5 days/week) than control animals (Morimoto, Izumi et al. 2016). It is possible that the lack of statistical differences in gene expression of ZnO- and control-exposed rats in the present study was due to the short 6-hr exposure duration. In the other studies (Adamcakova-Dodd et al. 2014; Morimoto et al. 2016) that reported significantly increased inflammatory markers, the exposure concentration/dose and/or duration was/were higher than the present study. Cumulatively, results from the present study suggest that a single 6-hr exposure to a ZnO nanoparticle aerosol has minimal inflammatory potential.

Future studies should be done to compare effects of acute and chronic exposures to aerosolized ZnO ENMs of different shapes and sizes to elucidate the potential toxicity of ZnO NPs in human health.

CONCLUSION

The present study suggests a single day inhalation exposure to ZnO NPs in rats results in acute but transient inflammation, as shown by a decrease in cell viability and an increase in macrophage and neutrophilic influx to the lungs (Figure3.3). These findings suggest that exposure to ZnO can result in short-term inflammation and transient lung injury. Statistically increased BALF protein levels at day 7 suggest persistent but mild injury with enhanced cell permeability. The cause for increased cell permeability could benefit from further study. Cumulatively these findings suggest ZnO ENM are not innocuous when inhaled into the lungs and cause short term lung injury and inflammation that resolves between 7 to 21 days post exposure.

ACKNOWLEDGEMENTS

TABLES

Table 3.1: Semi-quantitative histopathology severity scoring rubric

Score	Description
0	Normal. Thin alveolar walls, with very few free macrophages and no inflammatory cells in the lumen. Respiratory epithelium 1 cell-layer thick. Normal smooth muscle and submucosal layers. Vascular endothelium may contain some influxing monocytes and a few inflammatory cells. No visible particle agglomerates. Little/no cells at the pleura.
1	PMNs present in perivascular cuffs, airway submucosa, and alveolar airspaces. Influx of monocytes and macrophages into alveolar airspaces and monocytes in perivascular cuffs.
2	Presence of PMNs, macrophages, and monocytes in alveolar airspaces, along with cellular debris (exudate). Influxing cells in the perivascular cuffs and/or airway submucosa. Thickened alveolar walls.
3	Presence of PMNs and/or foamy and/or irregular macrophages (e.g., multi-nucleated, or exhibiting loss of membrane integrity) and cellular exudate in the airspaces.

Table 3.2. Aerosol characterization

Method	Endpoint (units)	Measurement
Gravimetry	Mass Concentration (mg ZnO/m^3)	4.23 ± 1.27
X-ray Fluorescence	Zn Mass Concentration (mg Zn/m^3)	2.25 ± 0.23
Cascade Impactor	Mass median aerodynamic diameter (μm)	3.57

FIGURES

Figure 3.1. Aerosol Nebulization System.

A 6-jet Collison nebulizer was used to aerosolize particles in suspension as aqueous

droplets. Water was removed by a heater and diffusion dryers. Krypton-85 beta

emission source neutralized particle charge. Dry particles were delivered to the nose-

only exposure chamber.

A   B
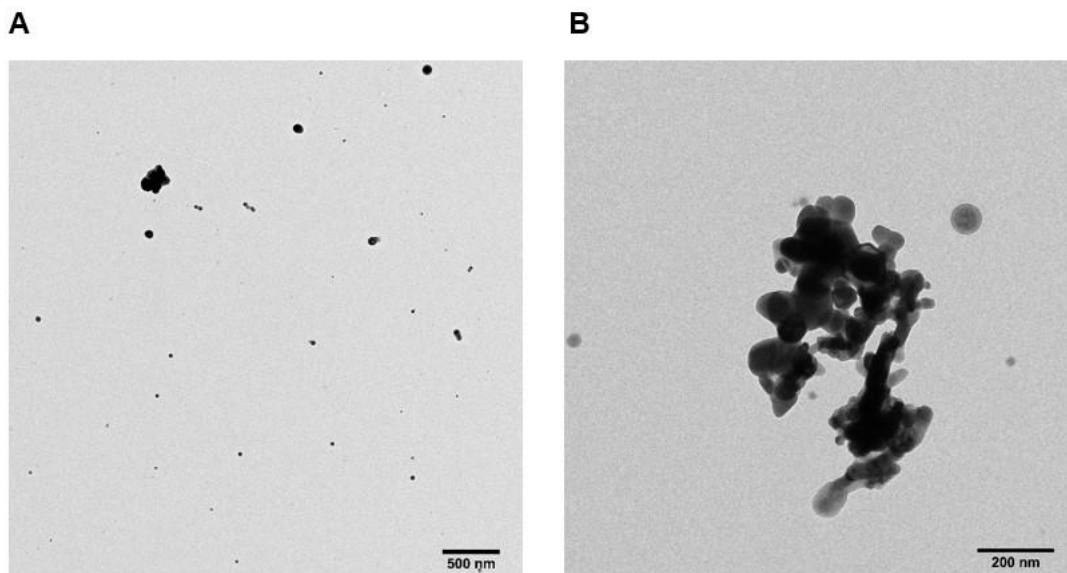
Figure 3.2. Morphology of aerosolized ZnO.

Transmission electron micrographs (TEM) of 50nm ZnO. Figure A is at a lower

magnification (scale bar, 500 nm). Figure B is at a higher magnification (scale bar, 200

nm) showing single and agglomerated ZnO nanoparticles.
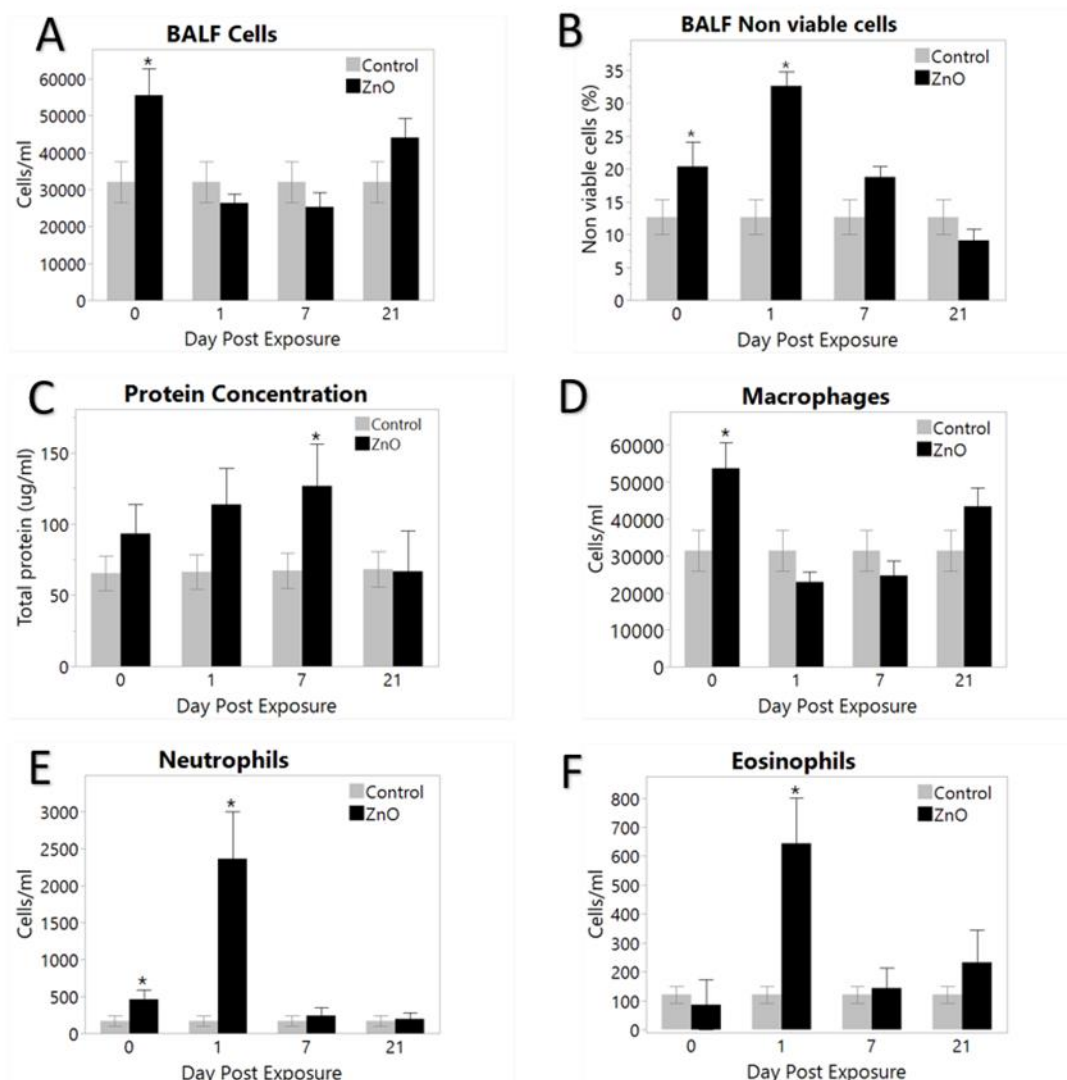
Figure 3.3. Total cells (A), Non-viable cells (B), Protein Concentration (C), Macrophages (D), Neutrophils (E) and Eosinophils (F) from bronchoalveolar lavage of rats exposed to filtered air (control) or ZnO. Rats were necropsied on days 0, 1, 7, or 21 post exposure. Statistical analysis was performed by ANOVA to compare between treatment groups. * = significant difference ($p < 0.05$) between control and ZnO exposed group for the same day.
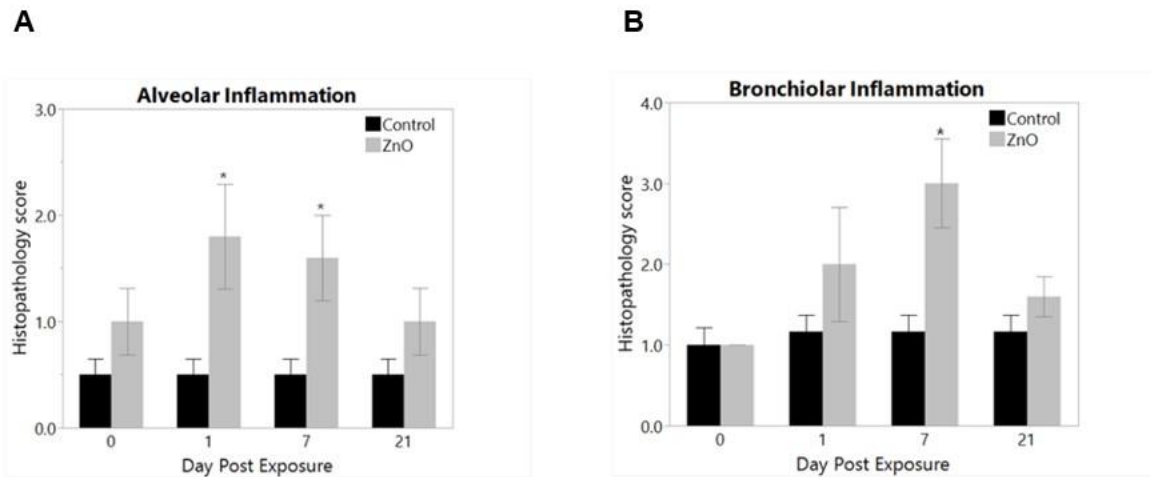
Figure 3.4. Histopathologic changes in alveolar and airway inflammation were noted on days 1 and 7 post exposure to ZnO.

Graphs show semi quantitative histopathology scores from alveolar (A) and bronchiolar (B) lung regions of rats exposed to filtered air (control) and ZnO by inhalation. Rats were necropsied on day 0, 1, 7, or 21 post exposure. Statistical analysis was performed by ANOVA to compare between treatment groups. * = significantly different ($p < 0.05$) between control and ZnO exposed group on same day.
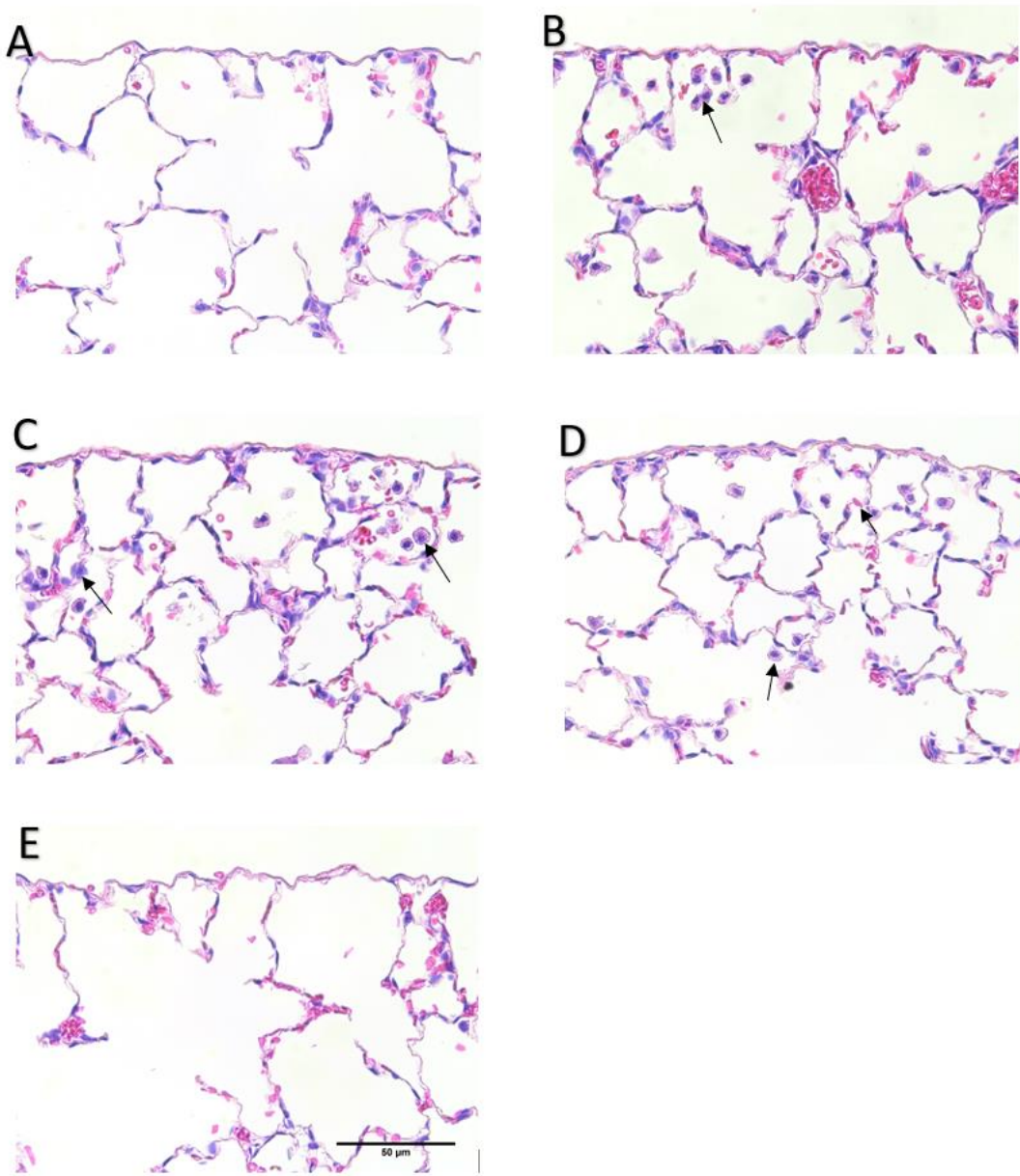
Figure 3.5. Representative brightfield microscopy subpleural images of H & E stained lung tissue sections at 40X magnification showing control animals (**A**) and animals exposed to ZnO on day 0 PE (**B**), day 1 PE (**C**), day 7 PE (**D**) and day 21 PE (**E**). Arrows indicate the presence of increased number of macrophages in the subpleural alveoli of the lungs. (Scale bar= 50μm)
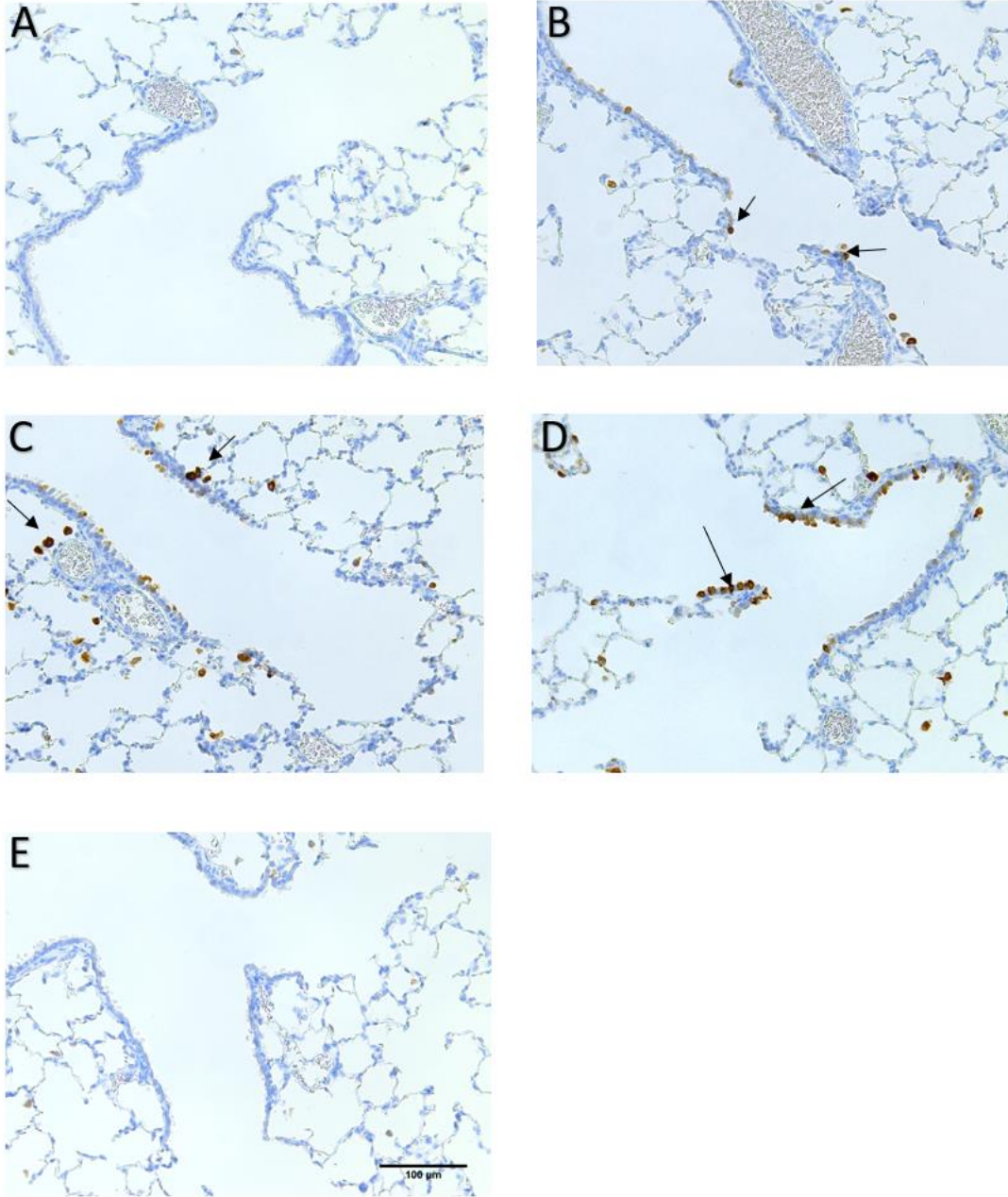
Figure 3.6. Lung tissue sections, at 20X magnification, immunochemically stained with anti-heme oxygenase-1 for control (**A**) post-exposure day 0 (**B**), day 1 (**C**), day 7 (**D**), day 21 (**E**). Arrows point to cells with heme oxygenase-1, a marker for oxidative stress. Positive cells appear to be both macrophages and selected Club cells of the terminal bronchioles. No positive staining was noted at 21 days post exposure to ZnO. (Scale bar= 100μm)
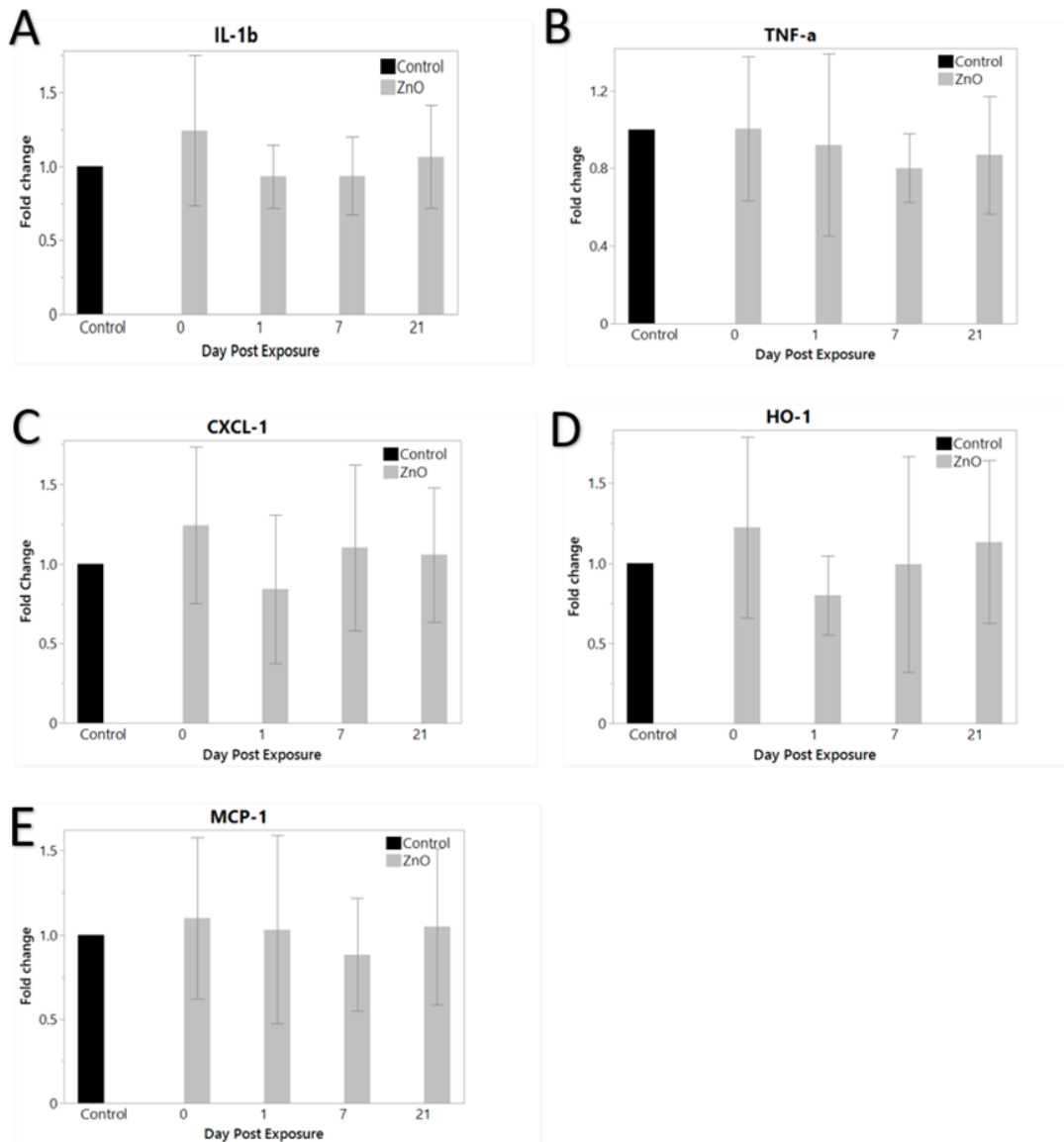
Figure 3.S.1. *IL-1β* (**A**), *TNFα* (**B**), *CXCL-1* (**C**), *HO-1* (**D**) and *MCP-1* (**E**) in lung homogenates in control animals and ZnO exposed animals. Rats were necropsied on days 0, 1, 7, or 21 post exposure. Statistical analysis was performed by ANOVA to compare between treatment groups. No significant differences were observed between control and ZnO exposed groups in any time point.

REFERENCES

1. Adamcakova-Dodd, Andrea, Larissa V Stebounova, Jong Sung Kim, Sabine U Vorrink, Andrew P Ault, Patrick T O'Shaughnessy, Vicki H Grassian, and Peter S Thorne. 2014. 'Toxicity assessment of zinc oxide nanoparticles using sub-acute and sub-chronic murine inhalation models', *Particle and fibre toxicology*, 11: 1-15.

2. Anderson, D. S., E. S. Patchin, R. M. Silva, D. L. Uyeminami, A. Sharmah, T. Guo, G. K. Das, J. M. Brown, J. Shannahan, T. Gordon, L. C. Chen, K. E. Pinkerton, and L. S. Van Winkle. 2015. 'Influence of particle size on persistence and clearance of aerosolized silver nanoparticles in the rat lung', *Toxicol Sci*, 144: 366-81.

3. Araujo, Jesus A, Min Zhang, and Fen Yin. 2012. 'Heme oxygenase-1, oxidation, inflammation, and atherosclerosis', *Frontiers in pharmacology*, 3: 119.

4. Areecheewakul, Sudartip, Andrea Adamcakova-Dodd, Brittany E Givens, Benjamin R Steines, Yifang Wang, David K Meyerholz, Nathanial J Parizek, Ralph Altmaier, Ezazul Haque, and Patrick T O'Shaughnessy. 2020. 'Toxicity assessment of metal oxide nanomaterials using in vitro screening and murine acute inhalation studies', *NanoImpact*, 18: 100214.

5. Beltran-Huarac, Juan, Zhenyuan Zhang, Georgios Pyrgiotakis, Glen DeLoid, Nachiket Vaze, and Philip Demokritou. 2018. 'Development of reference metal and metal oxide engineered nanomaterials for nanotoxicology research using high throughput and precision flame spray synthesis approaches', *NanoImpact*, 10: 26-37.

6. Buzea, Cristina, Ivan I Pacheco, and Kevin Robbie. 2007. 'Nanomaterials and nanoparticles: sources and toxicity', *Biointerphases*, 2: MR17-MR71.

7. Cho, Wan-Seob, Rodger Duffin, Sarah EM Howie, Chris J Scotton, William AH Wallace, William MacNee, Mark Bradley, Ian L Megson, and Ken Donaldson. 2011. 'Progressive severe lung injury by zinc oxide nanoparticles; the role of Zn2+ dissolution inside lysosomes', *Particle and fibre toxicology*, 8: 1-16.

8. Chuang, Hsiao-Chi, Hung-Tzu Juan, Chun-Nung Chang, Yuan-Horng Yan, Tzu-Hsuen Yuan, Jyh-Seng Wang, Hao-Cheng Chen, Yaw-Huei Hwang, Chii-Hong Lee, and Tsun-Jen Cheng. 2014. 'Cardiopulmonary toxicity of pulmonary exposure to occupationally relevant zinc oxide nanoparticles', *Nanotoxicology*, 8: 593-604.

9. De Matteis, Valeria. 2017. 'Exposure to inorganic nanoparticles: routes of entry, immune response, biodistribution and in vitro/in vivo toxicity evaluation', *Toxics*, 5: 29.

10. Dobrucka, Renata, Jolanta Dlugaszewska, and Mariusz Kaczmarek. 2018. 'Cytotoxic and antimicrobial effects of biosynthesized ZnO nanoparticles using of Chelidonium majus extract', *Biomedical microdevices*, 20: 1-13.

11. du Bois, Roland M, Marjolein Drent, Sonoko Nagai, and Paola Rottoli. 'THE CLINICAL UTILITY OF BRONCHOALVEOLAR LAVAGE CELLULAR ANALYSIS IN INTERSTITIAL LUNG DISEASE: AN ATS CLINICAL PRACTICE GUIDELINE'.

12. Elsabahy, Mahmoud, and Karen L Wooley. 2013. 'Cytokines as biomarkers of nanoparticle immunotoxicity', *Chemical Society Reviews*, 42: 5552-76.

13. Gao, Lifeng, Sheng-Tao Yang, Shaorui Li, Yuguang Meng, Haifang Wang, and Hao Lei. 2013. 'Acute toxicity of zinc oxide nanoparticles to the rat olfactory system after intranasal instillation', *Journal of Applied Toxicology*, 33: 1079-88.

14. Jacobsen, Nicklas Raun, Tobias Stoeger, Sybille Van Den Brûle, Anne Thoustrup Saber, Andrea Beyerle, Giulia Vietti, Alicja Mortensen, Józef Szarek, Hans Christian Budtz, and Ali Kermanizadeh. 2015. 'Acute and subacute pulmonary toxicity and mortality in mice after intratracheal instillation of ZnO nanoparticles in three laboratories', *Food and Chemical Toxicology*, 85: 84-95.

15. Jiang, Shengjie, Kaili Lin, and Ming Cai. 2020. 'ZnO nanomaterials: current advancements in antibacterial mechanisms and applications', *Frontiers in Chemistry*, 8.

16. Kao, Yi-Yun, Yi-Chun Chen, Tsun-Jen Cheng, Yin-Mei Chiung, and Pei-Shan Liu. 2012. 'Zinc oxide nanoparticles interfere with zinc ion homeostasis to cause cytotoxicity', *Toxicological sciences*, 125: 462-72.

17. Klein, Christoph L, Karin Wiench, Martin Wiemann, Lan Ma-Hock, Ben van Ravenzwaay, and Robert Landsiedel. 2012. 'Hazard identification of inhaled nanomaterials: making use of short-term inhalation studies', *Archives of Toxicology*, 86: 1137-51.

18. Kołodziejczak-Radzimska, Agnieszka, and Teofil Jesionowski. 2014. 'Zinc oxide—from synthesis to application: a review', *Materials*, 7: 2833-81.

19. Landsiedel, Robert, Lan Ma-Hock, Hans-Juergen Haussmann, Ben van Ravenzwaay, Martin Kayser, and Karin Wiench. 2012. 'Inhalation studies for the

safety assessment of nanomaterials: status quo and the way forward', *Wiley Interdisciplinary Reviews: Nanomedicine and Nanobiotechnology*, 4: 399-413.

20. Livak, Kenneth J, and Thomas D Schmittgen. 2001. 'Analysis of relative gene expression data using real-time quantitative PCR and the 2− ΔΔCT method', *methods*, 25: 402-08.

21. Madl, Amy K, and Kent E Pinkerton. 2009. 'Health effects of inhaled engineered and incidental nanoparticles', *Critical reviews in toxicology*, 39: 629-58.

22. Monsé, Christian, Olaf Hagemeyer, Monika Raulf, Birger Jettkant, Vera van Kampen, Benjamin Kendzia, Vitali Gering, Günther Kappert, Tobias Weiss, and Nadin Ulrich. 2018. 'Concentration-dependent systemic response after inhalation of nano-sized zinc oxide particles in human volunteers', *Particle and fibre toxicology*, 15: 1-11.

23. Morimoto, Yasuo, Hiroto Izumi, Yukiko Yoshiura, Taisuke Tomonaga, Takako Oyabu, Toshihiko Myojo, Kazuaki Kawai, Kazuhiro Yatera, Manabu Shimada, and Masaru Kubo. 2016. 'Evaluation of pulmonary toxicity of zinc oxide nanoparticles following inhalation and intratracheal instillation', *International journal of molecular sciences*, 17: 1241.

24. Pietroiusti, Antonio, Helene Stockmann-Juvala, Francesca Lucaroni, and Kai Savolainen. 2018. 'Nanomaterial exposure, toxicity, and impact on human health', *Wiley Interdisciplinary Reviews: Nanomedicine and Nanobiotechnology*, 10: e1513.

25. Saptarshi, Shruti R, Bryce N Feltis, Paul FA Wright, and Andreas L Lopata. 2015. 'Investigating the immunomodulatory nature of zinc oxide nanoparticles at sub-

cytotoxic levels in vitro and after intranasal instillation in vivo', *Journal of nanobiotechnology*, 13: 1-11.

26. Sawant, Kirti V, Krishna Mohan Poluri, Amit K Dutta, Krishna Mohan Sepuru, Anna Troshkina, Roberto P Garofalo, and Krishna Rajarathnam. 2016. 'Chemokine CXCL1 mediated neutrophil recruitment: role of glycosaminoglycan interactions', *Scientific reports*, 6: 1-8.

27. Seaton, Anthony, Lang Tran, Robert Aitken, and Kenneth Donaldson. 2010. 'Nanoparticles, human health hazard and regulation', *Journal of the Royal Society Interface*, 7: S119-S29.

28. Siddiqi, Khwaja Salahuddin, Aziz ur Rahman, and Azamal Husen. 2018. 'Properties of zinc oxide nanoparticles and their activity against microbes', *Nanoscale research letters*, 13: 1-13.

29. Silva, R. M., D. S. Anderson, J. Peake, P. C. Edwards, E. S. Patchin, T. Guo, T. Gordon, L. C. Chen, X. Sun, L. S. Van Winkle, and K. E. Pinkerton. 2016. 'Aerosolized Silver Nanoparticles in the Rat Lung and Pulmonary Responses over Time', *Toxicol Pathol*, 44: 673-86.

30. Silva, Rona M, Donald S Anderson, Lisa M Franzi, Janice L Peake, Patricia C Edwards, Laura S Van Winkle, and Kent E Pinkerton. 2015. 'Pulmonary effects of silver nanoparticle size, coating, and dose over time upon intratracheal instillation', *Toxicological sciences*, 144: 151-62.

31. Singh, Sanjiv. 2019. 'Zinc oxide nanoparticles impacts: cytotoxicity, genotoxicity, developmental toxicity, and neurotoxicity', *Toxicology mechanisms and methods*, 29: 300-11.

32. Subramaniam, Vimala Devi, Suhanya Veronica Prasad, Antara Banerjee, Madhumala Gopinath, Ramachandran Murugesan, Francesco Marotta, Xiao-Feng Sun, and Surajit Pathak. 2019. 'Health hazards of nanoparticles: understanding the toxicity mechanism of nanosized ZnO in cosmetic products', *Drug and chemical toxicology*, 42: 84-93.

33. Swain, Partha S, Somu BN Rao, Duraisamy Rajendran, George Dominic, and Sellappan Selvaraju. 2016. 'Nano zinc, an alternative to conventional zinc as animal feed supplement: A review', *Animal Nutrition*, 2: 134-41.

34. Untergasser, Andreas, Ioana Cutcutache, Triinu Koressaar, Jian Ye, Brant C. Faircloth, Maido Remm, and Steven G. Rozen. 2012. 'Primer3--new capabilities and interfaces', *Nucleic acids research*, 40: e115-e15.

35. Vandebriel, Rob J, and Wim H De Jong. 2012. 'A review of mammalian toxicity of ZnO nanoparticles', *Nanotechnology, science and applications*, 5: 61.

36. Vogel, Ulla, and Flemming R Cassee. 2018. "dose-dependent ZnO particle-induced acute phase response in humans warrants re-evaluation of occupational exposure limits for metal oxides." In.: BioMed Central.

37. Wang, Dejun, Haibo Li, Zihong Liu, Jingyang Zhou, and Tianliang Zhang. 2017. 'Acute toxicological effects of zinc oxide nanoparticles in mice after intratracheal instillation', *International journal of occupational and environmental health*, 23: 11-19.

38. Wang, Ping, Lin Zhang, Yanxia Liao, Juan Du, Mengying Xu, Wen Zhao, Shuxian Yin, Guilan Chen, Yu Deng, and Yiran Li. 2020. 'Effect of intratracheal instillation

of ZnO nanoparticles on acute lung inflammation induced by lipopolysaccharides in mice', *Toxicological sciences*, 173: 373-86.

39. Wiesmann, Nadine, Wolfgang Tremel, and Juergen Brieger. 2020. 'Zinc oxide nanoparticles for therapeutic purposes in cancer medicine', *Journal of Materials Chemistry B*, 8: 4973-89.

40. Yadav, Amita, Vandana Saini, and Sarika Arora. 2010. 'MCP-1: chemoattractant with a role beyond immunity: a review', *Clinica chimica acta*, 411: 1570-79.

41. Yoshiura, Yukiko, Yuri Fujisawa, Taisuke Tomonaga, Hiroto Izumi, Takako Oyabu, Toshihiko Myojo, Masaru Kubo, Manabu Shimada, and Yasuo Morimoto. 2019. 'Comparison of Responses in Rat Lung Following Inhalation and Intratracheal Administration of Nanoparticles.' in, *In Vivo Inhalation Toxicity Screening Methods for Manufactured Nanomaterials* (Springer).

CHAPTER 4

Pulmonary Response in Sprague Dawley Rats Following a Single Exposure to Aerosolized Graphene Oxide

ABSTRACT

Graphene oxide (GO) is a two-dimensional (2-D) planar nanomaterial which is widely used in drug delivery systems, biosensors, medical imaging, electronics, and energy storage. With increased commercial use, there may be a potential risk for the inhalation of these aerosolized planar 2D nanomaterials under special conditions to affect human health. GO nanoparticles have been reported to cause toxic effects by dermal and oral routes of exposure. However, limited information is available on the inhalation of GO, which could represent a route of exposure, should GO suspensions become aerosolized. Therefore, the purpose of this study was to examine short-term inhalation of 2-D GO suspensions for acute and transient inflammation of the respiratory tract. Male and female Sprague Dawley rats eight weeks of age were randomly assigned to sham control (n=12) or GO exposed groups (n=24). Exposure to aerosolized GO (400nm x 400nm) was for a single 6-hour period in a nose-only inhalation chamber to attain maximal exposure. Particle aerosol was characterized by gravimetric and cascade impactor measurements, along with transmission electron microscopy. Animals were examined 1 and 7 days post-exposure. Bronchoalveolar lavage (BAL) was collected from the right lung to assess protein concentration, cell number, viability, and cell differentials. The left lung was inflation-fixed, embedded and sectioned for histopathological analysis. The caudal lobe from the right lung was used for the analysis of selected inflammatory gene expression. Aerosolized GO mass was 2.28 +/- 0.73 mg/m^3. Mass median aerodynamic diameter of the aerosolized GO was 2.37 μm. No statistically significant differences were observed for cell differentials, cell number, cell viability or protein concentration between the control and exposed animals

for both male and female rats. There were no significant histopathological differences or gene expression of inflammatory markers. Inhalation of aerosolized GO demonstrated no observed pulmonary toxicity in rats at the concentration used in this study following a single day of exposure.

INTRODUCTION

The exponential growth of nanotechnology has introduced a diverse number of engineered nanomaterials (ENMs) to multiple commercial markets. ENMs are used widely in electronics, agriculture, textiles, medicine and cosmetics. Graphene, a relatively new nanomaterial, is a planar 2-dimensional carbon-based product that exhibits unique electronic, optical, magnetic and thermal properties (Zhou and Liang 2014). Graphene is a good conductor of heat and electricity (Park, Lee et al. 2015). However, it has been found that micromechanical cleavage of bulk graphene for mass production results in low productivity which is not suitable for large scale applications. This has led to the conversion of graphene to graphene oxide (Paredes, Villar-Rodil et al. 2008). Graphene oxide (GO) is an oxidized derivative of graphene. The chemical structure of GO contains oxygen functional groups such as epoxy, hydroxyl, carbonyl and carboxylic forms (Gao 2015). These functional groups stabilize GO sheets in water and other solvents, thus making it easier to handle (Paredes, Villar-Rodil et al. 2008, Rhazouani, Gamrani et al. 2021). Interestingly, GO can be reduced to mimic pristine graphene. Reduced graphene oxides (rGO) have less oxygen groups and possess properties similar to pristine graphene (Pei and Cheng 2012).

Oxygen functional groups contribute to the use of GO in photo catalyzers, photonics, electronics, composites, electron field emission and energy storage devices (Singh, Herrera et al. 2018). Graphene-based materials (GBM) are also used in the biomedical and biotechnological fields in cancer therapy as vehicles for drug/gene delivery, scaffolds for tissue engineering, cell imaging and antibacterial substrates (Zhou and Liang 2014). GO can also be used as electrode material in batteries due to

their high surface area. The fluorescent properties of GBM are also utilized in biosensor and disease diagnosis. They can detect proteins and DNA and help in diagnosing HIV, human cervical cancer and human breast cancer cells (Song, Chen et al. 2011). Photothermal activity of graphene is used for enhancing the safety and efficacy of chemotherapeutics in cancer treatment. (Zhou and Liang 2014). The large-scale production and application of graphene has raised concerns regarding its toxicity.

Increased applications of GBM has elevated the risk of exposure to humans and the environment during the manufacture and handling of these materials. Workers handling graphene can be exposed via inhalation dispersed in the air (Pecoraro, D'Angelo et al. 2018). However, the relative toxicity of GBM is less studied than other carbon-based products, such as carbon nanotubes (Pecoraro, D'Angelo et al. 2018). There are 250 scientific publications reporting graphene toxicity but only 70 publications include in vivo toxicity in laboratory animals (Pelin, Sosa et al. 2018). Therefore, there remain concerns regarding the safety of GBM. There is no occupational exposure limit (OEL) currently available for the family of graphene nanomaterials including GO/rGO (Di Cristo, Grimaldi et al. 2020). Exposure of humans to nanomaterials in the occupational setting is primarily through inhalation. Studies have shown that the air in production facilities contain graphene nanoforms that could present a risk to worker's health (Lee, Han et al. 2016, Spinazzè, Cattaneo et al. 2016, Park, Bleeker et al. 2017). Thus, OEL and other regulatory parameters are critical to ensure the occupational safety of workers.

Inhalation studies are more comparable to human exposure and are critical in the safety assessment of environmental and occupational exposures (Landsiedel, Ma-Hock

et al. 2012). There have been few inhalation studies performed to assess the toxicity of a number of GBMs following acute exposure (Han, Kim et al. 2015). No inhalation study has been done to examine the pulmonary response following acute exposure to rGO. Although, GO and rGO are from the same graphene family, their biological responses can be different due to their unique physicochemical properties (Mittal, Kumar et al. 2016). Therefore, we selected rGO to study.

To better understand the toxicity of rGO after acute inhalation exposure, Sprague Dawley rats were exposed to aerosols of rGO in a nose-only inhalation chamber for 6 hours and allowed to recover for 1 day and 7 days. Pulmonary responses were assessed by bronchoalveolar lavage fluid, lung histology and gene expression studies.

MATERIALS AND METHODS

Reduced Graphene Oxide Nanomaterial

Reduced graphene oxide (rGO) 400nm x 400 nm in diameter was provided by the National Institutes of Health (NIH) Health Effects of Nanomaterials Consortium in aqueous dispersion. Physicochemical characterization of the ENMs was performed by the T.H. Chan School of Public Health-National Institute of Environmental Health Sciences (HSPH-NIEHS) Nanosafety Center at Harvard University. rGO was synthesized using a modified Hummer's method and liquid phase exfoliation. Elemental analysis was determined by X-ray photoelectron spectroscopy. The crystalline structure and imaging was analyzed by Raman spectroscopy and transmission electron microscopy (TEM) respectively.

Nose-only Inhalation Exposure System

A rGO ENM aerosol was generated to facilitate a more realistic inhalation exposure scenario. The aerosol nebulization system (Figure 1) was designed at the University of California, Davis, Center for Health and the Environment (Anderson, Patchin et al. 2015, Silva, Anderson et al. 2016). Briefly, a BGI 6-jet Collison nebulizer (Waltham, Massachusetts) was used to aerosolize ENM suspensions as fine droplets. The suspension in the nebulizer was constantly stirred and kept on ice to reduce ENM aggregation. An oil-free compressor (California Air Tools, San Diego, California) was used to generate compressed air for the nebulizer. The compressed air was dehumidified using compressed air dryers (Wilkerson, Richland, MI) and filtered with a Motor Gard M-610 filter (Motor Gard, Manteca, California) to aerosolize the suspension. The suspension droplets were passed through a custom-fabricated heater and two diffusion dryers (TSI, Shoreview, Minnesota) to remove water and create dry particle aggregates. The aggregates were passed through a Krypton-85 charge neutralizer to reduce static charge and minimize agglomeration of the dried particles entering the 48-port nose-only exposure system. Steel piping connected all the components of the system. The pressure in the nebulizer was 20 psi, while the exposure chamber was at 0.5 to 1 inch of negative water pressure compared to the room air pressure.

During the time of exposure, each rat was housed in a cylindrical nose-only exposure tube (Teague Enterprises, Woodland, California). The tubes were connected to the exposure system for the rGO aerosol exposure or placed on a table in the same room as the exposure system for the filtered air (control) exposure.

Exposure Characterization

Temperature and relative humidity of the exposure system were monitored during the 6-hour exposure period. Four mass concentration, three TEM, three x-ray fluorescence (XRF), and two cascade impactor samples were collected. Total mass concentration was determined by gravimetric measurement of 25-mm Pallflex membrane filters (TX40HI20-WW, Pall Life Sciences, Port Washington, New York). These filters were placed in a portable sampler connected to a nose-only port for sampling of the aerosol within the inhalation system at 1 L/min for 15 minutes.

An eight-stage Mercer style cascade impactor was used to determine the particle agglomerate size range. A 25-mm Pallflex membrane filter was used on each stage to collect particles at a flow rate of 1 L/min for 30 minutes. For visualization of rGO ENM by transmission electron microscopy (TEM), aerosolized samples were collected on a formvar-carbon film supported on a 400-mesh copper grid (3 mm in diameter; Ted Pella, Reading, California). Images were acquired using a Phillips CM-12 TEM operating at 120 kV (Anderson, Patchin et al. 2015).

Animal Protocol

The inhalation study was conducted in agreement with regulations set by University of California, Davis Institutional Animal Care and Use Committee (IACUC) institutional animal care and use committee under NIH guidelines. Male (n=12) and female (n=12) Sprague Dawley rats 12 weeks of age were purchased from Envigo Laboratory (Fremont, California). Prior to exposure, the animals were housed two per cage, with Purina 5001 regular laboratory rodent diet (Newco Distributors, Rancho Cucamonga, California) and water provided ad libitum. Rats were acclimated in nose-

only exposure tubes daily for one week prior to the experiment. The residence time in the tubes was gradually increased to acclimate rats to a single 6-hour exposure to filtered air or aerosolized rGO.

The animals were randomly assigned to two treatment group and two control groups with 6 males and 6 females/treatment group and 3 males and 3 females/timepoint/control group.

Necropsy, Bronchoalveolar lavage and Tissue collection

At necropsy performed on days 1 and 7 post exposure to aerosolized rGO, an overdose of Beuthanasia-D (7.5 ml/kg) (MWI Veterinary Supply Company, Los Angeles, CA, 90074) was used for euthanasia. Control animals, exposed to filtered air, were necropsied on day 2 post exposure. Cardiac puncture was performed, and blood was collected in a 12-ml round bottom tube for centrifugation at 2000 revolutions per min (rpm) for 15 min. The resulting blood plasma was collected and stored at -80°C for later use.

Following blood collection, the trachea was cannulated, and the left main bronchus was clamped. The right middle, caudal and accessory lobes were lavaged, flash-frozen, and stored at -80°C for later use. Briefly, the right lobes were lavaged three times with a single 7-ml aliquot of sterile phosphate-buffered saline (PBS Sigma Aldrich, St. Louis, MO) in a 12-ml syringe for collection of bronchoalveolar lavage fluid (BALF). The BALF was collected in a 15-ml round bottom tube and centrifuged for 15 min at 2000 rpm and 4°C. The resulting BALF supernatant was decanted and stored for further analysis, while the cell pellet was resuspended in 2 ml of sterile PBS. Trypan blue was

used to count the total viable and non-viable cells. A 100-µl aliquot of resuspended cells was used to prepare cytospin slides for cell differentials.

The left lung was unclamped and inflation-fixed at a hydrostatic pressure of 30 cm with 4% paraformaldehyde for 1 hour. The fixed lung was subsequently stored in 4% paraformaldehyde for 24 hours before transfer to 70% ethanol.

Histological Analysis

The left lung was cut into four transverse slices (cranial to caudal), dehydrated in a graded series of ethanol (70%, 95% and 100%), placed through three series of toluene and paraffin, and embedded in paraffin in cassettes. The paraffin sections were cut to 5-µm thickness using a microtome (HM 355, Microm, Walldorf, Germany) and placed on Superfrost slides (Fisher Scientific, Pittsburgh, PA) for histopathologic or immunohistochemical staining.

For H&E-staining tissue sections were deparaffinized, stained with Harris hematoxylin (American MasterTech), differentiating solution (American MasterTech), Bluing solution (American MasterTech), and eosin Y (American MasterTech) before coverslipping.

Histopathologic Assessment

Semi-quantitative histologic analysis of lung tissue sections stained with hematoxylin and eosin (H&E) was performed to determine the presence of cellular infiltrates, epithelial abnormalities, and mucous hyperplasia. The levels of inflammation and cellularity were evaluated in the alveolar, perivascular, bronchiolar, and pleural regions of the lungs for each rat using a previously described method (Silva, Anderson

116

et al. 2015). 5 sections per rat were evaluated. Briefly, the severity and extent of pathology were determined using a severity score ranging from 0–3; 0 being normal and 3 being markedly inflamed in a particular region of the tissue (Table 4.1). The extent score was defined as the relative area of tissue observed with pathological changes. Extent scores included 0 (no lung involvement), 1 ($\leq 1/3^{rd}$ lung involvement), 2 ($>1/3^{rd}$ to ½ involvement) and 3 ($>1/2$ involvement). The overall score of lung inflammation was determined by multiplying severity and extent scores (Overall score = severity × extent).

Gene Expression

TRI-Reagent® (Sigma Aldrich) was used to homogenize the right caudal lobe and preserve ribonucleic acid (RNA). RNA was extracted according to the manufacturer's instructions of an RNA isolation kit (Zymo Research, Irvine, CA) and converted to complementary deoxyribonucleic acid (cDNA) using Applied Biosystems' High-Capacity cDNA Reverse Transcription Kit (Foster City, CA). Gene-specific forward and reverse primer (0.2 μm), cDNA (2 μl/reaction), and SYBR Green nucleic acid stain (10 μl/reaction; Applied Biosystems) were used for quantitative polymerase chain reaction (qPCR). Using the ΔΔ-Ct method, gene expression of inflammatory markers interleukin-1β (*IL-1β*), chemokine ligand-1 *(CXCL-1),* tumor necrosis factor-α *(TNF-α),* and monocyte chemoattractant protein-1 *(MCP-1)* and oxidative stress marker hemeoxygenase-1 *(HO-1)* were analyzed and standardized to the expression of the Ribosomal Protein S13 (RPS13) housekeeping gene (Livak and Schmittgen 2001). Gene primers were designed using Primer3 primer design software (Untergasser, Cutcutache et al. 2012).

Statistical Analysis

JMP 13 statistical software (Cary, NC) was used for the sample size calculation and data analysis. Outliers for BALF and histopathology data were determined by box plots. The cleaned data were then assessed for deviations from the assumptions of the Analysis of Variance (ANOVA) and transformed to meet the requirements of normality and equal variance as needed. ANOVAs and post-hoc Tukey's tests for each BALF endpoint were performed at a significance level of $p \leq 0.05$ to determine the main effects between the independent variables (post-exposure necropsy day and treatment).

RESULTS

Aerosol Characterization

Elemental analysis of rGO provided by NIEHS yielded 78% carbon and 22% oxygen. 0 bacteria/mg was detected in the suspension.

Samples were taken during the 6 hour exposure period to rGO and the results were expressed as an average of samples taken. The mean mass concentration of rGO was 2.28 ± 0.73 mg/m^3 standard deviation (Table 4.2). The mass median aerodynamic diameter was 2.37 µm (Table 4.2). Figure 2 shows the TEM images of rGO images in the exposure chamber.

BALF Analysis

The results from analyzing BAL cells did not show any statistically significant difference between the exposed and control group. There were no differences in total cells or cell viability between the BAL of animals exposed to GO and FA. Similarly, the

cell differential analysis did not show any significant changes in macrophages, neutrophils, eosinophils or lymphocytes between the control and GO exposed animals at 1 or 7 days post-exposure. Protein concentration in BAL supernatant did not show any significant differences between the two groups of animals at 1 or 7 days post-exposure. Data are pooled as no differences between male and female animals were observed.

Histopathologic Analysis

Histopathologic analysis of the lung tissue sections did not show any pathological changes between the GO exposed group of animals and animals exposed to FA. A semiquantitative analysis resulted in 0 scores for all animals, data not shown.

Gene Expression

Expression of *IL-1β, TNF-α, CXCL-1, MCP-1* and *HO-1* were analyzed on day 1 and day 7 post exposure to GO. No statistically significant changes were observed between animals exposed to GO and FA.

Discussion

The exponential use of rGO has increased the risk of human exposure but there are limited inhalation experiments performed to evaluate its toxicity (Sanchez, Jachak et al. 2012). The present acute inhalation study did not find any evidence for significant toxicity of rGO based on the analyses of BALF, lung histology or gene expression. Cell counts, cell differentials and protein analysis of BALF were analyzed to determine pulmonary injury, inflammation and vascular injury. No statistically significant differences were observed in total cells, cell viability, macrophages, neutrophils, eosinophils or protein concentration in BALF recovered from rats exposed to rGO on

post-exposure time points 1 and 7 days, compared to control animals exposed to filtered air only. Similarly, histological assessment of H&E-stained lung tissue sections showed a normal pulmonary architecture of the airways and bronchiolar epithelium lining all airways. The alveolar lung parenchyma also demonstrated no significant changes due to exposure to rGO. No statistically significant changes were observed between male and female rats.

In our experiment, we chose an inhalation study to represent maximal exposure mimicking an occupational and workplace scenario for human exposure to rGO (Heitbrink, Lo et al. 2015). We exposed rats in a nose-only inhalation chamber for 6 hours and allowed a recovery period of 1 day and 7 days post-exposure. The 400 x 400 nm rGO provided by NIEHS was fully characterized before and during the experiment. In the present study, mean mass concentration of rGO was 2.28 ± 0.73 mg/m^3 standard deviation. No occupational exposure limit has been established for graphene-based materials as limited data are available on airborne graphene concentrations on workplace. However, airborne concentration of graphene nanoplatelets during the collection of products from the discharge vessels at a single manufacturing site was 2.27 and 0.017 mg/m^3 (Heitbrink, Lo et al. 2015). This concentration range is comparable to the concentration of rGO we used in our study.

Our study found little toxicity following exposure this is comparable to a study done by (Ma-Hock, Strauss et al. 2013), no significant toxicity was seen when rats were exposed to similar concentrations of graphene nanomaterials (0.5 and 2.5 mg/m^3) in a nose-only inhalation chamber for 6 hours/ day for 5 consecutive days. However, exposure to 10 mg/m^3 of graphene resulted in an increase in total cells, neutrophils and

lymphocytes in BALF, but without any statistically significant changes. Similar results were observed in another nose-only inhalation study where rats were exposed to GO (0.76, 2.60 or 9.78 mg/m^3) for 6 hours/day for 5 days followed by necropsy of animals on day 1, 3 and 21 post-exposure. No significant effects were observed in BALF, histological analysis or BAL-cytokines (Kim, Jo et al. 2018). In a more recent study, mice were injected with GO (5, 10, 50 and 100 mg/kg) into a tail vein once daily for 7 days. Low concentrations of GO (5 and 10 mg/kg) did not induce any inflammatory changes in the lung whereas higher concentrations (50 and 100 mg/kg) induced histopathological lung changes demonstrated by alveolar septa thickening and inflammatory cells infiltration. They concluded pulmonary toxicity exerted by GO is dose-dependent for this route of exposure (Zhang, Ouyang et al. 2021). Intratracheal instillation of graphene nanoplatelets resulted in a pulmonary inflammation demonstrated by inflammatory cytokines in BAL, which were highest on day 14 and decreased by day 28(Park, Lee et al. 2015). Differences in the results can be explained by different route of exposure in these studies. Tail vein injection and intratracheal instillation delivers a much higher dose than nose-only inhalation. When ENMs are not delivered in a natural way, the distribution in the lungs will be different compared to the inhalation route (Madl and Pinkerton 2009). A different inflammatory response was observed in mice who were exposed to either GO or rGO, most likely due to the overall total mass delivered to the lungs. Intratracheal instillation of 18, 54 and 162 µg/mouse resulted in strong acute inflammation with changes in lung histology in mice exposed to GO, whereas minimal inflammation was observed in mice exposed to rGO (Bengtson, Knudsen et al. 2017). So, the less inflammatory response exerted by rGO can likely be

explained by the absence of a high hydroxyl-functionalization (O-H) group, an important factor for acute inflammation, found in GO (Bengtson, Knudsen et al. 2017).

In summary, the present study suggests single 6-hour exposure to rGO aerosols in a given dose does not induce any inflammatory reaction. Future studies need to be done to evaluate the long term toxicity of rGO and help in establishing OEL.

CONCLUSION

The results of this study suggest a single inhalation exposure to aerosols of rGO (400 x 400 nm) for 6 hours does not exert any toxic effects in rats at a dose 2.28 ± 0.73 mg/m^3. This indicates that rGO at this selected dose is rather inert. However, more studies with different concentrations are needed to confirm the toxic levels of rGO and to establish the OEL.

ACKNOWLEDGEMENTS

TABLES

Table 4.1: Semi-quantitative histopathology severity scoring rubric

Score	Description
0	Normal. Thin alveolar walls, with very few free macrophages and no inflammatory cells in the lumen. Respiratory epithelium 1 cell-layer thick. Normal smooth muscle and submucosal layers. Vascular endothelium may contain some influxing monocytes and a few inflammatory cells. No visible particle agglomerates. Little/no cells at the pleura.
1	PMNs present in perivascular cuffs, airway submucosa, and alveolar airspaces. Influx of monocytes and macrophages into alveolar airspaces and monocytes in perivascular cuffs.
2	Presence of PMNs, macrophages, and monocytes in alveolar airspaces, along with cellular debris (exudate). Influxing cells in the perivascular cuffs and/or airway submucosa. Thickened alveolar walls.
3	Presence of PMNs and/or foamy and/or irregular macrophages (e.g., multi-nucleated, or exhibiting loss of membrane integrity) and cellular exudate in the airspaces.

Table 4.2. Aerosol characterization

| Method	Endpoint (units)	Measurement
Gravimetry	Mass Concentration (mg rGO/m^3)	2.28 ± 0.73
Cascade Impactor	Mass median aerodynamic diameter (μm)	2.37

FIGURES

**Figure 4.1. Aerosol Nebulization System.**

A 6-jet Collison nebulizer was used to aerosolize particles in suspension as aqueous droplets. Water was removed by a heater and diffusion dryers. Krypton-85 beta emission source neutralized particle charge. Dry particles were delivered to the nose-only exposure chamber.
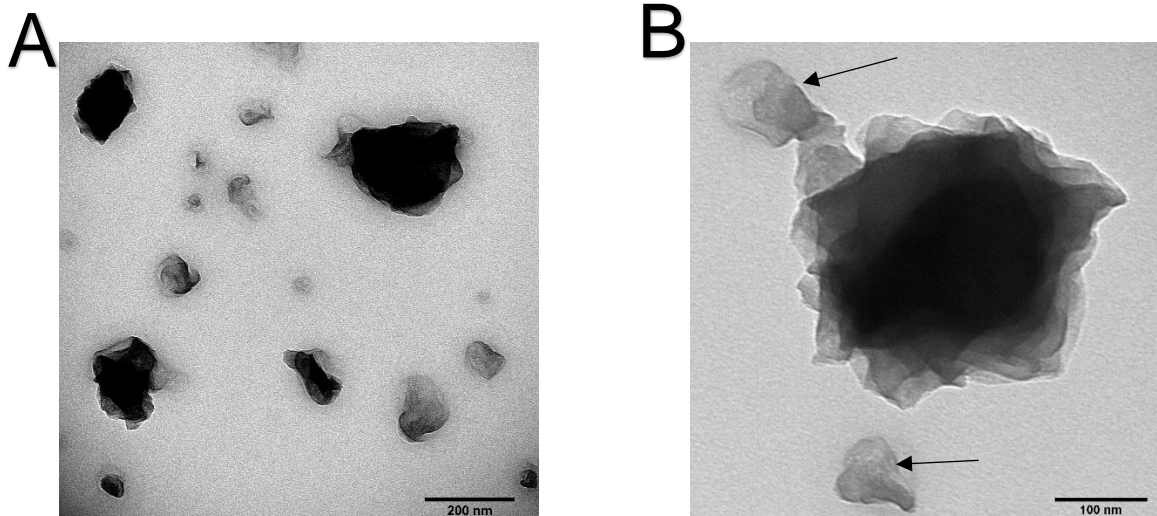
Figure 4.2. Morphology of aerosolized rGO

Transmission electron micrographs (TEM) of aerosolized 400 x 400 nm GO. Figure A is at a lower magnification (scale bar, 200 nm). Figure B is at a higher magnification (scale bar, 100 nm) showing the formation of a single agglomerated GO nanoparticle following aerosolization prior to inhalation. Please note the presence of individual planar 2-D GO nanoparticles (arrow) in this agglomerate.
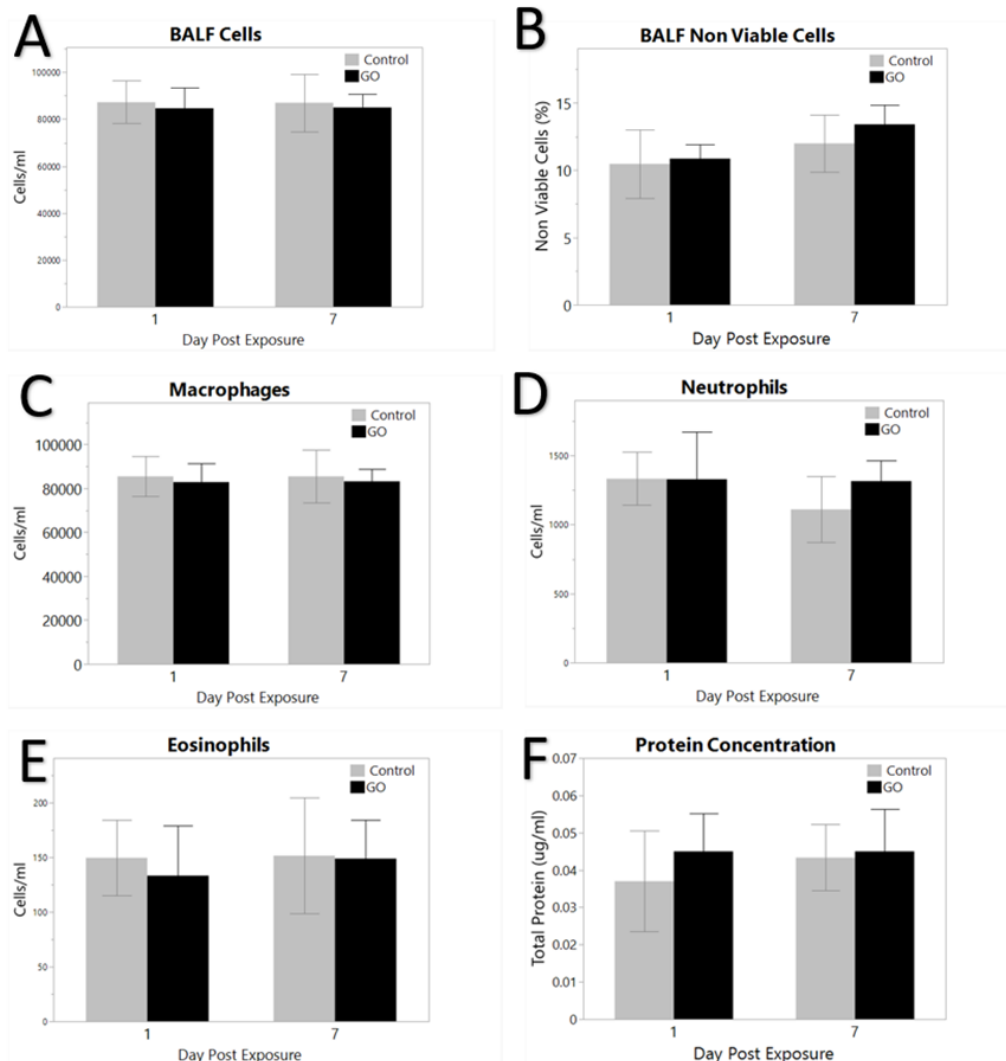
Figure 4.3. Total cells (A), Non-viable cells (B), Macrophages (C), Neutrophils (D), Eosinophils (E) and Protein Concentration (F) from bronchoalveolar lavage of rats exposed to filtered air (control) or rGO. Rats were necropsied on days 1 and 7 post exposure. Statistical analysis was performed by ANOVA to compare between treatment and control group. (n=6 control rats/time point and n=12 rGO exposed rats/time point).
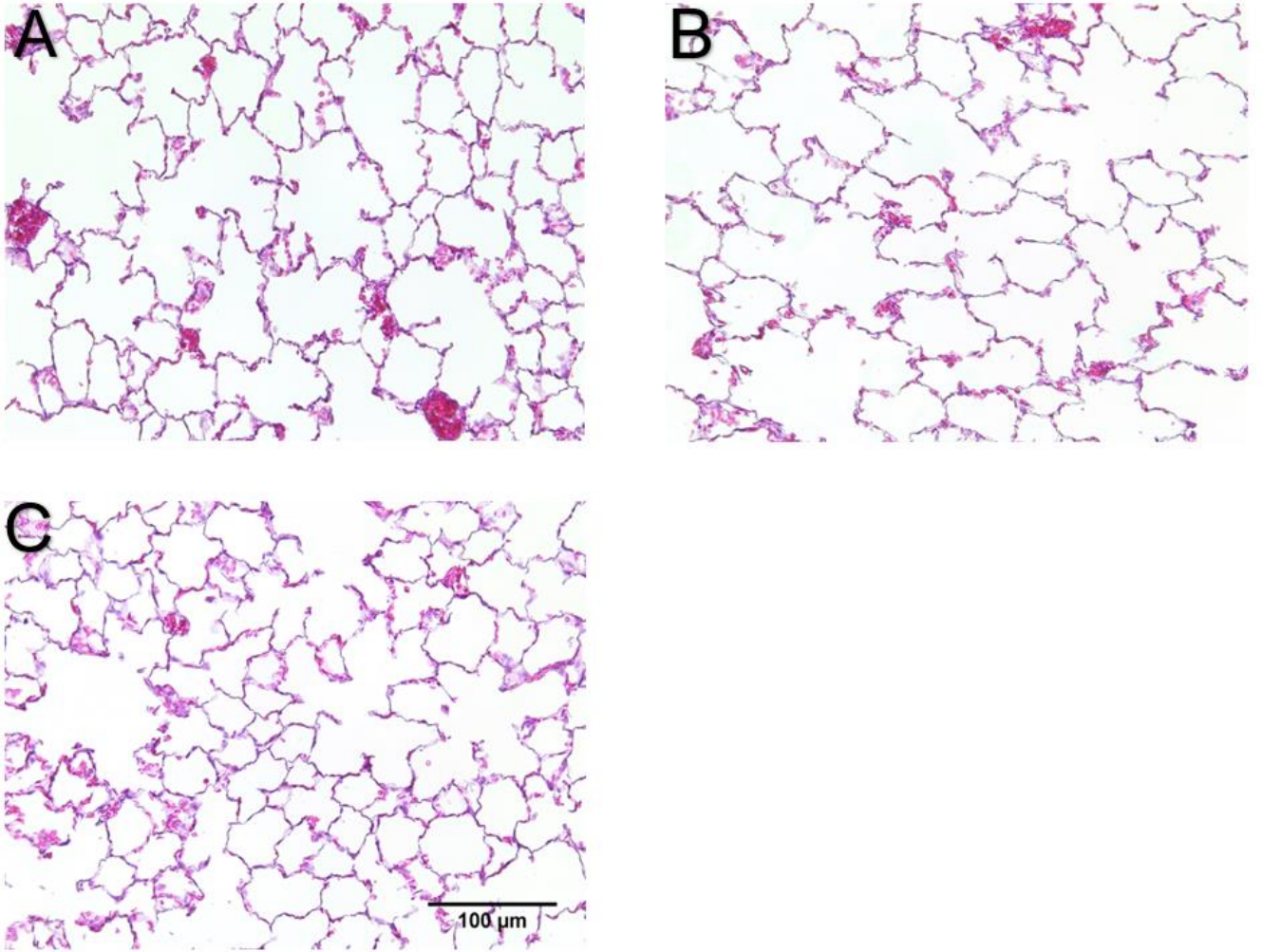
Figure 4.4. Representative brightfield microscopy images H & E stained lung tissue sections at 20X magnification showing control animals (**A**) and animals exposed to GO on day 1 PE (**B**) and day 7 PE (**C**).

REFERENCES

1. Anderson, D. S., E. S. Patchin, R. M. Silva, D. L. Uyeminami, A. Sharmah, T. Guo, G. K. Das, J. M. Brown, J. Shannahan, T. Gordon, L. C. Chen, K. E. Pinkerton, and L. S. Van Winkle. 2015. 'Influence of particle size on persistence and clearance of aerosolized silver nanoparticles in the rat lung', *Toxicol Sci*, 144: 366-81.

2. Bengtson, Stefan, Kristina B Knudsen, Zdenka O Kyjovska, Trine Berthing, Vidar Skaug, Marcus Levin, Ismo K Koponen, Abhay Shivayogimath, Timothy J Booth, and Beatriz Alonso. 2017. 'Differences in inflammation and acute phase response but similar genotoxicity in mice following pulmonary exposure to graphene oxide and reduced graphene oxide', *PloS one*, 12: e0178355.

3. Di Cristo, L, B Grimaldi, T Catelani, E Vázquez, PP Pompa, and S Sabella. 2020. 'Repeated exposure to aerosolized graphene oxide mediates autophagy inhibition and inflammation in a three-dimensional human airway model', *Materials Today Bio*, 6: 100050.

4. Gao, Wei. 2015. 'The chemistry of graphene oxide.' in, *Graphene oxide* (Springer).

5. Han, Sung Gu, Jin Kwon Kim, Jae Hoon Shin, Joo Hwan Hwang, Jong Seong Lee, Tae-Gyu Kim, Ji Hyun Lee, Gun Ho Lee, Keun Soo Kim, and Heon Sang Lee. 2015. 'Pulmonary responses of sprague-dawley rats in single inhalation exposure to graphene oxide nanomaterials', *BioMed Research International*, 2015.

6. Heitbrink, William A, Li-Ming Lo, and Kevin H Dunn. 2015. 'Exposure controls for nanomaterials at three manufacturing sites', *Journal of occupational and environmental hygiene*, 12: 16-28.

7. Kim, Young Hun, Mi Seong Jo, Jin Kwon Kim, Jae Hoon Shin, Jin Ee Baek, Hye Seon Park, Hyo Jin An, Jong Seong Lee, Boo Wook Kim, and Hoi Pin Kim. 2018. 'Short-term inhalation study of graphene oxide nanoplates', *Nanotoxicology*, 12: 224-38.

8. Landsiedel, Robert, Lan Ma-Hock, Hans-Juergen Haussmann, Ben van Ravenzwaay, Martin Kayser, and Karin Wiench. 2012. 'Inhalation studies for the safety assessment of nanomaterials: status quo and the way forward', *Wiley Interdisciplinary Reviews: Nanomedicine and Nanobiotechnology*, 4: 399-413.

9. Lee, Ji Hyun, Jong Hun Han, Jae Hyun Kim, Boowook Kim, Dhimiter Bello, Jin Kwon Kim, Gun Ho Lee, Eun Kyung Sohn, Kyungmin Lee, and Kangho Ahn. 2016. 'Exposure monitoring of graphene nanoplatelets manufacturing workplaces', *Inhalation toxicology*, 28: 281-91.

10. Livak, Kenneth J, and Thomas D Schmittgen. 2001. 'Analysis of relative gene expression data using real-time quantitative PCR and the 2− ΔΔCT method', *methods*, 25: 402-08.

11. Ma-Hock, Lan, Volker Strauss, Silke Treumann, Karin Küttler, Wendel Wohlleben, Thomas Hofmann, Sibylle Gröters, Karin Wiench, Bennard van Ravenzwaay, and Robert Landsiedel. 2013. 'Comparative inhalation toxicity of multi-wall carbon nanotubes, graphene, graphite nanoplatelets and low surface carbon black', *Particle and fibre toxicology*, 10: 1-20.

12. Madl, Amy K, and Kent E Pinkerton. 2009. 'Health effects of inhaled engineered and incidental nanoparticles', *Critical reviews in toxicology*, 39: 629-58.

13. Mittal, Sandeep, Veeresh Kumar, Nitesh Dhiman, Lalit Kumar Singh Chauhan, Renu Pasricha, and Alok Kumar Pandey. 2016. 'Physico-chemical properties based differential toxicity of graphene oxide/reduced graphene oxide in human lung cells mediated through oxidative stress', *Scientific reports*, 6: 1-16.

14. Paredes, JI, S Villar-Rodil, Amelia Martínez-Alonso, and JMD Tascon. 2008. 'Graphene oxide dispersions in organic solvents', *Langmuir*, 24: 10560-64.

15. Park, Eun-Jung, Gwang-Hee Lee, Beom Seok Han, Byoung-Seok Lee, Somin Lee, Myung-Haing Cho, Jae-Ho Kim, and Dong-Wan Kim. 2015. 'Toxic response of graphene nanoplatelets in vivo and in vitro', *Archives of Toxicology*, 89: 1557-68.

16. Park, Margriet VDZ, Eric AJ Bleeker, Walter Brand, Flemming R Cassee, Merel van Elk, Ilse Gosens, Wim H de Jong, Johannes AJ Meesters, Willie JGM Peijnenburg, and Joris TK Quik. 2017. 'Considerations for safe innovation: the case of graphene', *ACS nano*, 11: 9574-93.

17. Pecoraro, Roberta, Daniele D'Angelo, Simona Filice, Silvia Scalese, Fabiano Capparucci, Fabio Marino, Carmelo Iaria, Giulia Guerriero, Daniele Tibullo, and Elena M Scalisi. 2018. 'Toxicity evaluation of graphene oxide and titania loaded nafion membranes in zebrafish', *Frontiers in physiology*, 8: 1039.

18. Pei, Songfeng, and Hui-Ming Cheng. 2012. 'The reduction of graphene oxide', *Carbon*, 50: 3210-28.

19. Pelin, Marco, Silvio Sosa, Maurizio Prato, and Aurelia Tubaro. 2018. 'Occupational exposure to graphene based nanomaterials: risk assessment', *Nanoscale*, 10: 15894-903.

20. Rhazouani, Asmaa, Halima Gamrani, Mounir El Achaby, Khalid Aziz, Lhoucine Gebrati, Md Sahab Uddin, and Faissal Aziz. 2021. 'Synthesis and toxicity of graphene oxide nanoparticles: A literature review of in vitro and in vivo studies', *BioMed Research International*, 2021.

21. Sanchez, Vanesa C, Ashish Jachak, Robert H Hurt, and Agnes B Kane. 2012. 'Biological interactions of graphene-family nanomaterials: an interdisciplinary review', *Chemical research in toxicology*, 25: 15-34.

22. Silva, R. M., D. S. Anderson, J. Peake, P. C. Edwards, E. S. Patchin, T. Guo, T. Gordon, L. C. Chen, X. Sun, L. S. Van Winkle, and K. E. Pinkerton. 2016. 'Aerosolized Silver Nanoparticles in the Rat Lung and Pulmonary Responses over Time', *Toxicol Pathol*, 44: 673-86.

23. Silva, Rona M, Donald S Anderson, Lisa M Franzi, Janice L Peake, Patricia C Edwards, Laura S Van Winkle, and Kent E Pinkerton. 2015. 'Pulmonary effects of silver nanoparticle size, coating, and dose over time upon intratracheal instillation', *Toxicological sciences*, 144: 151-62.

24. Singh, Dinesh Pratap, Carlos Eugenio Herrera, Brijesh Singh, Shipra Singh, Rajesh Kumar Singh, and Rajesh Kumar. 2018. 'Graphene oxide: An efficient material and recent approach for biotechnological and biomedical applications', *Materials Science and Engineering: C*, 86: 173-97.

25. Song, Yujun, Yong Chen, Lingyan Feng, Jinsong Ren, and Xiaogang Qu. 2011. 'Selective and quantitative cancer cell detection using target-directed functionalized graphene and its synergetic peroxidase-like activity', *Chemical Communications*, 47: 4436-38.

26. Spinazzè, Andrea, Andrea Cattaneo, Davide Campagnolo, Valentina Bollati, Pier Alberto Bertazzi, and Domenico M Cavallo. 2016. 'Engineered nanomaterials exposure in the production of graphene', *Aerosol Science and Technology*, 50: 812-21.

27. Untergasser, Andreas, Ioana Cutcutache, Triinu Koressaar, Jian Ye, Brant C. Faircloth, Maido Remm, and Steven G. Rozen. 2012. 'Primer3--new capabilities and interfaces', *Nucleic acids research*, 40: e115-e15.

28. Zhang, Lei, Shuge Ouyang, Hongbo Zhang, Mingke Qiu, Yuxin Dai, Shuqing Wang, Yang Wang, and Jingmin Ou. 2021. 'Graphene oxide induces dose-dependent lung injury in rats by regulating autophagy', *Experimental and Therapeutic Medicine*, 21: 1-11.

29. Zhou, Xianfeng, and Feng Liang. 2014. 'Application of graphene/graphene oxide in biomedicine and biotechnology', *Current medicinal chemistry*, 21: 855-69.

CHAPTER 5

Inhalation of Silver Silicate Nanoparticles Leads to Transient and Differential Microglial Activation in the Rodent Olfactory Bulb

ABSTRACT

Engineered silver nanoparticles (AgNPs), including silver silicate nanoparticles (Ag-SiO$_2$ NPs), are used in a wide variety of medical and consumer applications. Inhaled AgNPs have been found to translocate to the olfactory bulb (OB) after inhalation and intranasal instillation. However, the biological effects of Ag-SiO$_2$ NPs and their potential nose-to-brain transport have not been evaluated. The present study assessed whether inhaled Ag-SiO$_2$ NPs can elicit microglial activation in the OB. Adult Sprague-Dawley rats inhaled aerosolized Ag-SiO$_2$ NPs at a concentration of 1 mg/ml for six hours. On day 0, 1, 7, and 21 post-exposure, rats were necropsied and OB were harvested. Immunohistochemistry on OB tissues were performed with anti-ionized calcium binding adapter molecule 1 and heme oxygenase-1 as markers of microglial activation and oxidative stress, respectively. Aerosol characterization indicated Ag-SiO$_2$ NPs were sufficiently aerosolized with moderate agglomeration and high-efficiency deposition in the nasal cavity and olfactory epithelium. Findings suggested that acute inhalation of Ag-SiO$_2$ NPs elicited transient and differential microglial activation in the OB without significant microglial recruitment or oxidative stress. The delayed and differential pattern of microglial activation in the OB implied that inhaled Ag-SiO$_2$ may have translocated to the central nervous system via intra-neuronal pathways.

INTRODUCTION

Silver nanoparticles (AgNPs), including silver silicate nanoparticles (Ag-SiO$_2$ NPs), are engineered transition-metal nanomaterials with diverse commercial applications. AgNPs are one of the most widely used metallic nanoparticles due to their broad-antimicrobial properties.[1] AgNPs are used in wound dressings and as protective coatings for medical supplies.[2-3] AgNPs are also used in various consumer products, from cosmetics to food storage containers.[4] Exposure to AgNPs can occur through dermal and ocular absorption, oral ingestion, or inhalation.[5-9] Inhalation of AgNPs may occur during manufacturing or usage of aerosolized commercial products or drug therapies containing silver, such as over-the-counter nasal spray treatments for respiratory infections. AgNPs are manufactured in various forms, with different compositions, sizes, shapes, and surface coatings, all of which confer unique physical and chemical properties.[10-12] Silver silicate (Ag-SiO$_2$) is a type of AgNPs supported on silica, which reduces particle agglomeration.[13] Ag-SiO$_2$ NPs are also used as antimicrobial additives for wound dressings and in catalytic reduction of toxic dyes in industries.[14-16]

Inhaled AgNPs can become entrapped in the fluid lining layer over the olfactory mucosa before reaching the olfactory epithelium.[17] From there, several possible pathways to the central nervous system (CNS) have been suggested. These include the 1) intra-neuronal pathway via uptake into olfactory nerve and trigeminal nerve, with retrograde axonal transport through neurons to the brain; 2) extra-neuronal pathway via transcellular transport across the sustentacular cells and paracellular transport across the tight junctions between sustentacular cells and olfactory sensory neurons; 3)

systemic pathway through translocation across the rich vasculature of the respiratory

epithelium, absorption into lymphatics, ingestion following clearance of NPs via the

mucociliary escalator with subsequent gastrointestinal absorption into the hepatic portal

circulation.[18-20] Intra-neuronal nose-to-brain translocation via the olfactory nerve

pathway is also utilized by viruses such as herpesvirus, influenza A virus, and SAR-

CoV-2 virus, which are similarly sized to AgNPs, to gain access to the CNS.[21-22]

AgNPs have been found in the olfactory bulb (OB) following inhalation of

AgNPs.[23-26(p1873)] Previous studies suggested that NPs can reach the OB via the

olfactory pathway, similar to how odorant information is relayed to the CNS.[26-28] The OB

receives odorant molecules from the olfactory epithelium in the nasal cavity via the

olfactory sensory nerve fascicles.[29(p1)] The OB has a lamellar structure with several

histologically distinct layers (Figure 1).[30] These layers, in the order of most superficial to

deep, include the glomerular layer (GL), external plexiform layer (EPL), mitral cell layer

(MCL), internal plexiform layer (IPL), and granule cell layer (GCL). Odorant molecules

from the nasal cavity arrive at the GL of the OB before information is relayed to cells of

the deeper layers of the OB and finally the primary olfactory cortex.[29(p2)]

Microglia are resident macrophages of the CNS and are beneficial in immune

surveillance, synaptic plasticity, neuronal repair, and neurogenesis.[31-34] However,

prolonged and/or excessive microglial activation following inhalation of NPs can be

detrimental due to associated upregulation of toll-like receptors and release of pro-

inflammatory cytokines and chemokines.[35-37] Inhaled AgNPs may be sufficiently

immunogenic to elicit an *in vivo* pro-inflammatory response in the OB via microglial

activation.[26(p1874)] The cytotoxicity of AgNPs is thought to be primarily due to the release of ionic silver (Ag^+) into the biological environment.[38-40]

The primary objectives of the present study were to determine whether acutely inhaled Ag-SiO$_2$ NPs activate resting microglia in the OB, and if there is differential activation of microglia in different histological layers of the OB. Rats were exposed to aerosols of Ag-SiO$_2$, and their OB were harvested immediately after exposure on day 0 (D0) and on post-exposure day 1, 7 and 21 (D1, D7, D21 respectively). 10-μm-thick OB sections were immunostained for anti-ionized calcium binding adapter molecule 1 (anti-Iba1) to identify the site and morphology of microglia in the OB and with heme oxygenase-1 (HO-1) as a marker of oxidative stress in the OB.

MATERIALS AND METHODS

Powdered Ag-SiO$_2$ NPs

The Ag-SiO$_2$ NPs used in the present study were synthesized, characterized, and supplied in powder form by the National Institute of Environmental Health Sciences Centers for Nanotechnology Health Implications Research Consortium. Ag-SiO$_2$ NPs were synthesized by flame spray pyrolysis as silver (~8 nm) supported on silica (~7 nm) (3.79% w/w).[41-42] The powdered Ag-SiO$_2$ NPs were on average 10.64 nm ± 7.10 nm in diameter before suspension in endotoxin-free water to a 1 mg/ml concentration for aerosolization. The primary particle size, primary particle size distribution, and size factor were characterized by transmission electron microscope (TEM) image analysis. Crystallinity, density, and chemical composition were characterized by X-ray diffraction, pycnometer, and inductively coupled plasma mass spectrometry (ICP-MS) respectively.

Animal Care

Adult, twelve-week-old male Sprague-Dawley rats were obtained from Envigo laboratory (Fremont, California). Upon arrival, the rats were randomly assigned to two exposure groups, Ag-SiO$_2$ ($n = 4$ per time point) or filtered air ($n = 8$; pooled from D1 and D21 post-exposure). The rats were housed two per cage in filter-top polycarbonate cages in an animal facility with high-efficiency particulate air filters, maintained in a twelve-hour dark/light cycle under standard temperature and given *ad libitum* access to a standard laboratory rodent diet (Purina 5001, Newco Distributors, Rancho Cucamonga, California) and water. Rats were allowed to acclimate for at least one week prior to the experimental exposure. During the acclimation period, the rats were conditioned to remain in the inhalation exposure tubes (Teague Enterprises, Woodland, CA) for progressively longer periods. The conditioning exercises were performed to minimize confinement stress during the experimental exposure. Animals were handled following guidelines from the National Institutes of Health and Institutional Animal Care and Use Committee of the University of California, Davis.

Aerosolization of Ag-SiO$_2$ NPs

Rats were exposed to either filtered room air or Ag-SiO$_2$ aerosol generated by the aerosol nebulization system located at the Center for Health and the Environment, University of California, Davis (Figure 5.2). The Ag-SiO$_2$ suspension was sonicated (QSonica Sonicators; 500 W, 20kHz, 90% Amp), kept on ice to reduce particle aggregation, and aerosolized with a BGI 6-jet Collision nebulizer (Waltham, MA) into fine droplets. Air for the nebulizer was compressed with an oil-free compressor (California Air Tools, San Diego, CA), dehumidified with compressed air dryers (Wilkerton, Richland, MI), and filtered with a Motor Gard M-610 filter (Motor Gard,

Manteca, CA). The fine nebulized droplets passed through a custom-fabricated heater and two diffusion dryers (TSI, Shoreview, MN) to remove any remaining water. The resulting dried particles then passed through a Krypton-85 charge-neutralizer to reduce static and minimize particle agglomeration before entering the 48-port nose-only exposure system connected by steel piping.[43]

Nose-Only Inhalation Exposure

Rats were placed into the nose-only exposure tubes, one rat per tube, for a single, six-hour exposure to either filtered air or aerosolized Ag-SiO$_2$. Rats were monitored for their presence and activity while in the inhalation chamber for the entire duration of the exposure period. The average temperature and humidity in the exposure room was 56°F and 54% respectively.

Characterization of the Aerosolized Ag-SiO$_2$ NPs

Air samples were collected throughout the six-hour exposure period, and aerosol characterization was performed using a protocol previously described.[44] Briefly, the mass concentration and particle size distribution of the aerosolized Ag-SiO$_2$ NPs were determined via gravimetry and an eight-stage Mercer-style cascade impactor, respectively, using samples collected onto 25-mm diameter Pallflex membrane filters (catalog number 28150-925, Pall Life Sciences, Port Washington, NY). The silver mass was determined by X-ray fluorescence (XRF; Chester Labnet, Tigard, OR) with samples collected on 25-mm diameter Pall Teflo filters (catalog number 28139-131, Pall Life Sciences, Port Washington, NY); and the average particle diameter was measured using aerosolized particles collected onto formvar carbon film (carbon grids 200 mesh,

catalog number FCF200-Cu, Electron Microscopy Sciences, Hatfields, PA) and examined via a Phillips CM-12 transmission electron microscope operating at 120kV.

Tissue Collection and Preparation

Ag-SiO$_2$ NPs-exposed rats were euthanized on D0 (immediately after the exposure), D1, D7, and D21 post-exposure with an intraperitoneal injection of Beuthanasia-D at 7.5 ml/kg (MWI Veterinary Supply Company, Los Angeles, CA 90074). Control animals were necropsied on D1 and D21 after the exposure. Cardiac puncture was performed, and blood was collected in a 12-ml round bottom tube for centrifugation at 2000 revolutions per min (rpm) for 15 min. The resulting blood plasma was collected and stored at -80°C for later use. Following blood collection, the trachea was cannulated, and the left main bronchus was clamped. The right middle, caudal and accessory lobes were lavaged, flash-frozen, and stored at -80°C for later use. Briefly, the lobes were lavaged three times with a single 7-ml aliquot of sterile phosphate-buffered saline (PBS, Sigma Aldrich, St.Louis, MO) in a 12-ml syringe for collection of bronchoalveolar lavage fluid (BALF). The BALF was collected in a 15-ml round bottom tube and centrifuged for 15 min at 2000 rpm and 4°C. The resulting BALF supernatant was decanted and stored for further analysis, while the cell pellet was resuspended in 2 ml of sterile PBS. Trypan blue was used to count the total viable and non-viable cells. A 100-µl aliquot of resuspended cells was used to prepare cytospin slides for cell differentials. The left lung was unclamped and inflation-fixed at a hydrostatic pressure of 30 cm with 4% paraformaldehyde for 1 hour. The fixed lung was subsequently stored in 4% paraformaldehyde for 24 hours before transfer to 70% ethanol. (A separate

manuscript evaluating pulmonary toxicity caused by inhalation of Ag-SiO$_2$ is being prepared).

The heads were decapitated, brains were removed, and the remaining head was fixed in 4% paraformaldehyde for 24 hours and stored in 70% ethanol. The heads and nasal cavities were decalcified along with the OB using 0.5-M ethylenediaminetetraacetic acid (EDTA, pH = 8; Thermo Fisher Scientific) at room temperature for 2 weeks. A total of four transverse sections of nasal cavity per rat were obtained following a standard protocol.[45] Then, one sagittal section of the decalcified heads was obtained per rat. Sagittal tissue orientation was chosen so that the nasal cavity and OB tissues are on the same slide for silver detection in the nose and the OB with autometallography. All tissues were embedded in Paraplast (Fisher Scientific, Swedesboro, NJ), cut with a microtome to 5-µm and 10-µm thick sections and put onto slides (catalog number 12-550015, Fisherbrand, Fisher Scientific).

Immunohistochemistry

For each rat, three slides of OB were immunostained for anti-Iba1, and one slide of OB was immunostained for HO-1 to visualize microglia and assess for oxidative stress, respectively. The OB sections were deparaffinized in three changes of toluene for 5 minutes each and rehydrated in 100%, 95%, and 70% ethanol for 2 minutes each before immersion in EDTA (Thermo Fisher Scientific, pH = 8) at 123°C for 2 minutes, and 85°C for 10 seconds. The sections were then cooled for 45 minutes and washed for 5 minutes under gentle running tap water. Endogenous peroxidase was blocked with 3% hydrogen peroxide for 10 minutes, followed by a quick dip in distilled water and three washes in phosphate-buffered saline with 1000µl Tween 20 (PBST; Sigma

Aldrich, St. Louis, MO) at 2 minutes each. Nonspecific proteins were blocked with Protein Block (catalog number X0909; Dako, Carpinteria, CA) for 20 minutes at room temperature. The sections incubated with anti-Iba1 (ab 153696, Abcam Inc., Cambridge, MA), at a 1:1000 dilution with PBST, were incubated overnight at room temperature. The sections incubated with HO-1 (ab 13243, Abcam Inc., Cambridge, MA) at a 1:700 dilution with PBST were incubated for 1 hour at room temperature. Negative-control tissue sections were not incubated with the primary antibody. Sections were then washed in PBST following a protocol of two washes of brief twenty dips followed by two washes at 5 minutes each. The sections were then incubated with the secondary antibody, horseradish peroxidase-labeled polymer for rabbit (catalog number K4403; Dako), for 30 minutes at room temperature and washed twice in PBST with occasional agitation for 5 minutes each. Each section was incubated with 100 μl of 3,3'-Diaminobenzidine (DAB) and substrate (catalog number K3468; Dako) for 5 minutes at room temperature. DAB solution was tipped off each section onto lab paper. Sections were washed briefly in distilled water twice and counterstained with Harris Hematoxylin (MasterTech, Inc., Lodi, CA) and coverslipped with ClearMount permanent mounting medium (Thermo Fisher Scientific). IHC staining was evaluated qualitatively.

Microglial Visualization and Characterization

The OB sections immunostained for Iba1 were divided into four histologically distinct layers for photomicrography. These layers consisted of the olfactory nerve layer (ONL), glomerular layer (GL), external plexiform layer (EPL), and inner layers (IL). Each IL consisted of the mitral cell layer, internal plexiform layer, and granule cell layer, grouped as one layer because these layers were difficult to distinguish from each other

144

at 20X magnification. Microglial abundance and morphology were evaluated in three

randomly sampled non-overlapping fields per histologically distinct layer for a total of

twelve fields per histological section, one section per animal, four animals in each Ag-

SiO_2 post-exposure group and eight animals in sham control at 20X magnification on a

Zeiss AxioLab.A1 microscope. All microglia were manually counted in each of the

twelve randomly captured, non-overlapping fields to determine microglial abundance,

and microglial morphology was evaluated to determine resting and activation states.

The ratio of activated to resting microglia was calculated for sham control and each of

the five exposure groups. The protocol was repeated for each of the four histologically

distinct layers (ONL, GL, EPL, and IL) in the OB sections. Four investigators evaluated

microglial abundance and morphology in a blinded fashion, and their scores were

averaged.

Microglial morphology was categorized as resting or activated as a mean of

evaluating the OB response to inhalation of Ag-SiO_2 and as an indirect assessment of

NP translocation to the CNS. Microglial morphology is associated with different

microglial phenotypes.[46-47] Resting microglia surveils for changes in the

microenvironment and has a small cell body with extensively ramified processes. The

processes are highly motile, undergoing continuous cycles of *de novo* formation and

disappearance without a net change in the total number of processes to dynamically

scan the environment without disturbing pre-existing neuronal structures.[48-49] Once

microglia sense changes in the microenvironment such as the presence of pro-

inflammatory stimuli such as lipopolysaccharide and interferon gamma or cytokines

such as interleukin 4 and interleukin 10, they change their morphology into an amoeboid

form with enlarged cell bodies and retracted, thickened processes to mediate phagocytic activity, suppress inflammation, or mediate tissue remodeling.[50] This study classified microglia as resting or activated based on previously accepted criteria.[26-27,51] Resting microglia were defined as cells with at least two highly ramified processes extending at least twice the length of a small nucleus. Activated microglia were defined as cells with significantly shortened ramified processes extending from a slightly enlarged cell nucleus.

Oxidative Stress

The OB sections immunostained for HO-1 were treated in similar fashion as sections immunostained for Iba1. HO-1 expression was evaluated qualitatively, as present or not present, in twelve randomly sampled non-overlapping fields per histologically distinct layers per histological section, one section per animal, four animals in each Ag-SiO$_2$ post-exposure group and eight animals in sham control at 20X magnification on a Zeiss AxioLab.A1 microscope.

Statistical Analysis

Data were analyzed with Jamovi 1.6 statistical software (Sydney, Australia). No animals were excluded from statistical analysis. Shapiro-Wilk and Levene's tests were performed to confirm normality and homoscedasticity, respectively.[26(p1872)] Statistically significant differences in microglial abundance and microglial activation were determined by Welch's one-way ANOVAs. Games-Howell post hoc tests were used to identify significant differences between specific groups. These tests were performed at a significance level of $p < 0.05$. Data are presented as group means ± standard error.

RESULTS

146

Ag-SiO$_2$ Aerosol Characterization

Aerosol characterization suggested that the Ag-SiO$_2$ NPs in nanopure water were sufficiently aerosolized with moderate agglomeration. The mean Ag-SiO$_2$ aerosol mass concentration measured by gravimetry was 4.9 ± 2.3 mg/m^3, and the Ag concentration measured by XRF was 0.17 ± 0.01 mg/m^3. These results suggested that suspension of Ag-SiO$_2$ NPs in nanopure water did not alter the mass concentration of the aerosol. The median aerosol diameter measured by cascade impactor was 1.9 ± 0.3 µm, and the size (diameter) distribution of the Ag-SiO$_2$ NPs based on TEM ranged from 21 to 370 nm (Figures 5.3 and 5.4). The aerosol diameter measured by the cascade impactor suggested that there was particle agglomeration, but size distribution based on TEM suggested that approximately 50% of Ag-SiO$_2$ NPs were less than 100 nm in diameter and small enough to be deposited in the nasal epithelium.[52]

Transient and Differential Microglial Activation in the OB Without Microglial Recruitment

Microglial morphology in the OB was categorized as resting or activated (Figure 5.5). Microglial numbers were counted to determine microglial abundance in the OB (Figure 5.6, panel A) and in each histologically distinct layer of the OB in sham control and Ag-SiO$_2$ post-exposure groups (Figure 5.6, panels B, C, D, and E). The ratio for activated to resting microglia were calculated for the entire OB (Figure 5.7, panel A) and for each histologically distinct layer of the OB (Figure 5.7, panels B, C, D, and E) in sham control and Ag-SiO$_2$. After Ag-SiO$_2$ versus filtered air exposure, there was significant ($p = 0.02$) microglial activation in the OB, compared to sham control, with elevated ratios of activated to resting microglia noted on D1 and D7 post-exposure and

a return to control concentration by D21 (Figure 5.7, panel A). In the ONL, there was a notable but non-significant ($p = 0.08$) increase in the ratio of activated to resting microglia on D1 and D7 compared to sham control (Figure 5.7, panel B). In contrast, the GL of the OB in exposed rats demonstrated a significant increase ($p = 0.01$) compared to sham control in the proportion of activated to resting microglia on post-exposure D1 (Figure 5.7, panel C, and Figure 8). In the EPL and IL, there were no notable inter-group differences in the ratio of activated to resting microglia (Figure 5.7, panel D and E). There was no significant difference in microglial abundance between sham control versus exposed group at any time point post exposure, which suggested a lack of microglial recruitment (Figure 5.6).

Mild Oxidative Stress in the OB

Sparse HO-1 immunoreactivity was noted in the ONL on D0 and the EPL on D1 and D7 (Figure 5.9). Negative and sham controls showed no immunoreactivity.

DISCUSSION

The primary objectives of the present study were to determine whether acute inhalation of Ag-SiO$_2$ NPs induced microglial activation and, and if so, whether microglial activation differed between the distinct histologic layers of the OB. Based on our results, we concluded that an acute (single, six-hour) inhalation exposure to Ag-SiO$_2$ NPs elicited slightly delayed and transient microglial activation on D1 and D7 post-exposure, particularly in the GL, without significant microglial recruitment to the OB. There was also evidence of mild oxidative stress in the OB at D0, D1, and D7 post-exposure. The temporal and differential pattern of microglial activation in the OB implied

that inhaled Ag-SiO$_2$ NPs are immunogenic in the biologic environment and may have translocated to the CNS via intra-neuronal and systemic pathways to induce a mild pro-inflammatory response.

In this study, the aerosolized silver concentration averaged 5.6 ± 2.0 mg/m^3. The Occupational Safety and Health Administration (OSHA) set the exposure limit for silver at 0.01 mg/m^3 per 8-hour time weighted average.[53] Maximal time weighted average of aerosolized silver concentration of up to 0.289 mg/m^3 has been detected in silver manufacturing plants.[54] Our study's aerosolized silver concentration can be correlated to an environment with high occupational exposure to aerosolized silver without personal safety measures.

A trend was observed for an increased ratio of activated-to-resting microglia in groups exposed to Ag-SiO$_2$ NPs compared to filtered air controls, with the highest elevation noted on D1 and D7 post-exposure, which returned to control concentration by D21 (Figure 5.7, panel A). These observations suggested a transient pro-inflammatory response in the OB to inhaled Ag-SiO$_2$ NPs. The inflammatory response mediated by microglia can help directly sequester NPs for digestion. Microglial cells may recognize NPs through surface toll-like receptors (TLR2 and TLR4) and can internalize NPs via phagocytosis, micropinocytosis, and clathrin-mediated endocytosis.[36-37,55-56] Microglia may also be activated to remodel damaged neuronal tissues, as AgNPs and Ag$^+$ have been shown to induce apoptosis mediated by reactive oxygen species and phagocytosis mediated by tissue necrosis factor-α and interleukin-1β.[38,57-59]

Activation of microglia in the OB implied that inhaled Ag-SiO$_2$ NPs may have translocated to the CNS to induce a pro-inflammatory response. However, it is unclear

from the present study which route NPs take to enter the CNS. Delayed microglial activation, on D1 and D7 post-exposure without significant activation on D0 is suggestive of intra-neuronal pathway as a possible route for inhaled Ag-SiO$_2$ NPs to arrive at the OB. This presumption is supported by previous studies, which demonstrated that particles traveling from the olfactory epithelium to the OB take minutes to make this journey via extra-neuronal pathways, 18-36 minutes via fast axonal transport (a type of intra-neuronal transport), and approximately 5 days with slow axonal transport (another type of intra-neuronal transport).[20,27]

Systemic pathway is another possible route for Ag-SiO$_2$ NPs to enter the CNS. A kinetic time course study showed that inhaled AgNPs of similar diameter to ours were detected in the OB with peak concentration immediately after a six-hour inhalation exposure period and again at seven-day post-exposure.[60] Patchin et al[26] found significant microglial activation in the OB immediately after exposure to similarly sized inhaled AgNPs and at one- and seven-day post-exposure. These temporal profiles are similar to our finding of microglial activation in the OB on D1 and D7 post-exposure. The first peak in Ag deposition and early microglial activation may represent translocation of NPs via the intra-neuronal olfactory pathway as well as systemic absorption of NPs via the gastrointestinal tract and the hepatic portal circulation. Recordati et al[61] showed that ingestion of AgNPs was correlated with structural alteration of the blood-brain barrier, which may facilitate AgNPs entry to the CNS. The second peak in Ag deposition and delayed microglial activation may represent NPs entering the systemic circulation and lymphatics following delayed clearance from the nasal cavity and lungs.[26,60,62]

Recruitment of additional microglia to the OB is another marker of pro-inflammatory response that has been reported following exposure to NP.[63] We did not find a significant increase in the number of microglia in the OB in animals exposed to Ag-SiO$_2$ NPs compared to controls at any post-exposure time point (Figure 5.6). This suggested a non-inflammatory response to inhaled Ag-SiO$_2$ NPs. This is further supported by an mild oxidative stress response indicated by sparse HO-1 immunostaining in the OB. These findings, taken altogether, suggested an insignificant inflammatory response in the OB to inhaled Ag-SiO$_2$ NPs. The exposure time to NPs in this study (single, six-hour inhalation) may not be sufficiently long to elicit microglial recruitment to the OB. Wang et al[63] found microglial recruitment to the OB following every other day instillation of NPs over a period of forty days. Second, the silicate core of the Ag-SiO$_2$ NPs conferred stability to the structure and may have caused the AgNPs to oxidize more slowly to Ag$^+$, thus minimizing injury to cells in the OB.[13] Aggregation of Ag-SiO$_2$ NPs during aerosolization, as shown by the aerosol diameter measured by the cascade impactor, may have also reduced NPs deposition onto the nasal epithelium, which in turn diminished cellular uptake efficiency and cytotoxic effects on microglial cells in the OB. This presumption is supported by previous studies that demonstrated decreased cellular uptake rates of large-sized NPs compared to smaller-sized NPs of the same composition.[64-65] Further studies with sub-acute and chronic exposure durations are needed to fully evaluate the extent of Ag-SiO$_2$ NP-induced inflammation in the OB.

Differential activation of microglia was noted among the histologically distinct layers of the OB. This differential activation of microglia may potentially be due to NPs

failing to penetrate deeper into the OB. However, previous studies found metal NPs along with associated microglial activation and histologic brain remodeling in the OB and more distant brain regions such as the hippocampus, striatum, and lateral ventricle following inhalation and intranasal instillation of metal NPs.[37,58,63,66-67] These findings suggested that the acute inhalation exposure duration may have precluded delivery of a dose of metal NPs equivalent to chronic inhalation or intranasal instillation leading to less NPs deposition onto the olfactory epithelium, less NPs translocation to the deeper layers of the OB, and less microglial activation than expected.

The major limitation of this study is that the activation of microglia in the OB showed implied rather than actual translocation of AgNPs from the nasal cavity to the OB. We were unable to visualize or quantify silver in the nasal cavity, the olfactory nerves, or in the OB using autometallography or ICP-MS. Other studies used these methods to demonstrate presence of silver in these tissues, but we were unable to replicate this result.[25-26] One reason for this may be due to the interaction between EDTA used for decalcification of the nasal cavity and the silver enhancement solution used in autometallography. Autometallography utilizes gold to initiate the reduction of ionic silver to metallic silver.[68] EDTA is commonly used as a metal chelator and is capable of chelating gold.[69-71] These reagents may have cross-reacted to cause gold to precipitate out of the solution rather than aid in ionic silver reduction for visualization. Another explanation may be that the amount of AgNPs deposited was insufficient for direct silver visualization due to the low dose of exposure or due to NP agglomeration precluding efficient NP deposition onto the nasal epithelium as discussed above.

Further studies are needed to investigate the in *vivo* translocation of inhaled Ag-SiO$_2$ NPs to the CNS.

Another limitation of the study was that we did not differentiate between activated microglia from CNS-associated macrophages, which have a similar amoeboid morphology. Microglia and CNS-associated macrophages are resident immune cells of the CNS but reside in different niches. Microglia reside in the brain parenchyma, whereas CNS-associated macrophages are non-parenchymal and reside in peripheral regions such as the perivascular space, choroid plexus, and meninges.[72] Iba-1, the immunohistochemical marker chosen for this study, is widely used to highlight microglia, but it can also bind to macrophages.[73-74] Our OB sections likely had perivascular macrophages but not choroidal or meningeal macrophages, as these structures were not attached to the OB sections used for analysis. Without differentially staining for these cells, we may have classified some perivascular macrophages as activated microglia. However, perivascular macrophages are normal immune cells of the CNS and are present in both sham control as well as exposure groups. Moreover, perivascular macrophages may also proliferate in response to CNS injury.[75] Therefore, by comparing the ratio of activated to resting microglia rather than total count of activated microglia, we were still able to utilize morphometric analysis of microglia to indirectly assess the inflammatory response in the OB in response to inhaled Ag-SiO$_2$ NPs. Further studies are needed to assess the activation pattern of microglia and CNS-associated macrophages following inhalation of Ag-SiO$_2$ NPs, as their activation pattern may have implications on the route NPs may take to enter the CNS. Activation of microglia but not CNS-associated macrophages may suggest a primarily intra-neuronal

153

transport of NPs to the CNS to induce an inflammatory response in parenchymal immune cells. On the contrary, activation of CNS-associated macrophages but not microglia may suggest a primarily extra-neuronal or systemic transport of NPs.
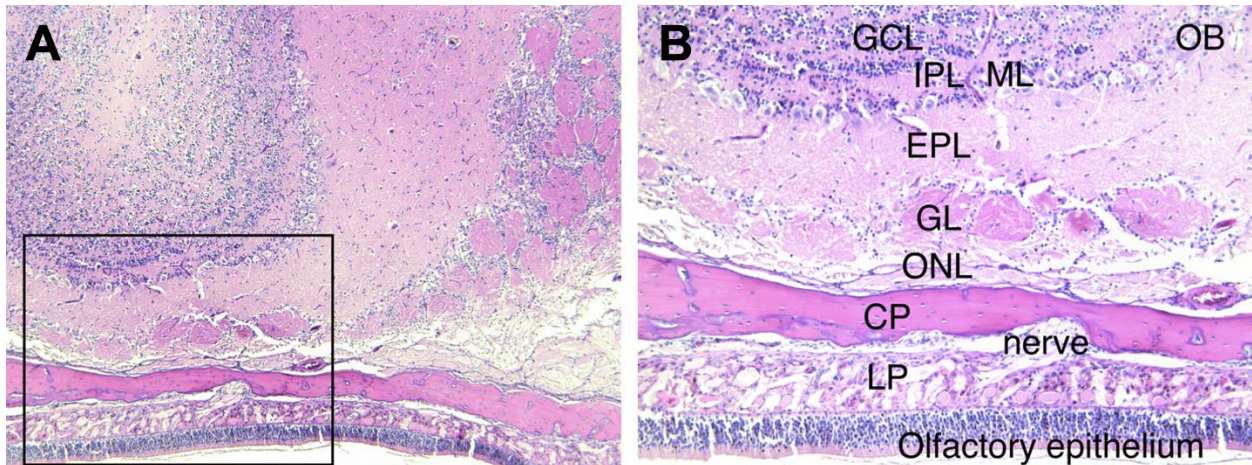
CONCLUSION

Acute inhalation of Ag-SiO$_2$ NPs elicited transient and differential microglial activation without significant microglial recruitment to the OB. The delayed and differential pattern of microglial activation in the OB implied that inhaled Ag-SiO$_2$ NPs may have translocated to the CNS via intra-neuronal pathway. The absence of significant microglial recruitment and mild oxidative stress in the OB was indicative of an insignificant inflammatory response in the OB that might reflect the short duration of the acute inhalation exposure, the chemical stability of the Ag-SiO$_2$ NPs conferred by the silicate core, or moderate Ag-SiO$_2$ NPs agglomeration during aerosolization that interfered with NPs deposition onto the nasal epithelium, which in turn diminish the number of NPs available to reach distant organs to induce cytotoxic effects.

ACKNOWLEDGEMENTS

Figure 5.1. Representative brightfield microscopy images of 5-μm thick, hematoxylin- and eosin-stained tissue sections of rat nasal tissue and olfactory bulb (OB). Panel **A** shows a transverse section of the OB at 5X magnification. Box identifies a section of the OB shown in panel B at 10X magnification. Panel **B** shows the lamellar structure composed of histologically distinct layers of the OB. Abbreviations: CP – cribriform plate; EPL – external plexiform layer; GCL – granular cell layer; GL – glomerular layer; IPL – internal plexiform layer; LP – lamina propria; ML – mitral cell layer.

Figure 5.2: Aerosolization and exposure system.
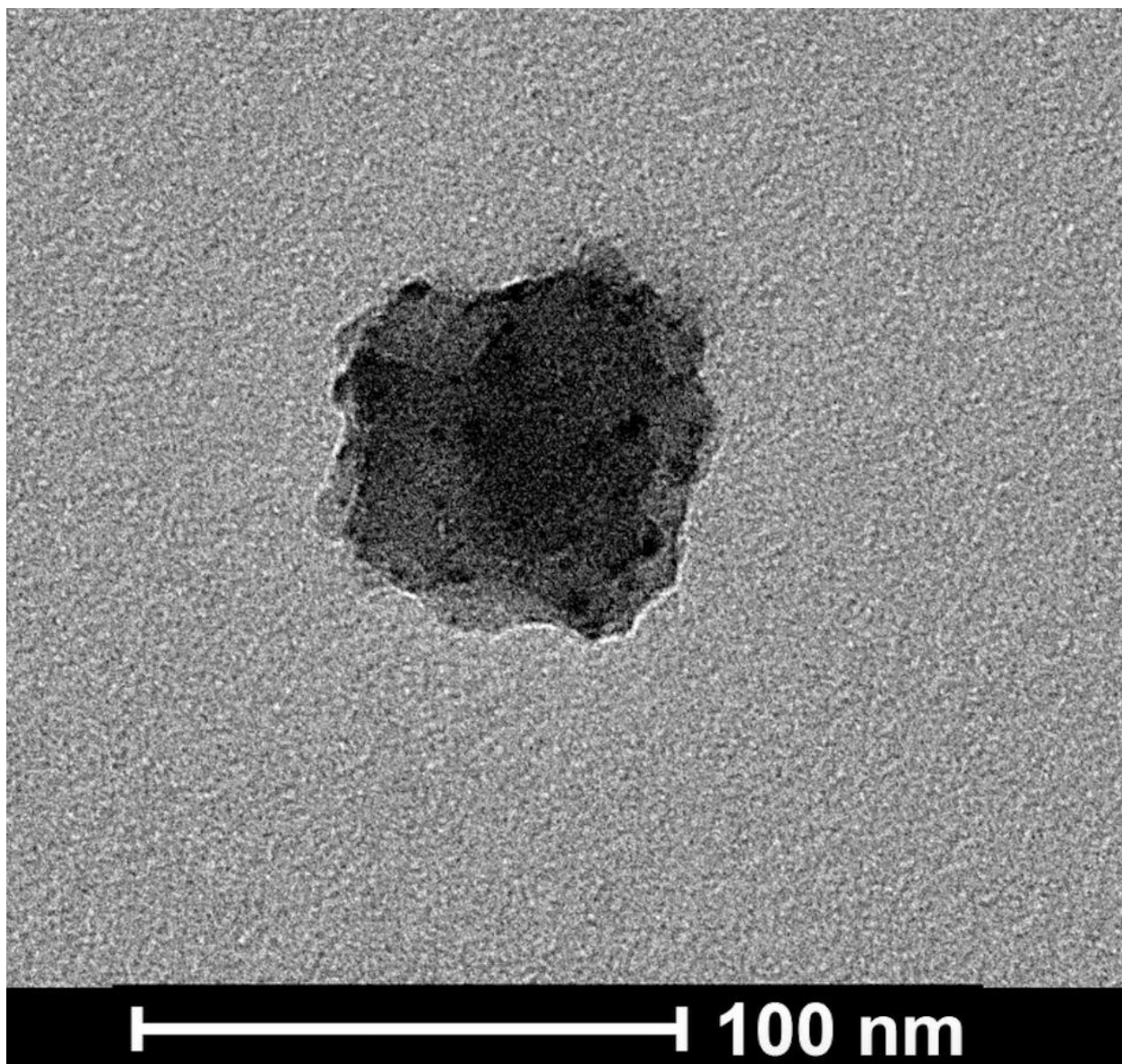
Figure 5.3. Transmission electron microscopy image at 120kX magnification of a silver silicate (Ag-SiO$_2$) nanoparticle obtained during a single, six-hour aerosolization period.
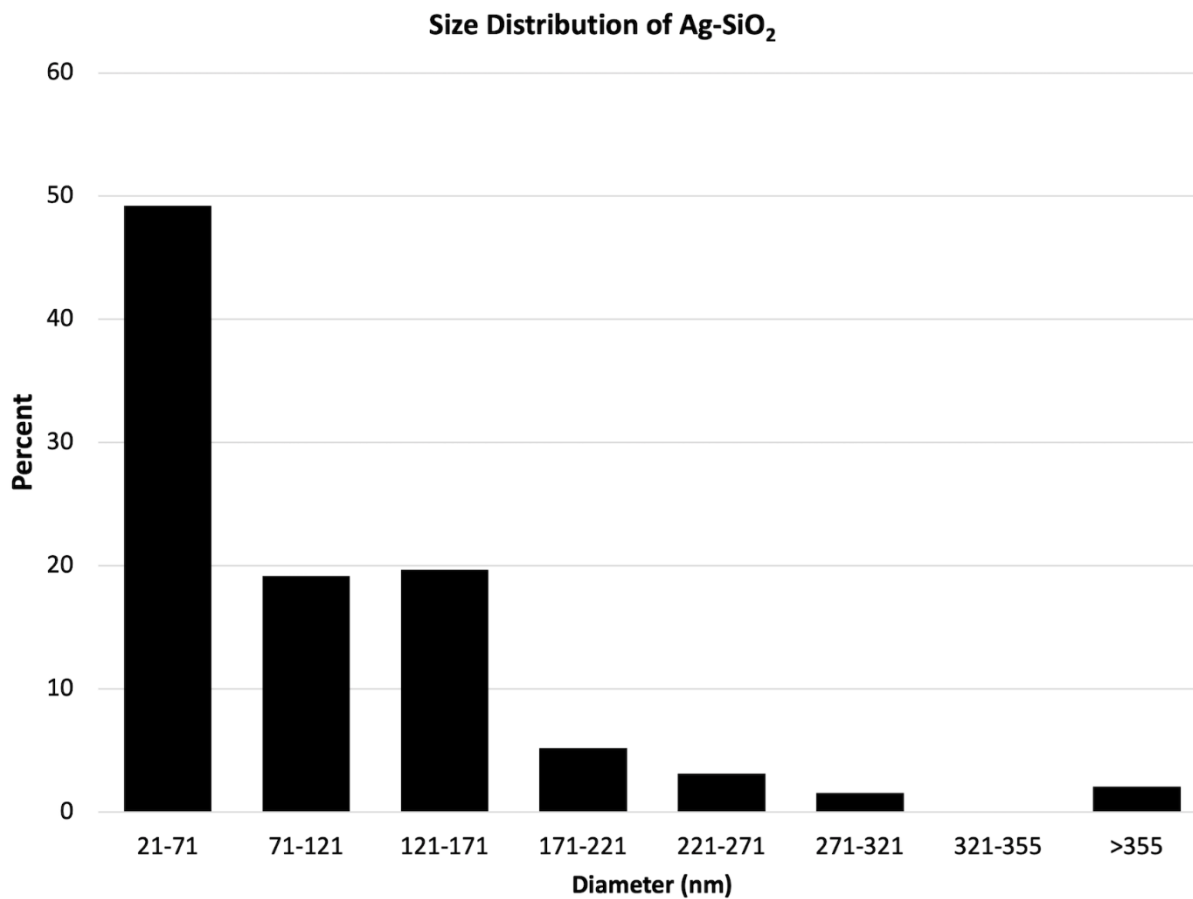
Figure 5.4. Graph of the size (diameter) distribution of aerosolized silver silicate (Ag-SiO$_2$) nanoparticles measured by transmission electron microscopy.
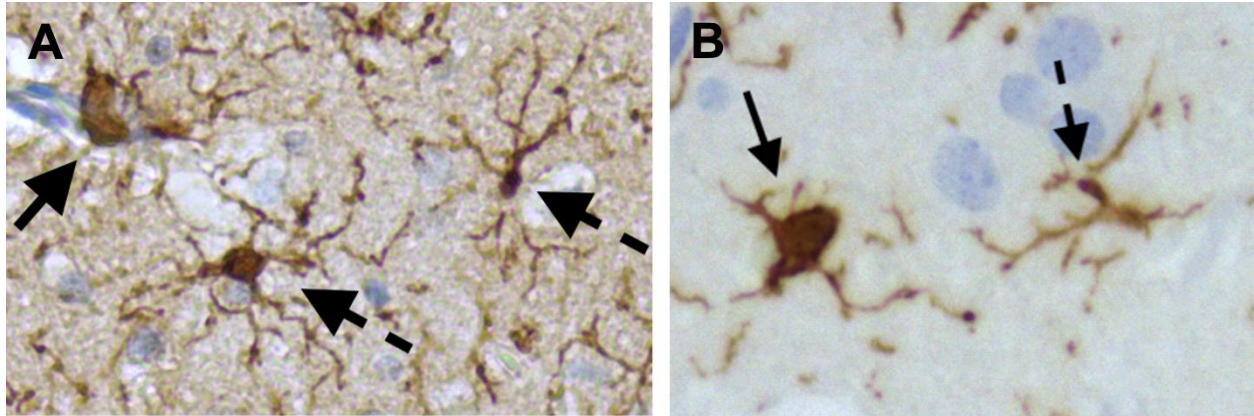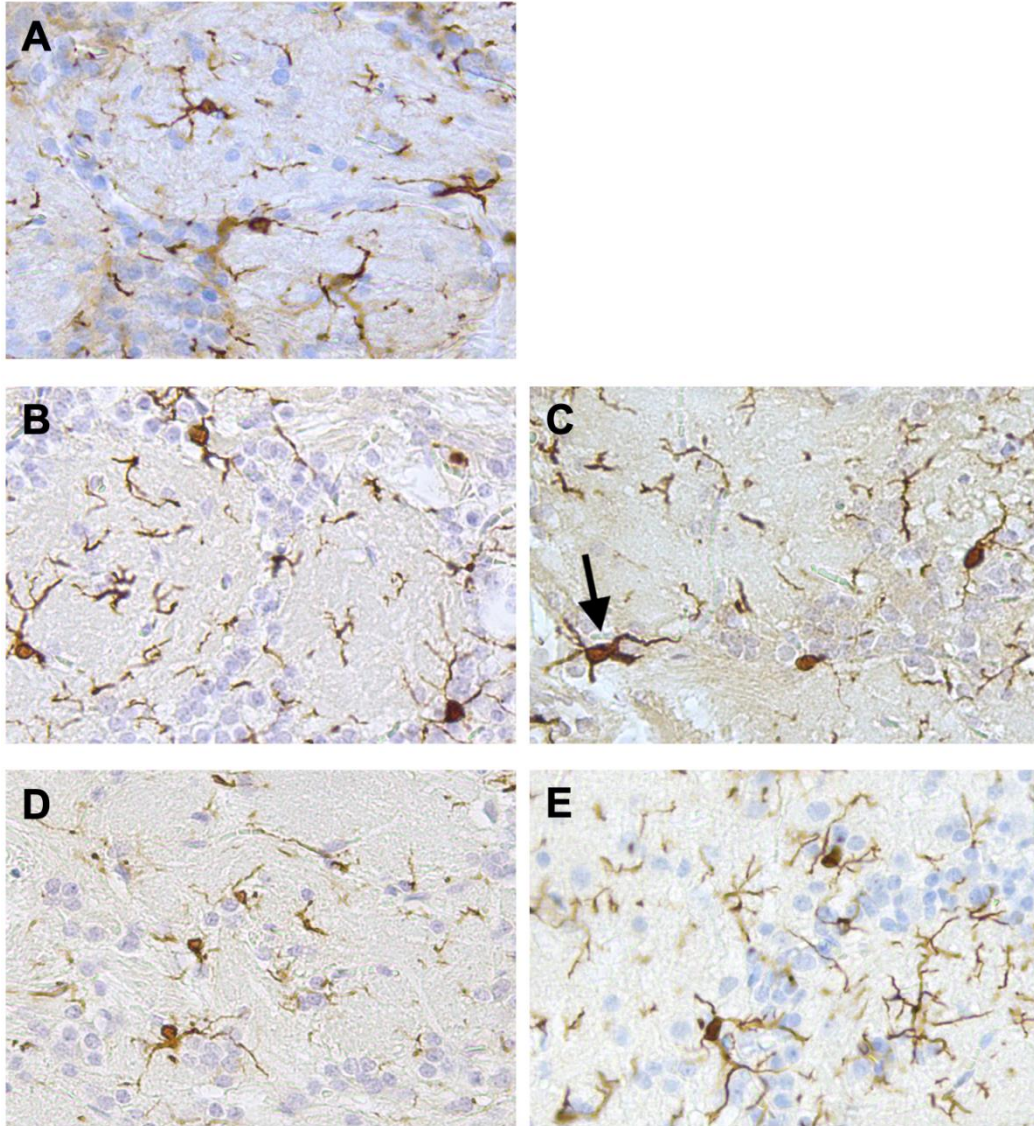
Figure 5.5. Representative brightfield microscopy images of olfactory bulb tissue sections, at 20X magnification, with anti-ionized calcium-binding adapter molecule 1 (anti-Iba1; panel **A**) and anti-heme oxygenase-1 (anti-HO-1; panel **B**) immunohistochemical stains. Resting microglia are indicated by arrows and characterized by a small cell body with ramified processes. Activated microglia are indicated by arrowheads and characterized by a large cell body with retracted processes.
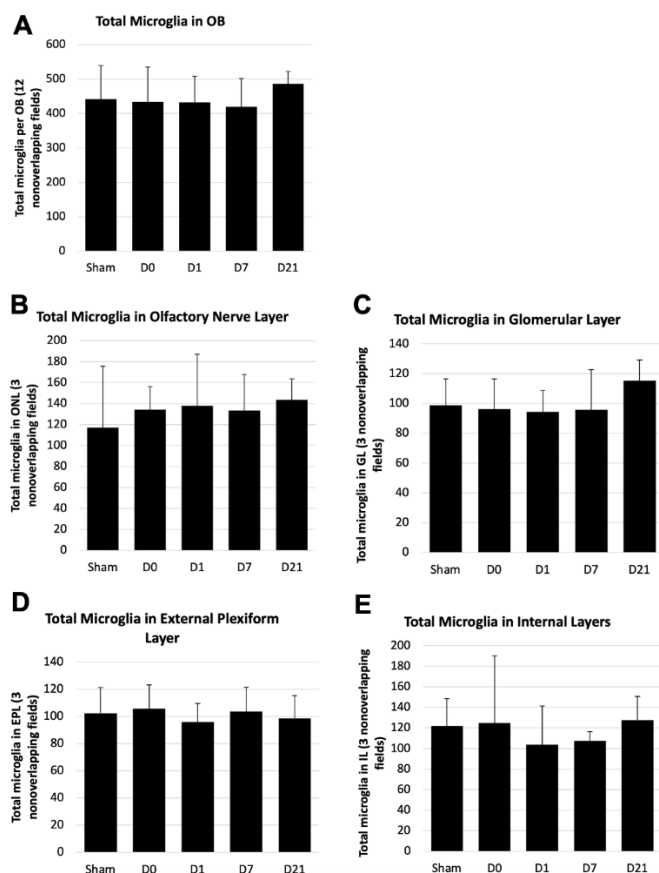
Figure 5.6. Total (panel **A**) and differential (panel **B-E**) microglial cell counts in the olfactory bulb (OB). Microglial cells were counted in twelve non-overlapping fields per animal. Differential microglial cell counts were determined using three non-overlapping fields per histologically distinct layer per olfactory bulb per animal. The analysis was done at 20X magnification, and four animals in each Ag-SiO$_2$ post-exposure group and eight animals in sham control were examined. Welch's one-way ANOVAs and post hoc Games-Howell tests were used to compare groups exposed to filtered air (control) or aerosolized silver silicate nanoparticles and euthanized 0-, 7-, 14-, or 21-days post-exposure (D0, D7, D14, and D21, respectively). Each value shown in the graphs is a group mean $\pm$ standard error.
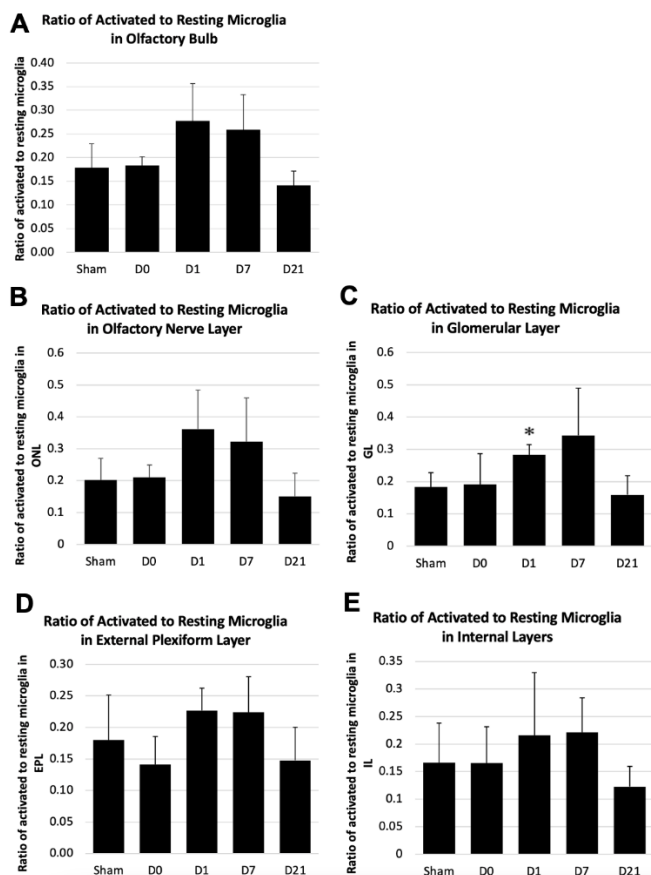
Figure 5.7. Inter-group comparisons of the ratio of activated to resting microglia in the olfactory bulb (panel **A**) and histologically distinct layers of the olfactory bulb (panels **B-E**). Microglia were morphometrically evaluated in twelve non-overlapping fields per olfactory bulb (OB) per animal, with three fields per histologically distinct layer. The analysis was done at 20X magnification, and four animals in each Ag-SiO$_2$ post-exposure group and eight animals in sham control were examined. Welch's one-way ANOVAs and post hoc Games-Howell tests were used to compare groups exposed to filtered air (sham control) or aerosolized silver silicate nanoparticles and euthanized 0-, 7-, 14-, or 21-days post-exposure (D0, D7, D14, and D21, respectively). Each value shown in the graphs is a group mean $\pm$ standard error. The asterisk (*) represents a significant ($p = 0.01$) difference from the sham control group.

Figure 5.8: Representative brightfield microscopy images of the glomerular layer of the olfactory bulb tissue sections, at 20X magnification, with anti-ionized calcium-binding adapter molecule 1 immunohistochemical stain to visualize microglial cells [sham control (**A**), day 0 post-exposure (**B**), day 1 post-exposure (**C**), day 7 post-exposure (**D**), day 21 post-exposure (**E**)]. Arrowhead points to activated microglia.
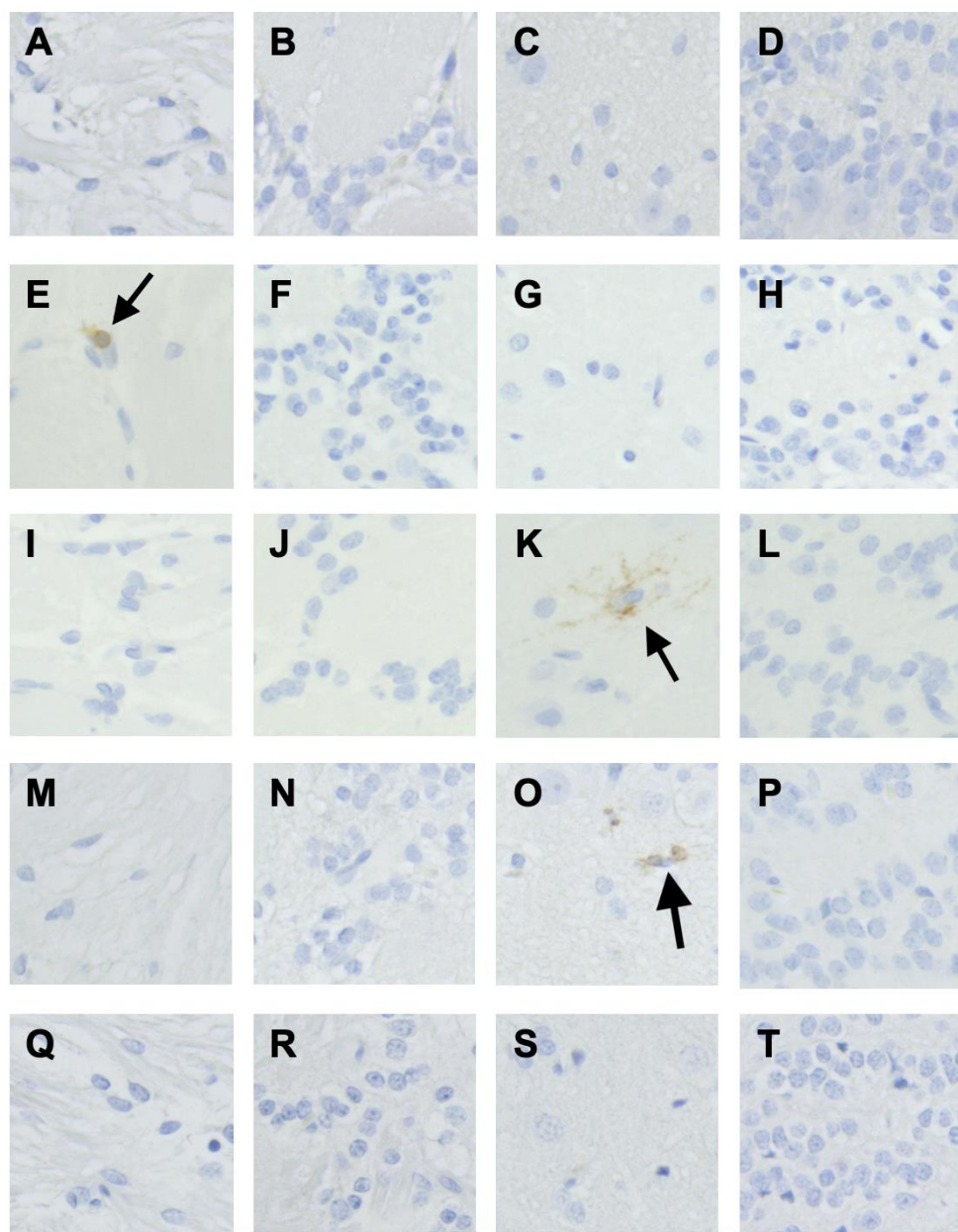
Figure 5.9: Representative brightfield microscopy images of olfactory bulb tissue sections, at 20X magnification, with anti-heme oxygenase-1 immunohistochemical stain showing immunostaining on post-exposure day 0 (A), day 1 (B), and day 7 (C). Arrowheads point to cells with heme oxygenase-1 staining, a marker for oxidative stress.

REFERENCES

1. Shao Y, Wu C, Wu T, et al. Green synthesis of sodium alginate-silver nanoparticles and their antibacterial activity. *International Journal of Biological Macromolecules*. 2018;111:1281-1292. doi:10.1016/j.ijbiomac.2018.01.012

2. Kumar R, Howdle S, Münstedt H. Polyamide/silver antimicrobials: Effect of filler types on the silver ion release. *Journal of Biomedical Materials Research Part B: Applied Biomaterials*. 2005;75B(2):311-319. doi:10.1002/jbm.b.30306

3. Burdușel AC, Gherasim O, Grumezescu AM, Mogoantă L, Ficai A, Andronescu E. Biomedical Applications of Silver Nanoparticles: An Up-to-Date Overview. *Nanomaterials (Basel)*. 2018;8(9). doi:10.3390/nano8090681

4. Lem KW, Choudhury A, A. Lakhani A, et al. Use of Nanosilver in Consumer Products. *NANOTEC*. 2012;6(1):60-72. doi:10.2174/187221012798109318

5. Larese FF, D'Agostin F, Crosera M, et al. Human skin penetration of silver nanoparticles through intact and damaged skin. *Toxicology*. 2009;255(1):33-37. doi:10.1016/j.tox.2008.09.025

6. George R, Merten S, Wang TT, Kennedy P, Maitz P. *In vivo* analysis of dermal and systemic absorption of silver nanoparticles through healthy human skin: Dermal absorption of nanocrystaline silver. *Australasian Journal of Dermatology*. 2014;55(3):185-190. doi:10.1111/ajd.12101

7. Kim S, Gates BL, Chang M, et al. Transcorneal delivery of topically applied silver nanoparticles does not delay epithelial wound healing. *NanoImpact*. 2021;24:100352. doi:10.1016/j.impact.2021.100352

8. Johnston HJ, Hutchison G, Christensen FM, Peters S, Hankin S, Stone V. A review of the in vivo and in vitro toxicity of silver and gold particulates: Particle attributes and biological mechanisms responsible for the observed toxicity. *Critical Reviews in Toxicology*. 2010;40(4):328-346. doi:10.3109/10408440903453074

9. Bourquin J, Milosevic A, Hauser D, et al. Biodistribution, Clearance, and Long-Term Fate of Clinically Relevant Nanomaterials. *Advanced Materials*. 2018;30(19):1704307. doi:https://doi.org/10.1002/adma.201704307

10. Suresh AK, Pelletier DA, Wang W, Morrell-Falvey JL, Gu B, Doktycz MJ. Cytotoxicity Induced by Engineered Silver Nanocrystallites Is Dependent on Surface Coatings and Cell Types. *Langmuir*. 2012;28(5):2727-2735. doi:10.1021/la2042058

11. Jo DH, Kim JH, Lee TG, Kim JH. Size, surface charge, and shape determine therapeutic effects of nanoparticles on brain and retinal diseases. *Nanomedicine: Nanotechnology, Biology and Medicine*. 2015;11(7):1603-1611. doi:10.1016/j.nano.2015.04.015

12. Riaz Ahmed KB, Nagy AM, Brown RP, Zhang Q, Malghan SG, Goering PL. Silver nanoparticles: Significance of physicochemical properties and assay interference on the interpretation of in vitro cytotoxicity studies. *Toxicology in Vitro*. 2017;38:179-192. doi:10.1016/j.tiv.2016.10.012

13. Jiang ZJ, Liu CY, Sun LW. Catalytic Properties of Silver Nanoparticles Supported on Silica Spheres. *J Phys Chem B*. 2005;109(5):1730-1735. doi:10.1021/jp046032g

14. Chu CY, Peng FC, Chiu YF, et al. Nanohybrids of Silver Particles Immobilized on Silicate Platelet for Infected Wound Healing. *PLOS ONE*. 2012;7(6):e38360. doi:10.1371/journal.pone.0038360

15. Egger S, Lehmann RP, Height MJ, Loessner MJ, Schuppler M. Antimicrobial Properties of a Novel Silver-Silica Nanocomposite Material. *Applied and Environmental Microbiology*. Published online May 2009. doi:10.1128/AEM.01658-08

16. Mannu R, Karthikeyan V, Veerappa MM, et al. Facile Use of Silver Nanoparticles-Loaded Alumina/Silica in Nanofluid Formulations for Enhanced Catalytic Performance toward 4-Nitrophenol Reduction. *Int J Environ Res Public Health*. 2021;18(6):2994. doi:10.3390/ijerph18062994

17. Neves J das, Arzi RS, Sosnik A. Molecular and cellular cues governing nanomaterial–mucosae interactions: from nanomedicine to nanotoxicology. *Chemical Society Reviews*. Published online 2020. doi:10.1039/C8CS00948A

18. Illum L. Transport of drugs from the nasal cavity to the central nervous system. *European Journal of Pharmaceutical Sciences*. 2000;11(1):1-18. doi:10.1016/S0928-0987(00)00087-7

19. Crowe TP, Greenlee MHW, Kanthasamy AG, Hsu WH. Mechanism of intranasal drug delivery directly to the brain. *Life Sciences*. 2018;195:44-52. doi:10.1016/j.lfs.2017.12.025

20. Selvaraj K, Gowthamarajan K, Karri VVSR. Nose to brain transport pathways an overview: potential of nanostructured lipid carriers in nose to brain targeting.

Artificial Cells, Nanomedicine, and Biotechnology. Published online November 17, 2018:1-8. doi:10.1080/21691401.2017.1420073

21. van Riel D, Verdijk R, Kuiken T. The olfactory nerve: a shortcut for influenza and other viral diseases into the central nervous system. *The Journal of Pathology*. 2015;235(2):277-287. doi:10.1002/path.4461

22. Meinhardt J, Radke J, Dittmayer C, et al. Olfactory transmucosal SARS-CoV-2 invasion as a port of central nervous system entry in individuals with COVID-19. *Nat Neurosci*. 2021;24(2):168-175. doi:10.1038/s41593-020-00758-5

23. Ji JH, Jung JH, Kim SS, et al. Twenty-Eight-Day Inhalation Toxicity Study of Silver Nanoparticles in Sprague-Dawley Rats. *Inhalation Toxicology*. 2007;19(10):857-871. doi:10.1080/08958370701432108

24. Sung JH, Ji JH, Park JD, et al. Subchronic Inhalation Toxicity of Silver Nanoparticles. *Toxicological Sciences*. 2009;108(2):452-461. doi:10.1093/toxsci/kfn246

25. Genter MB, Newman NC, Shertzer HG, Ali SF, Bolon B. Distribution and Systemic Effects of Intranasally Administered 25 nm Silver Nanoparticles in Adult Mice. *Toxicol Pathol*. 2012;40(7):1004-1013. doi:10.1177/0192623312444470

26. Patchin ES, Anderson DS, Silva RM, et al. Size-Dependent Deposition, Translocation, and Microglial Activation of Inhaled Silver Nanoparticles in the Rodent Nose and Brain. *Environmental Health Perspectives*. 2016;124(12):1870-1875. doi:10.1289/EHP234

27. Hopkins LE, Patchin ES, Chiu PL, Brandenberger C, Smiley-Jewell S, Pinkerton KE. Nose-to-brain transport of aerosolised quantum dots following acute

exposure. *Nanotoxicology*. 2014;8(8):885-893.

doi:10.3109/17435390.2013.842267

28. Elder A, Gelein R, Silva V, et al. Translocation of Inhaled Ultrafine Manganese Oxide Particles to the Central Nervous System. *Environmental Health Perspectives*. 2006;114(8):1172-1178. doi:10.1289/ehp.9030

29. de Castro F. Wiring olfaction: the cellular and molecular mechanisms that guide the development of synaptic connections from the nose to the cortex. *Front Neurosci*. Published online 2009. doi:10.3389/neuro.22.004.2009

30. Kosada T, Kosada K. Olfactory Bulb Anatomy. In Squire LR, ed, *Encyclopedia of Neuroscience*. 1st ed. Academic Elsevier; 2009:59-69.

31. Wake H, Moorhouse AJ, Jinno S, Kohsaka S, Nabekura J. Resting Microglia Directly Monitor the Functional State of Synapses In Vivo and Determine the Fate of Ischemic Terminals. *J Neurosci*. 2009;29(13):3974-3980.

doi:10.1523/JNEUROSCI.4363-08.2009

32. Tremblay MÈ, Stevens B, Sierra A, Wake H, Bessis A, Nimmerjahn A. The Role of Microglia in the Healthy Brain. *J Neurosci*. 2011;31(45):16064-16069.

doi:10.1523/JNEUROSCI.4158-11.2011

33. Schafer DP, Lehrman EK, Kautzman AG, et al. Microglia Sculpt Postnatal Neural Circuits in an Activity and Complement-Dependent Manner. *Neuron*.

2012;74(4):691-705. doi:10.1016/j.neuron.2012.03.026

34. Squarzoni P, Oller G, Hoeffel G, et al. Microglia Modulate Wiring of the Embryonic Forebrain. *Cell Reports*. 2014;8(5):1271-1279.

doi:10.1016/j.celrep.2014.07.042

35. Tin-Tin-Win-Shwe, Yamamoto S, Ahmed S, Kakeyama M, Kobayashi T, Fujimaki H. Brain cytokine and chemokine mRNA expression in mice induced by intranasal instillation with ultrafine carbon black. *Toxicology Letters*. 2006;163(2):153-160. doi:10.1016/j.toxlet.2005.10.006

36. Hutter E, Boridy S, Labrecque S, et al. Microglial Response to Gold Nanoparticles. *ACS Nano*. 2010;4(5):2595-2606. doi:10.1021/nn901869f

37. Ze Y, Sheng L, Zhao X, et al. TiO2 Nanoparticles Induced Hippocampal Neuroinflammation in Mice. *PLOS ONE*. 2014;9(3):e92230. doi:10.1371/journal.pone.0092230

38. Foldbjerg R, Olesen P, Hougaard M, Dang DA, Hoffmann HJ, Autrup H. PVP-coated silver nanoparticles and silver ions induce reactive oxygen species, apoptosis and necrosis in THP-1 monocytes. *Toxicology Letters*. 2009;190(2):156-162. doi:10.1016/j.toxlet.2009.07.009

39. Wang X, Ji Z, Chang CH, et al. Use of Coated Silver Nanoparticles to Understand the Relationship of Particle Dissolution and Bioavailability to Cell and Lung Toxicological Potential. *Small*. 2014;10(2):385-398. doi:10.1002/smll.201301597

40. Wang L, Zhang T, Li P, et al. Use of Synchrotron Radiation-Analytical Techniques To Reveal Chemical Origin of Silver-Nanoparticle Cytotoxicity. *ACS Nano*. 2015;9(6):6532-6547. doi:10.1021/acsnano.5b02483

41. Beltran-Huarac J, Zhang Z, Pyrgiotakis G, DeLoid G, Vaze N, Demokritou P. Development of reference metal and metal oxide engineered nanomaterials for nanotoxicology research using high throughput and precision flame spray

synthesis approaches. *NanoImpact*. 2018;10:26-37.

doi:10.1016/j.impact.2017.11.007

42. Zhang T, Gaffrey MJ, Thomas DG, et al. A proteome-wide assessment of the oxidative stress paradigm for metal and metal-oxide nanomaterials in human macrophages. *NanoImpact*. 2020;17:100194. doi:10.1016/j.impact.2019.100194

43. Raabe OG, Bennick JE, Light ME, Hobbs CH, Thomas RL, Tillery MI. An improved apparatus for acute inhalation exposure of rodents to radioactive aerosols. *Toxicol Appl Pharmacol*. 1973;26(2):264-273. doi:10.1016/0041-008x(73)90261-5

44. Anderson DS, Patchin ES, Silva RM, et al. Influence of Particle Size on Persistence and Clearance of Aerosolized Silver Nanoparticles in the Rat Lung. *Toxicological Sciences*. 2015;144(2):366-381. doi:10.1093/toxsci/kfv005

45. Ruehl-Fehlert C, Kittel B, Morawietz G, et al. Revised guides for organ sampling and trimming in rats and mice--part 1. *Exp Toxicol Pathol*. 2003;55(2-3):91-106.

46. Hanisch UK, Kettenmann H. Microglia: active sensor and versatile effector cells in the normal and pathologic brain. *Nat Neurosci*. 2007;10(11):1387-1394. doi:10.1038/nn1997

47. Olah M, Biber K, Vinet J, W.G.M. Boddeke H. Microglia Phenotype Diversity. *CNSNDDT*. 2011;10(1):108-118. doi:10.2174/187152711794488575

48. Davalos D, Grutzendler J, Yang G, et al. ATP mediates rapid microglial response to local brain injury in vivo. *Nature Neuroscience.* 2005;8(6):752-758. doi:10.1038/nn1472

49. Nimmerjahn A, Kirchhoff F, Helmchen F. Resting Microglial Cells Are Highly Dynamic Surveillants of Brain Parenchyma in Vivo. *Science*. 2005;308(5726):1314-1318. doi:doi:10.1126/science.1110647

50. Cherry JD, Olschowka JA, O'Banion MK. Neuroinflammation and M2 microglia: the good, the bad, and the inflamed. *Journal of Neuroinflammation*. 2014;11(1):98. doi:10.1186/1742-2094-11-98

51. Stence N, Waite M, Dailey ME. Dynamics of microglial activation: A confocal time-lapse analysis in hippocampal slices. *Glia*. 2001;33(3):256-266. doi:10.1002/1098-1136(200103)33:3<256::AID-GLIA1024>3.0.CO;2-J

52. Garcia GJM, Kimbell JS. Deposition of inhaled nanoparticles in the rat nasal passages: Dose to the olfactory region. *Inhalation Toxicology*. 2009;21(14):1165-1175. doi:10.3109/08958370902882713

53. Occupational Safety and Health Administration. *Silver, Metal, and Soluble Compounds (as Ag+)*. 1988. Accessed March 2, 2022. https://www.osha.gov/chemicaldata/519

54. Lee JH, Ahn K, Kim SM, Jeon KS, Lee JS, Yu IJ. Continuous 3-day exposure assessment of workplace manufacturing silver nanoparticles. *J Nanopart Res*. 2012;14(9):1134. doi:10.1007/s11051-012-1134-8

55. Luther EM, Petters C, Bulcke F, et al. Endocytotic uptake of iron oxide nanoparticles by cultured brain microglial cells. *Acta Biomaterialia*. 2013;9(9):8454-8465. doi:10.1016/j.actbio.2013.05.022

56. Ye D, Raghnaill MN, Bramini M, et al. Nanoparticle accumulation and transcytosis in brain endothelial cell layers. *Nanoscale*. 2013;5(22):11153-11165. doi:10.1039/C3NR02905K

57. Wang J, Liu Y, Jiao F, et al. Time-dependent translocation and potential impairment on central nervous system by intranasally instilled TiO2 nanoparticles. *Toxicology*. 2008;254(1):82-90. doi:10.1016/j.tox.2008.09.014

58. Liu Y, Gao Y, Liu Y, Li B, Chen C, Wu G. Oxidative stress and acute changes in murine brain tissues after nasal instillation of copper particles with different sizes. *J Nanosci Nanotechnol*. 2014;14(6):4534-4540. doi:10.1166/jnn.2014.8290

59. Duffy CM, Ahmed S, Yuan C, Mavanji V, Nixon JP, Butterick T. Microglia as a Surrogate Biosensor to Determine Nanoparticle Neurotoxicity. *J Vis Exp*. 2016;(116):54662. doi:10.3791/54662

60. Andriamasinoro SN, Dieme D, Marie-Desvergne C, et al. Kinetic time courses of inhaled silver nanoparticles in rats. *Arch Toxicol*. 2022;96(2):487-498. doi:10.1007/s00204-021-03191-0

61. Recordati C, De Maglie M, Cella C, et al. Repeated oral administration of low doses of silver in mice: tissue distribution and effects on central nervous system. *Particle and Fibre Toxicology*. 2021;18(1):23. doi:10.1186/s12989-021-00418-x

62. Kim JK, Kim HP, Park JD, et al. Lung retention and particokinetics of silver and gold nanoparticles in rats following subacute inhalation co-exposure. *Part Fibre Toxicol*. 2021;18:5. doi:10.1186/s12989-021-00397-z

63. Wang Y, Wang B, Zhu MT, et al. Microglial activation, recruitment and phagocytosis as linked phenomena in ferric oxide nanoparticle exposure. *Toxicology Letters*. 2011;205(1):26-37. doi:10.1016/j.toxlet.2011.05.001

64. Zhu J, Liao L, Zhu L, et al. Size-dependent cellular uptake efficiency, mechanism, and cytotoxicity of silica nanoparticles toward HeLa cells. *Talanta*. 2013;107:408-415. doi:10.1016/j.talanta.2013.01.037

65. Wu M, Guo H, Liu L, Liu Y, Xie L. Size-dependent cellular uptake and localization profiles of silver nanoparticles. *Int J Nanomedicine*. 2019;14:4247-4259. doi:10.2147/IJN.S201107

66. Davenport LL, Hsieh H, Eppert BL, et al. Systemic and Behavioral Effects of Intranasal Administration of Silver Nanoparticles. *Neurotoxicol Teratol*. 2015;51:68-76. doi:10.1016/j.ntt.2015.08.006

67. Lebedová J, Nováková Z, Večeřa Z, et al. Impact of acute and subchronic inhalation exposure to PbO nanoparticles on mice. *Nanotoxicology*. 2018;12(4):290-304. doi:10.1080/17435390.2018.1438679

68. Danscher G. Autometallography: A new technique for light and electron microscopic visualization of metals in biological tissues (gold, silver, metal sulphides and metal selenides). *Histochemistry*. 1984;81(4):331-335. doi:10.1007/BF00514327

69. Oviedo C, Rodríguez J. EDTA: the chelating agent under environmental scrutiny. *Quím Nova*. 2003;26:901-905. doi:10.1590/S0100-40422003000600020

70. Flora SJS, Pachauri V. Chelation in Metal Intoxication. *Int J Environ Res Public Health*. 2010;7(7):2745-2788. doi:10.3390/ijerph7072745

71. Sreeprasad TS, Pradeep T. Reversible Assembly and Disassembly of Gold Nanorods Induced by EDTA and Its Application in SERS Tuning. *Langmuir*. 2011;27(7):3381-3390. doi:10.1021/la104828e

72. Herz J, Filiano AJ, Smith A, Yogev N, Kipnis J. Myeloid cells and their relationship with the central nervous system. *Immunity*. 2017;46(6):943-956. doi:10.1016/j.immuni.2017.06.007

73. Sasaki Y, Ohsawa K, Kanazawa H, Kohsaka S, Imai Y. Iba1 is an actin-cross-linking protein in macrophages/microglia. *Biochem Biophys Res Commun*. 2001;286(2):292-297. doi:10.1006/bbrc.2001.5388

74. Jurga AM, Paleczna M, Kuter KZ. Overview of General and Discriminating Markers of Differential Microglia Phenotypes. *Frontiers in Cellular Neuroscience*. 2020;14. Accessed April 22, 2022. https://www.frontiersin.org/article/10.3389/fncel.2020.00198

75. Greenhalgh AD, Zarruk JG, Healy LM, et al. Peripherally derived macrophages modulate microglial function to reduce inflammation after CNS injury. *PLOS Biology*. 2018;16(10):e2005264. doi:10.1371/journal.pbio.2005264

CHAPTER 6

Conclusions and Future Research Directions

Over the last two decades, the use of products containing engineered nanomaterials (ENMs) has increased exponentially. Due to their unique physicochemical properties, they can be used in a wide variety of consumer products, industrial applications, medical treatments and drug delivery. There are currently 1800 ENM-based products on the market (Iftikhara, Azhara et al. 2021). The market size of ENMs in 2021 is 2.5 billion USD and is projected to reach 4 billion USD by 2028 (2022). ENMs are used in diverse consumer products including but not limited to antibacterial agents, paints, food additives, cosmetics, rubber-curing agents, textile UV-absorbers, contrast elements for magnetic resonance imaging, heating agents for cancer thermotherapy, and carriers for drug and gene delivery. When compared to their chemically identical bulk materials, nanomaterials possess a greater surface area to volume ratio, thus yielding a greater reactive surface area, unique physiochemical properties, while also possessing a potentially greater degree of toxicity than their bulk counterparts (Fischer and Chan 2007). With greater demands for engineered nanomaterials, this may pose increased risk for consumer and occupational exposure, especially for workers who manufacture, handle, and package ENMs and ENM-based products. Therefore, there is a significant need to better understand the hazards these materials may present and their effects on human health and the environment.

The Nanotechnology Health Implication Research (NHIR) Consortium formed by multiple academic and research instituions has focused on nanosafety research. NHIR provides ENMs to members of the consortium to assess possible toxicity in cell culture and for in vivo studies. Following in vitro studies performed by collaborators at UC Davis, two metal oxides, silver silicate (Ag-SiO$_2$) and zinc oxide (ZnO) and one carbon

based, graphene oxide (GO) ENMs were chosen for in vivo studies. Among all ENMs provided through NHIR, these ENMs had comparatively the highest toxicity found through in vitro studies.

Silver nanoparticles (AgNPs) are known to cause an inflammatory response in lung tissues. Inhalation of AgNPs in rats and mice have been shown to decrease lung function and increase pulmonary inflammation (Sung, Ji et al. 2008, Stebounova, Adamcakova-Dodd et al. 2011, Braakhuis, Gosens et al. 2014, Seiffert, Buckley et al. 2016, Silva, Anderson et al. 2016). However, no in vivo studies have been conducted with Ag-SiO$_2$ NPs, which are AgNPs on a silica support, designed to reduce particle agglomeration (Jiang, Liu et al. 2005).

A number of studies have examined the potential toxicity of ZnO ENMs using various exposure methods such as intranasal or intratracheal instillation, as well as oropharyngeal aspiration. Few studies have implemented an inhalation route which is physiologically more comparable to human exposure conditions (Gao, Yang et al. 2013, Jacobsen, Stoeger et al. 2015, Saptarshi, Feltis et al. 2015, Morimoto, Izumi et al. 2016, Wang, Li et al. 2017, Wang, Zhang et al. 2020). Some studies using chronic exposure to ZnO aerosols in a whole-body chamber have resulted in acute, but transient inflammation (Adamcakova-Dodd, Stebounova et al. 2014, Chuang, Juan et al. 2014, Morimoto, Izumi et al. 2016). Only a few studies (Klein, Wiench et al. 2012, Areecheewakul, Adamcakova-Dodd et al. 2020) have used a single-day, nose-only inhalation exposure to assess the toxicity of ZnO nanomaterials.

The toxicity of graphene-based nanomaterials have been the least studied carbon-based nanostructures compared to carbon nanotubes (Pecoraro, D'Angelo et al.

2018). As a result, there remain concerns regarding the safety of graphene-based

nanomaterials. There is no occupational exposure limit (OEL) currently available for the

family of graphene-based materials including graphene oxide (GO) /reduced graphene

oxide (rGO) (Di Cristo, Grimaldi et al. 2020). In addition, there are few inhalation studies

to assess the toxicity of a number of graphene-based materials following acute

exposure (Han, Kim et al. 2015). No inhalation study has been done to examine the

pulmonary response of acute exposure to rGO. Although, GO and rGO are from the

same graphene family, their biological responses can be different due to their unique

physicochemical properties (Mittal, Kumar et al. 2016). We have selected rGO for our

study.

The aims of our studies was to explore the potential implications of the three

ENMs studied in vitro at our institution that demonstrated toxicity, following acute one-

day inhalation to the respiratory tract. The focus of this study was in two regions of the

respiratory tract; the upper respiratory tract composed of the nasal cavity and the lower

respiratory tract formed by the bronchial tree and lung parenchyma. These two regions

of the respiratory system were selected for study, based on the unique patterns of

particle deposition for each of these regions and the potential implications for

nanoparticle deposition in each of these regions.

To address the aims of our study, an acute single-day nose-only inhalation

exposure to aerosols was done using young healthy Sprague Dawley rats. Aerosols

were well-characterized before and during each study. Experiments were conducted to

assess the pulmonary toxicity using BALF analysis and histological examination of the

lungs, and microglial activation of the olfactory bulb via histological examination. From these experiments, several conclusions can be drawn.

In our first study, the aerosolized silver silicate concentration averaged 4.9 ± 2.3 mg/m^3. The Occupational Safety and Health Administration (OSHA) set the exposure limit for silver at 0.01 mg/m^3 per 8-hour time weighted average. Maximal time weighted average concentration of aerosolized silver has been found to be up to 0.289 mg/m^3 in silver manufacturing plants (Lee, Ahn et al. 2012). The aerosolized silver concentration in our study can be considered as equivalent to an environment with high occupational exposure to aerosolized silver without personal safety measures. Similarly, the mean mass concentration of ZnO ENM aerosol was 4.23 ± 1.27 mg/m^3 standard deviation. This concentration is similar to the maximum recommended TWA limit for ZnO fume and respirable ZnO dust. For rGO the mean mass concentration was 2.28 ± 0.73 mg/m^3 standard deviation. No occupational exposure limit has been established for graphene-based materials as limited data are available on airborne graphene concentrations in the workplace. However, the airborne concentration of graphene nanoplatelets during product collection from the discharge vessels in the manufacturing site has been recorded as high as 2.27 and 0.017 mg/m^3 (Heitbrink, Lo et al. 2015). This concentration range is comparable to the rGO concentration we used in our study.

A single day of exposure to metal oxide-based ENMs (Ag-SiO$_2$ and ZnO) resulted in an acute, but transient pulmonary inflammatory response. In contrast, no inflammatory response was observed following acute exposure to 2D-carbon based ENM (rGO). In the Ag-SiO$_2$ study, total cells in the BAL was significantly increased on day 0, 1 and 7 post-exposure to Ag-SiO$_2$. Macrophages and neutrophils were increased

on day 0 and remained elevated through day 7 post-exposure to Ag-SiO$_2$. Of interest was the significant elevation of eosinophils on days 0 and 7 post-exposure to Ag-SiO$_2$ compared to animals exposed only to FA. By day 21, inflammatory cells returned levels similar to controls. No lung injury was demonstrated in the histological analysis of lung tissue sections. Similarly, in the ZnO inhalation study, the total number of cells recovered in BALF increased significantly immediately following the end of exposure, as well as the significant presence of non-viable cells in animals exposed to ZnO, compared to control animals on days 0, 1, and 7 days post-exposure. Macrophages and neutrophils in ZnO exposed animals were significantly increased immediately post-exposure (day 0), while neutrophils remained elevated along with an increase in eosinophil number 1 day post-exposure in ZnO exposed animals. A significant increase in protein concentration in BALF from day 0 to post-exposure day 7 suggested a mild, but statistically significant level of sustained injury and inflammation in animals exposed to ZnO. However, by 21 days post-exposure to ZnO, all biomarkers examined had returned to levels similar to control. In contrast to the Ag-SiO$_2$ and ZnO studies, a single day inhalation exposure to rGO did not demonstrate any toxicity based on analysis of BALF, lung histology or gene expression. The findings of this study suggested a single day of inhalation exposure to aerosols of rGO (400 x 400 nm) for 6 hours does not exert any toxic effects in rats at a dose 2.28 ± 0.73 mg/m^3.

Acute inhalation of Ag-SiO$_2$ NPs elicited transient and differential microglial activation without significant microglial recruitment to the OB. The absence of significant microglial recruitment and mild oxidative stress in the OB were indicative of an short-term inflammatory response in the OB that might reflect the relatively short duration of

inhalation exposure, the chemical stability of the Ag-SiO$_2$ NPs conferred by a silicate core, or the presence of a moderate Ag-SiO$_2$ NPs agglomeration during aerosolization that interfered with NPs deposition onto the nasal epithelium, and/or the limited uptake of NPs for transport to the OB to induce cytotoxic effects.

In conclusion, we conclude that the inhalation of ENMs is not harmless. However, the inflammatory response is acute and short-lived. Future studies are needed to evaluate the long-term toxicity of these ENMs.

Future Direction

Nanotechnology as a term was first introduced in 1959 by Nobel laureate Richard P. Feynman during his infamous lecture "There's Plenty of Room at the Bottom" (Feynman 1992). Although many studies are done to advance nanotechnology and its applications, toxicity screening and assessment for ENMs are still in the initial stages. Increased demands for ENM- based products are likely to lead to increasing scenarios for human exposure. Occupational and environmental exposures remain the greatest risk. There is a continued need for assessment and regulation of ENMs. Acute and chronic studies with different ENMs are necessary to better understand the mechanisms of pathophysiology and human health risks. As is expected with new material, initial studies have focused heavily on acute exposures and doses up to and including those likely to be encountered in the most exposed human populations, in manufacturing. Future studies are needed that use chronic low level exposures, and routes likely to be encountered by consumers or in the environment, instead of largely focusing on very acute high dose studies.

References

1. Adamcakova-Dodd, Andrea, Larissa V Stebounova, Jong Sung Kim, Sabine U Vorrink, Andrew P Ault, Patrick T O'Shaughnessy, Vicki H Grassian, and Peter S Thorne. 2014. 'Toxicity assessment of zinc oxide nanoparticles using sub-acute and sub-chronic murine inhalation models', *Particle and fibre toxicology*, 11: 1-15.

2. Areecheewakul, Sudartip, Andrea Adamcakova-Dodd, Brittany E Givens, Benjamin R Steines, Yifang Wang, David K Meyerholz, Nathanial J Parizek, Ralph Altmaier, Ezazul Haque, and Patrick T O'Shaughnessy. 2020. 'Toxicity assessment of metal oxide nanomaterials using in vitro screening and murine acute inhalation studies', *NanoImpact*, 18: 100214.

3. Braakhuis, Hedwig M, Ilse Gosens, Petra Krystek, John AF Boere, Flemming R Cassee, Paul HB Fokkens, Jan Andries Post, Henk Van Loveren, and Margriet VDZ Park. 2014. 'Particle size dependent deposition and pulmonary inflammation after short-term inhalation of silver nanoparticles', *Particle and fibre toxicology*, 11: 1-16.

4. Chuang, Hsiao-Chi, Hung-Tzu Juan, Chun-Nung Chang, Yuan-Horng Yan, Tzu-Hsuen Yuan, Jyh-Seng Wang, Hao-Cheng Chen, Yaw-Huei Hwang, Chii-Hong Lee, and Tsun-Jen Cheng. 2014. 'Cardiopulmonary toxicity of pulmonary exposure to occupationally relevant zinc oxide nanoparticles', *Nanotoxicology*, 8: 593-604.

5. Di Cristo, L, B Grimaldi, T Catelani, E Vázquez, PP Pompa, and S Sabella. 2020. 'Repeated exposure to aerosolized graphene oxide mediates autophagy

inhibition and inflammation in a three-dimensional human airway model',
Materials Today Bio, 6: 100050.

6. Feynman, Richard P. 1992. 'There's plenty of room at the bottom [data storage]',
Journal of microelectromechanical systems, 1: 60-66.

7. Fischer, Hans C, and Warren CW Chan. 2007. 'Nanotoxicity: the growing need
for in vivo study', *Current opinion in biotechnology*, 18: 565-71.

8. Gao, Lifeng, Sheng-Tao Yang, Shaorui Li, Yuguang Meng, Haifang Wang, and
Hao Lei. 2013. 'Acute toxicity of zinc oxide nanoparticles to the rat olfactory
system after intranasal instillation', *Journal of Applied Toxicology*, 33: 1079-88.

9. Han, Sung Gu, Jin Kwon Kim, Jae Hoon Shin, Joo Hwan Hwang, Jong Seong
Lee, Tae-Gyu Kim, Ji Hyun Lee, Gun Ho Lee, Keun Soo Kim, and Heon Sang
Lee. 2015. 'Pulmonary responses of sprague-dawley rats in single inhalation
exposure to graphene oxide nanomaterials', *BioMed Research International*,
2015.

10. Heitbrink, William A, Li-Ming Lo, and Kevin H Dunn. 2015. 'Exposure controls for
nanomaterials at three manufacturing sites', *Journal of occupational and
environmental hygiene*, 12: 16-28.

11. Iftikhara, Muhammad Muhammad Irfan, Irfan Azhara, Muhammad Sohaila, Zia Ur
Muhammad Nadeema, Rahman Farooqia, Ashar Hina Ayuba, Ayesha Fatimad
Muhammad Siddiquib, and Zia Wajid ur Rehmana. 2021. 'Sufficiency and toxicity
limits of metallic oxide nanoparticles in the biosphere', *Nanomaterials: Synthesis,
Characterization, Hazards and Safety*: 145.

12. Jacobsen, Nicklas Raun, Tobias Stoeger, Sybille Van Den Brûle, Anne Thoustrup Saber, Andrea Beyerle, Giulia Vietti, Alicja Mortensen, Józef Szarek, Hans Christian Budtz, and Ali Kermanizadeh. 2015. 'Acute and subacute pulmonary toxicity and mortality in mice after intratracheal instillation of ZnO nanoparticles in three laboratories', *Food and Chemical Toxicology*, 85: 84-95.

13. Jiang, Zhong-Jie, Chun-Yan Liu, and Lu-Wei Sun. 2005. 'Catalytic properties of silver nanoparticles supported on silica spheres', *The Journal of Physical Chemistry B*, 109: 1730-35.

14. Klein, Christoph L, Karin Wiench, Martin Wiemann, Lan Ma-Hock, Ben van Ravenzwaay, and Robert Landsiedel. 2012. 'Hazard identification of inhaled nanomaterials: making use of short-term inhalation studies', *Archives of Toxicology*, 86: 1137-51.

15. Lee, Ji Hyun, Kangho Ahn, Sun Man Kim, Ki Soo Jeon, Jong Seong Lee, and Il Je Yu. 2012. 'Continuous 3-day exposure assessment of workplace manufacturing silver nanoparticles', *Journal of Nanoparticle Research*, 14: 1-10.

16. Mittal, Sandeep, Veeresh Kumar, Nitesh Dhiman, Lalit Kumar Singh Chauhan, Renu Pasricha, and Alok Kumar Pandey. 2016. 'Physico-chemical properties based differential toxicity of graphene oxide/reduced graphene oxide in human lung cells mediated through oxidative stress', *Scientific reports*, 6: 1-16.

17. Morimoto, Yasuo, Hiroto Izumi, Yukiko Yoshiura, Taisuke Tomonaga, Takako Oyabu, Toshihiko Myojo, Kazuaki Kawai, Kazuhiro Yatera, Manabu Shimada, and Masaru Kubo. 2016. 'Evaluation of pulmonary toxicity of zinc oxide

nanoparticles following inhalation and intratracheal instillation', *International journal of molecular sciences*, 17: 1241.

18. "Nanoparticle Analysis Market to hit US$ 4 billion by 2028, Says Global Market Insights Inc." In. 2022. *GlobeNewswire*.

19. Pecoraro, Roberta, Daniele D'Angelo, Simona Filice, Silvia Scalese, Fabiano Capparucci, Fabio Marino, Carmelo Iaria, Giulia Guerriero, Daniele Tibullo, and Elena M Scalisi. 2018. 'Toxicity evaluation of graphene oxide and titania loaded nafion membranes in zebrafish', *Frontiers in physiology*, 8: 1039.

20. Saptarshi, Shruti R, Bryce N Feltis, Paul FA Wright, and Andreas L Lopata. 2015. 'Investigating the immunomodulatory nature of zinc oxide nanoparticles at sub-cytotoxic levels in vitro and after intranasal instillation in vivo', *Journal of nanobiotechnology*, 13: 1-11.

21. Seiffert, Joanna, Alison Buckley, Bey Leo, Nicholas G Martin, Jie Zhu, Ranran Dai, Farhana Hussain, Chang Guo, James Warren, and Alan Hodgson. 2016. 'Pulmonary effects of inhalation of spark-generated silver nanoparticles in Brown-Norway and Sprague–Dawley rats', *Respiratory research*, 17: 1-15.

22. Silva, R. M., D. S. Anderson, J. Peake, P. C. Edwards, E. S. Patchin, T. Guo, T. Gordon, L. C. Chen, X. Sun, L. S. Van Winkle, and K. E. Pinkerton. 2016. 'Aerosolized Silver Nanoparticles in the Rat Lung and Pulmonary Responses over Time', *Toxicol Pathol*, 44: 673-86.

23. Stebounova, Larissa V, Andrea Adamcakova-Dodd, Jong Sung Kim, Heaweon Park, Patrick T O'Shaughnessy, Vicki H Grassian, and Peter S Thorne. 2011.

'Nanosilver induces minimal lung toxicity or inflammation in a subacute murine inhalation model', *Particle and fibre toxicology*, 8: 1-12.

24. Sung, Jae Hyuck, Jun Ho Ji, Jin Uk Yoon, Dae Seong Kim, Moon Yong Song, Jayoung Jeong, Beom Seok Han, Jeong Hee Han, Yong Hyun Chung, and Jeongyong Kim. 2008. 'Lung function changes in Sprague-Dawley rats after prolonged inhalation exposure to silver nanoparticles', *Inhalation toxicology*, 20: 567-74.

25. Wang, Dejun, Haibo Li, Zihong Liu, Jingyang Zhou, and Tianliang Zhang. 2017. 'Acute toxicological effects of zinc oxide nanoparticles in mice after intratracheal instillation', *International journal of occupational and environmental health*, 23: 11-19.

26. Wang, Ping, Lin Zhang, Yanxia Liao, Juan Du, Mengying Xu, Wen Zhao, Shuxian Yin, Guilan Chen, Yu Deng, and Yiran Li. 2020. 'Effect of intratracheal instillation of ZnO nanoparticles on acute lung inflammation induced by lipopolysaccharides in mice', *Toxicological sciences*, 173: 373-86.